U.S. Department of Transportation
Federal Railroad Administration

Determination of Residual Stresses in Rails

Office of Research and Development
Washington, DC 20590

J. J. Groom

Battelle Columbus Laboratories
505 King Avenue
Columbus OH 43201

DOT/FRA/ORD-83/05
DOT-TSC-FRA-81-21

May 1983

This document is available to the public through the National Technical Information Service, Springfield, Virginia 22161.

NOTICE

This document is disseminated under the sponsorship of the Department of Transportation in the interest of information exchange. The United States Government assumes no liability for its contents or use thereof.

NOTICE

The United States Government does not endorse products or manufacturers. Trade or manufacturers' names appear herein solely because they are considered essential to the object of this report.

Technical Report Documentation Page

1. Report No. DOT/FRA/ORD-83/05	2. Government Accession No.	3. Recipient's Catalog No.
4. Title and Subtitle DETERMINATION OF RESIDUAL STRESSES IN RAILS		5. Report Date May 1983
		6. Performing Organization Code DTS-76
7. Author's) J.J. Groom		8. Performing Organization Report No. DOT-TSC-FRA-81-21
9. Performing Organization Name and Address Battelle Columbus Laboratories* 505 King Avenue Columbus OH 43201		10. Work Unit No. (TRAIS) RR219/R2309
		11. Contract or Grant No. DOT-TSC-1426
12. Sponsoring Agency Name and Address U.S. Department of Transportation Federal Railroad Administration Office of Research and Development Washington DC 20590		13. Type of Report and Period Covered Final Report
		14. Sponsoring Agency Code RRD-1

15. Supplementary Notes

*Under contract to: U.S. Department of Transportation
Research and Special Programs Administration
Transportation Systems Center
Cambridge MA 02142

16. Abstract

A destructive sectioning technique for measuring the complete three-dimensional residual stresses in a rail cross section was developed. The technique was applied to four tangent rail specimens: two 136-pound specimens were taken from FAST (Facility for Accelerated Service Testing), Pueblo, CO (83 and 270 MGT (million gross tons)) and two 132-pound specimens were obtained from revenue service (100 and 300 MGT). The results show that: 1) high compressive stresses exist in and near the tread surface of the rail, particularly near the edges of the wear pattern where the plastic flow of metal is extreme, 2) high tensile stresses are found just below the tread surface with peak stresses near the edges of the tread wear pattern, and 3) for the traffic ranges examined (83 to 300 MGT), the tensile stresses internal to the rail head increased with increasing MGT.

17. Key Words RAIL, RESIDUAL STRESS, FATIGUE, COMPRESSIVE STRESS, TENSILE STRESS, STRAIN	18. Distribution Statement DOCUMENT IS AVAILABLE TO THE PUBLIC THROUGH THE NATIONAL TECHNICAL INFORMATION SERVICE, SPRINGFIELD, VIRGINIA 22161

19. Security Classif. (of this report)	20. Security Classif. (of this page)	21. No. of Pages	22. Price
Unclassified	Unclassified	72	

Form DOT F 1700.7 (8-72) Reproduction of completed page authorized

METRIC CONVERSION FACTORS

Approximate Conversions to Metric Measures

Symbol	When You Know	Multiply by	To Find	Symbol
		LENGTH		
in	inches	*2.5	centimeters	cm
ft	feet	30	centimeters	cm
yd	yards	0.9	meters	m
mi	miles	1.6	kilometers	km
		AREA		
in^2	square inches	6.5	square centimeters	cm^2
ft^2	square feet	0.09	square meters	m^2
yd^2	square yards	0.8	square meters	m^2
mi^2	square miles	2.6	square kilometers	km^2
	acres	0.4	hectares	ha
		MASS (weight)		
oz	ounces	28	grams	g
lb	pounds	0.45	kilograms	kg
	short tons (2000 lb)	0.9	tonnes	t
		VOLUME		
tsp	teaspoons	5	milliliters	ml
Tbsp	tablespoons	15	milliliters	ml
fl oz	fluid ounces	30	milliliters	ml
c	cups	0.24	liters	l
pt	pints	0.47	liters	l
qt	quarts	0.95	liters	l
gal	gallons	3.8	liters	l
ft^3	cubic feet	0.03	cubic meters	m^3
yd^3	cubic yards	0.76	cubic meters	m^3
		TEMPERATURE (exact)		
°F	Fahrenheit temperature	5/9 (after subtracting 32)	Celsius temperature	°C

*1 in. = 2.54 cm (exactly). For other exact conversions and more detail tables see NBS Misc. Publ. 286. Units of Weight and Measures. Price $2.25 SD Catalog No. C13 10 286.

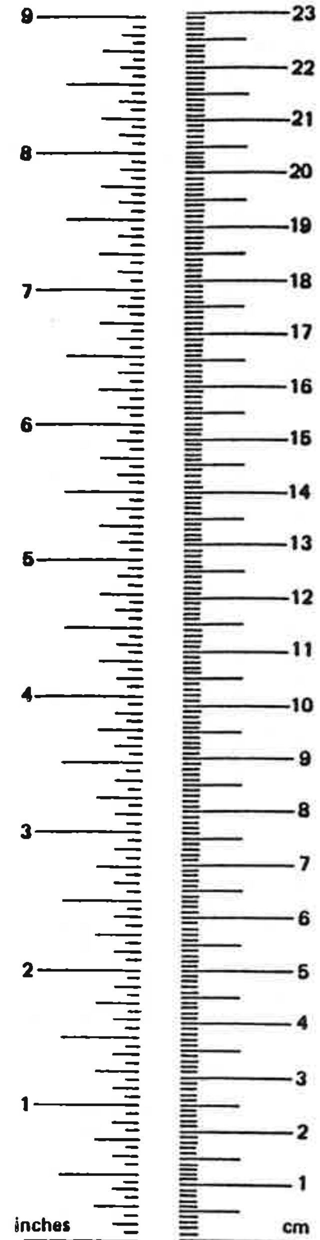

Approximate Conversions from Metric Measures

Symbol	When You Know	Multiply by	To Find	Symbol
		LENGTH		
mm	millimeters	0.04	inches	in
cm	centimeters	0.4	inches	in
m	meters	3.3	feet	ft
m	meters	1.1	yards	yd
km	kilometers	0.6	miles	mi
		AREA		
cm^2	square centimeters	0.16	square inches	in^2
m^2	square meters	1.2	square yards	yd^2
km^2	square kilometers	0.4	square miles	mi^2
ha	hectares (10,000 m^2)	2.5	acres	
		MASS (weight)		
g	grams	0.035	ounces	oz
kg	kilograms	2.2	pounds	lb
t	tonnes (1000 kg)	1.1	short tons	
		VOLUME		
ml	milliliters	0.03	fluid ounces	fl oz
l	liters	2.1	pints	pt
l	liters	1.06	quarts	qt
l	liters	0.26	gallons	gal
m^3	cubic meters	36	cubic feet	ft^3
m^3	cubic meters	1.3	cubic yards	yd^3
		TEMPERATURE (exact)		
°C	Celsius temperature	9/5 (then add 32)	Fahrenheit temperature	°F

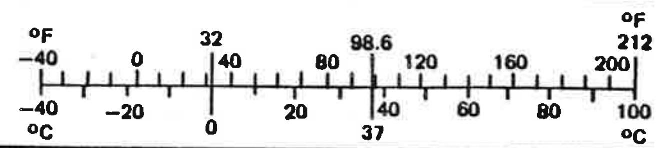

CONTENTS

LIST OF ILLUSTRATIONS

LIST OF ILLUSTRATIONS (Continued)

LIST OF TABLES

EXECUTIVE SUMMARY

This report presents part of the results of a study on rail material characterization for the correlation of rail defect growth and failure properties to better define rail defect mechanisms. The work was conducted as part of the Track Structures Program under the direction of the Transportation Systems Center, and sponsored by the Federal Railroad Administration. The results are presented in two volumes entitled:

Determination of Residual Stresses in Rails, FRA/ORD-83/05.
Fatigue Crack Initiation Properties of Rail Steels, FRA/ORD-82-05.

Fatigue cracks are a source of rail failure and subsequent train derailment. Residual stresses constitute an important driving force for the initiation and growth of fatigue cracks. Residual stresses are the result of several factors including the effects of the manufacturing/fabrication processes, the constraints and/or loadings due to the total track structure, and the live loads imposed during train passage. Detailed knowledge of the distribution and magnitudes of the residual stresses existing in rail is essential for the analysis of fatigue crack initiation and growth and fracture of rail. The objective of the work described in this report was to determine the residual stress levels and distribution in rail.

A destructive sectioning technique for measuring the complete three-dimensional residual stresses in rail cross sections (away from the bolted or welded joints) was developed. The technique was applied to four tangent rail specimens. Two 136-pound rail specimens were taken from FAST (83 and 270 MGT) and two 132-pound rail specimens were obtained from revenue service (100 and 300 MGT).

The results show that:

- High compressive stresses exist in and near the tread surface of the rail, particularly near the edges of the wear pattern where the plastic flow of metal is extreme.
- High tensile stresses are found just below the tread surface with peak stresses near the edges of the tread (and flange) wear pattern.
- For the traffic ranges examined (83 to 300 MGT), the tensile stresses internal to the rail head increase with increasing MGT.

1. INTRODUCTION

In its lifetime, a rail is subjected to loadings that cause localized plastic deformations within the rail cross section. The plastic deformations create stresses in the rail that remain even after the original loads are removed. These locked-in stresses are known as residual stresses. Residual stresses, in combination with the cyclic operational stresses, constitute one of the key factors of the internal rail environment in which cracks develop and grow. Therefore, specific knowledge of the residual stress patterns in rail cross sections is essential to any analysis which attempts to investigate fatigue and fracture of rail.

Frequently, the term "residual stress", as applied to rail, refers to the stress condition that is found in the rail in situ, i.e., the rail is constrained and loaded by the conditions of its existence in the total track structure (temperature, joints, tie plates, ties, fill, etc.). These conditions are exclusive of the additional "live" loads to be found during the passage of a train. It is possible, though not normally the case, that these conditions can cause the local plastic deformations described in the first paragraph above. If the rail were removed from these conditions, that is, completely freed from the track structure, its internal stress state would change, but it would still retain significant internal stresses as a vestige of the plastic deformations it experienced throughout its lifetime (including the deformations incurred as part of its manufacture). It is this latter (freed) residual stress state of the rail that is pursued in the work reported herein, and which is referred to as "residual stress" in the remainder of this report.

Various analytical attempts (1,2) have been made to determine the "freed" residual stress state of the rail, particularly with respect to the plastic deformations resulting from wheel/rail contact stresses. This is an extremely complex analytical problem and no definitive answers have resulted from these efforts. Numerous attempts have been made to experimentally determine the "freed" residual stress state of rail. These efforts have used faulty techniques (yielding erroneous results) and/or they have been limited in scope in terms of the extent of the cross section measured and in terms of determining what conditions affect the residual stress formation, and how they affect it. (3)

The main objective of the work described herein is to provide a detailed description of the residual stresses* throughout transverse cross sections of rail and to correlate the measured residual stress patterns and magnitudes with the affecting rail conditions. A key question to be answered is, "Does shakedown (the gradual change in the internal residual stress pattern toward a stable, unchanging pattern) actually occur?" In all of this work, the cross-sectional variations in residual stresses are examined only in that portion of the rail length away (from 3 to 4 feet minimum) from the rail joints (welded or spliced).

A necessary extension of the above objective is to codify the results in a simplified format that renders the results clear and in enough detail that they can be used by other investigators concerned with residual stresses in rails, e.g., fracture and fatigue.

*A similar study was conducted at United States Steel (USS) under a program funded by the Association of American Railroads. The results of that program should partially complement and overlap the subject work. [See reference 4.]

2. SUMMARY

One of the first tasks, and a major achievement in this program, was the development of a technique for measuring the three-dimensional residual stress throughout a rail cross section. The method used involved destructive sectioning of the rail specimen combined with an analytical procedure for resolving measurements of the sectioning effects into the original residual stress state of the rail specimen. Both the experimental and analytical portions of the technique were tested to verify/demonstrate the validity of the technique.

An experimental plan was developed by identifying the most likely affecting variables, by determining what ranges of these variables to investigate, and by balancing the foregoing factors with what specimens could realistically be obtained within the allowed budget. After several iterations, the specimen matrix shown in Figure 1 was accepted.

The main features of this test matrix are three test variables (tonnage, type of traffic, and curvature) of two levels each. The two levels of the tonnage variable were selected primarily to answer the question of shakedown. If shakedown occurs, the stable residual stress pattern should be well established by usage up to the first level, 60 to 150 MGT, and the pattern should remain relatively unchanged by substantial usage through the second level, 200 to 350 MGT. It is recognized that the high rail on curved track goes through a transition in the way it is loaded when the curvature becomes great enough to cause the wheel to go from lateral shear to flange loading. It is estimated that this slippage normally occurs at about 1 to 2 degrees curvature. The limitations on the number of specimens that could be examined and the limited availability of well-documented curved specimens caused the extremes of curvature (tangent and 5 degrees) to be selected for measurement. It must be noted that the shear phenomena will prevent any interpolation between these two data extremes for rail with curvature between tangent and 2 degrees.

Extremes on the type-of-traffic variable, such as heavy traffic (FAST track specimens) and light traffic, were preferred, but obtaining light traffic specimens from industry, particularly in tonnage ranges desired, did not appear feasible. The general traffic specimens 5, 6, 7, and 8 were furnished by Southern Railway System. The general type of traffic on the tangent track included heavy through light freight and a small percentage of passenger service (79 mph maximum speed).

Due to budget restraints which arose after development of the test matrix, only the tangent track specimens 1, 2, 5, and 6 were examined.

Since there were no data on what overall residual stress patterns could be expected in the rail, the first of the four tangent track specimens was heavily instrumented over its head* cross section. Some idea of the detail attempted on this specimen can be obtained from Figure 2, where the dense pattern of rosette strain gages applied to the head cross section is shown. Using the wealth of information obtained on the first specimen, the subsequent specimens were instrumented with fewer gages but with attention to verifying key features of the residual stress pattern and measurement technique.

The data were reduced through point by point calculations of the three-dimensional residual stresses within the rail cross section. Stress contour and vector plots were also prepared in order to convey the patterned information more clearly.

---

*Previous studies, though of a limited nature, have established that there are only relatively low residual stresses in the web and base of rails. Spot checks during the subject program confirmed this with two exceptions that could be the result of local mechanical working (dents).

TEST MATRIX

CURVATURE	TONNAGE: 60-150 MGT		TONNAGE: 200-300 MGT	
	TRAFFIC: Heavy	TRAFFIC: General	TRAFFIC: Heavy	TRAFFIC: General
Tan.	136 LB **1** (45 mph) 83 MGT	132 LB **5** (40 mph avg. 55 mph max.) 100 MGT	136 LB **2** (45 mph) 270 MGT	132 LB **6** (40 mph avg. 55 mph max.) 300 MGT
4-5° High Rail	**3**	132 LB **7** 100 MGT	**4**	131 LB **8** 300 MGT

Note: The large numbers in the matrix boxes denote the order of testing.

FIGURE 1. MATRIX OF TEST SPECIMENS FOR RESIDUAL STRESS MEASUREMENTS

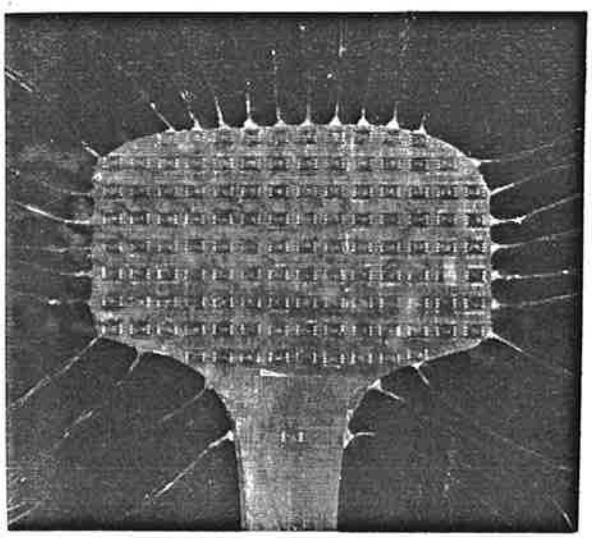

FIGURE 2. ROSETTE STRAIN GAGES ON HEAD CROSS SECTION, SPECIMEN 1

3. MAJOR CONCLUSIONS AND RESULTS

3.1 TECHNIQUE

The techniques used in this program were very successful in detailing the three-dimensional residual stress distributions in the specimens examined. The technique is applicable to those middle lengths of a rail away from its joint ends. Though the technique involves moderately exacting experimental measurements, the analytical conversion of the data to residual stresses was simplified through the adaptation of approximating assumptions. These assumptions have been shown to effect errors of less than 10 percent at points of significant residual stress over the major portion of the rail head. Errors of up to 44 percent occur in the very high compressive stress gradient found near the edge of the surface metal flow lip.

3.2 GENERAL PATTERNS OF RESIDUAL STRESS

General patterns of residual stress formation emerged from the measurements on tangent rail. These are revealed in Figures 3 and 4. Figure 3 shows the contours of the axial stresses in heavy traffic specimen 1, taken at 83 MGT. Flow of the surface metal laterally away from the top rail contact region, and particularly toward the gage side of the cross section, precipitates regions of acute compressive stress at the edges of these flow paths. A very high compressive stress* (>90 ksi) is found at the gage-side surface just below the edge of the flange wear pattern. These regions of compressive stress are not very deep at the edges of the wear pattern, but become deeper as they run across the head of the rail beneath the central tread region.

Closely allied to the regions of high compressive stress are regions of tensile stress. Note how the tensile stress regions seem to point peninsulas of tensile stress diagonally up toward the high compressive regions at the edges of the wear pattern. This is particularly visible in Figure 4, where the principal stresses in the plane of the cross section are shown. Note the high surface compressive stresses (inward arrows) at the edges of the wear (flow) region. But more importantly, note how high, in-plane, tensile stresses peak and point diagonally up toward the surface regions after running broadly and horizontally across the head underneath the center tread compressive zone. Both the axial and in-plane stresses drop off to low levels as the head narrows into the web.**

3.3 CONSISTENCY OF STRESS PATTERN ALONG RAIL LENGTH

The residual stress patterns, particularly those inside the rail and away from the surfaces, are consistent along the length of a tangent rail specimen. Checks on the uniformity of the stress patterns observed, with position along the length of the rail, were made. The principal compressive stresses over three feet along the centerline of the tread surface of specimens 1 and 2 vary as much as 34 percent from their average value. Two cross sections, 18 inches apart along the length of specimen 2, were subjected to identical transverse section measurements. The average variation in

---

*The results show stresses at a few points that may be in excess of the ultimate material strength. This probably arises from a condition where the strain relaxation upon sectioning went slightly plastic. The stress calculations that use these strains assume elastic relaxation, and therefore they produce an artificially high stress prediction. These points should be regarded as being highly stressed in the direction indicated (tensile or compressive), but the actual magnitude is somewhere between yield and ultimate.

**A region of high compressive stress (-35 to -65 ksi) may be observed in the lower field-side portion of Figures 3 and 4. This region does not appear to be associated with the contact surface of the rail, and this knot of compressive stress was not found in the other three specimens examined. It was noted during sectioning of specimens that apparently very hard spots would occur locally, as evidenced by repeated saw-tooth breakage over a 1/2- to 1-inch length of the cut. These spots occur only at a few locations whose distribution appears random. Perhaps these regions are artifacts of the manufacturing process.

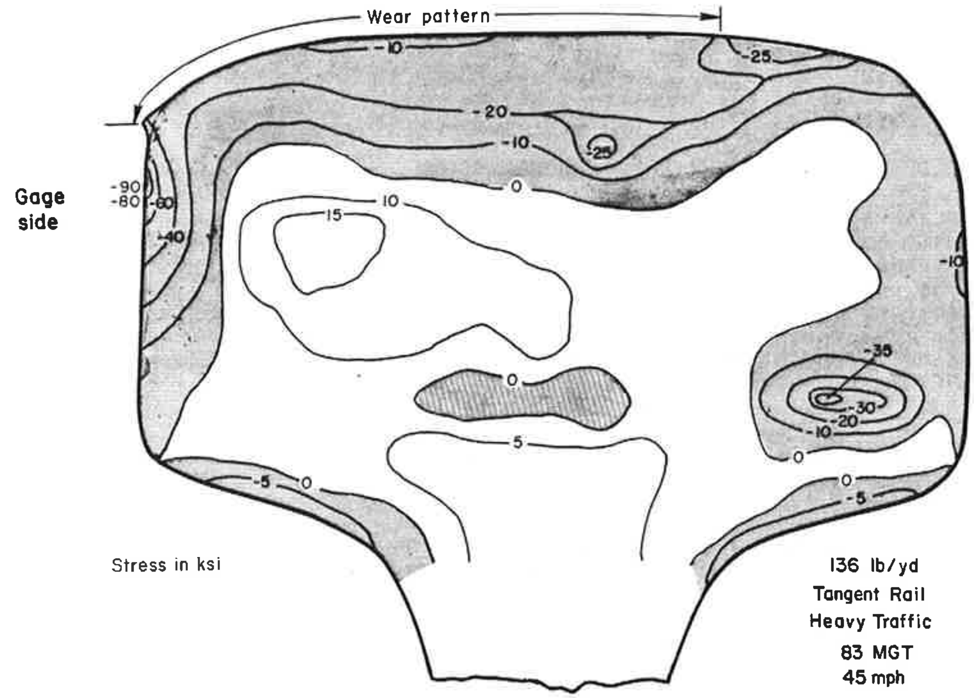

FIGURE 3. AXIAL RESIDUAL STRESS PATTERN

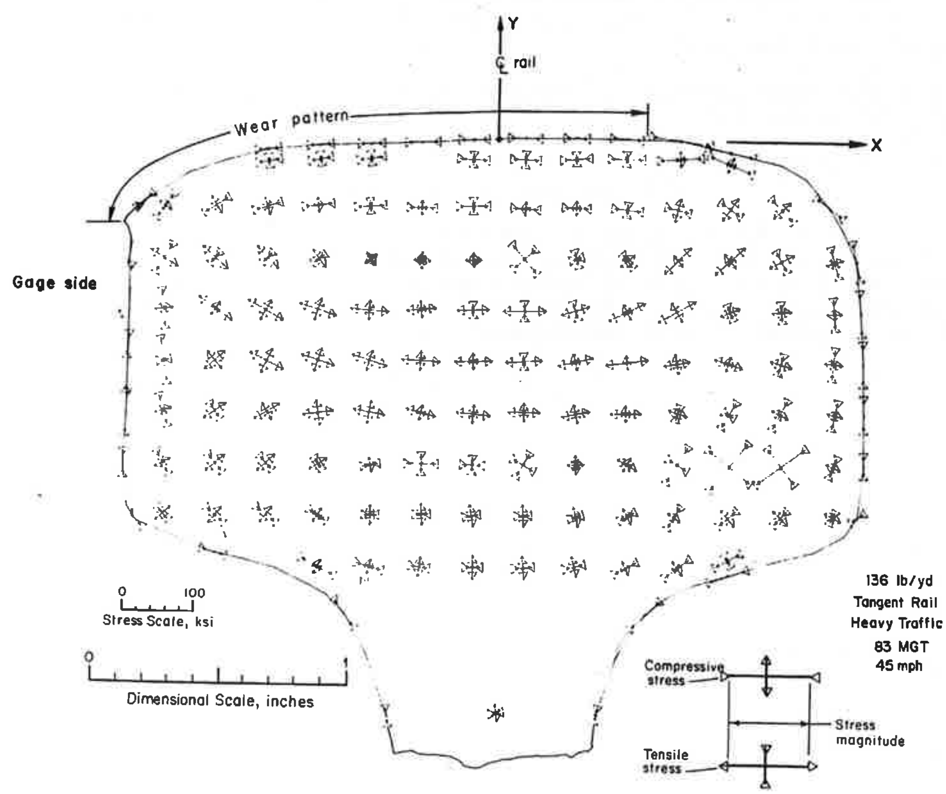

FIGURE 4. RESIDUAL STRESSES IN TRANSVERSE CROSS SECTION

internal (away from the surface) principal stress from one section to the next is 12 percent, with a maximum variation at one location of 26 percent. The orientations of these internal stresses from point to point are virtually identical. The variations in the stresses on the rail surfaces at these two sections average 25 percent, with a maximum variation at one location of 62 percent.

3.4 RESIDUAL STRESS MAGNITUDES AND SHAKEDOWN

The general stress patterns described above are present in all four tangent rail specimens. In terms of the stress magnitude, the surface and near-subsurface compressive stresses are the highest. Of these, the transverse stresses (those oriented around the periphery of the rail cross section and/or those lying in the transverse cross section) are greater than the axially oriented compressive stresses. Next in magnitude come the tensile stresses lying in the transverse cross section. The tensile stresses oriented in the axial direction have the lowest maximum values of all the residual stress component orientations. Table 1 lists the maximum values of each type of residual stress orientation for each of the tangent rail specimens.

The data from the four specimens* support the conclusion that shakedown does not occur within the range of 83 to 300 MGT for tangent rail under general-to-heavy traffic conditions. By looking at columns B and D in Table 1, it can be seen that the stresses (both compression and tension, lying in the transverse cross section of the rail) increase markedly with increased MGT. The axial tensile stresses (column E in Table 1) increase with MGT for the heavy traffic condition and register a slight decrease for the general traffic condition. Both the in-plane and axial stresses associated with the rail surfaces (columns A and C in Table 1) show a decrease with increased MGT. Perhaps flowing of the surface metal passes through a maximum stage after which the residual stresses in and near the rail surfaces are more evenly distributed and wear mechanisms erase the regions of acute stress.

The trend that emerges from the examination of these four tangent rail specimens is one of a general stress pattern within which the levels of stress are fluid, that is, the stress magnitudes change with time. Furthermore, these changes in stress magnitude at a point in the rail cross section are not merely the result of a moving (lowering) wear surface.

The increased pounding of tonnage (whether from general or heavy traffic) up into the 300 MGT level seems to drive the stresses in the transverse plane to higher levels within a general pattern that moves down into the rail head along with the wear surface. The axial tensile stresses inside the head also increase in this manner for heavy traffic, but remain relatively unchanged under general traffic.

The compressive stresses at and near the rail surface are more complex and difficult to predict. This is probably due to an intimate relationship between these stresses and the surface wear mechanisms and also to the fact that the stresses at the rail surface more closely reflect the random nature of the wheel contact loads that create the residual stress conditions.

*It must be recognized that examination of only four specimens (each differing from the others) represents a severely limited sampling.

TABLE 1. MAXIMUM RESIDUAL STRESSES MEASURED ON EACH OF TANGENT RAIL SPECIMENS

SPECIMEN NO. DESCRIPTION	MAXIMUM RESIDUAL STRESS COMPONENT, ksi				
	(A) PERIPHERAL ON THE SURFACE (COMPRESSIVE)	(B) IN THE TRANSVERSE PLANE SUBSURFACE (COMPRESSIVE)	(C) AXIAL (COMPRESSIVE)	(D) IN THE TRANS-VERSE PLANE (TENSILE)	(E) AXIAL (TENSILE)
1. Heavy Traffic 83 MGT	-142.7	-49.0	-91.0	41.0	17.3
2. Heavy Traffic* 270 MGT	-100.7	-66.5	-63.8	64.3	22.0
5. General Traffic 100 MGT	- 59.2	-34.3	-39.7	35.9	18.9
6. General Traffic 300 MGT	- 40.2	-59.8	-31.6	41.3	18.4

*The stresses shown are the maximums from either of two locations where measurements were made.

4. DISCUSSION

4.1 DEVELOPMENT OF THE TEST MATRIX

The primary objective of task 2 was to develop, analyze, and report data on three-dimensional residual stresses in rails in order that the likely state of residual stress in a rail can be readily determined for use in analyses. One of the major aspects of the above objective is the consistency of the residual stress pattern in a rail with continued cycles of loading. Does the rail approach a "shakedown" condition? The test matrix, shown in Figure 1, was developed with the above objective and the practical limitations of specimen collection and measurement in mind. This development is described below.

4.1.1 Excluded Parameters

From the outset it was obvious that it would be difficult to obtain rail specimens in which specific combinations of parameters were present or in which the actual affecting parameters were well known. In addition, the accurate measurement of three-dimensional stresses in rail is an expensive and time-consuming task. This placed practical limits on the number of measurements that could be made. And finally, some parameters that are likely to affect residual stress formation may not be realistic in terms of the existing or near-term spectrum of rail service. In view of the above considerations, it was necessary to judiciously select the set of affecting parameters to be examined experimentally.

By examining the literature and discussing the problem with experienced railroad personnel, a list of possible contributing factors, shown in Table 2, was developed. These factors, in effect, make up the rail service environment. All of the factors shown can affect the residual stress formation. An attempt was made to select the most significant parameters from this list; those selected are shown in Table 3.

TABLE 2. PARAMETERS AFFECTING RESIDUAL STRESSES IN RAIL

<u>Initial Rail Conditions</u>
- Size
- Physical Description (yield, hardness, composition, etc.)
- Manufacture/Mill

<u>Traffic</u>
- Type
- Speed
- Density

<u>Time in Service</u>
- Tonnage
- Wear

<u>Construction/Maintenance</u>
- Class
- Subgrade/Ballast
- Type (bolted, welded)
- Tie Spacing
- Installation Temperatures

<u>Territory</u>
- Tangent
- Curved
- Length of Grade
- Freeze/Thaw Cycles

<u>Flaws</u>
- Size
- Location
- Orientation

TABLE 3. INITIAL LIST OF IMPORTANT PARAMETERS

Rail Size
Rail Material/Manufacture
Type of Traffic
Curvature
Grade

The reasons for excluding some of the factors listed in Table 2 are as follows:

4.1.1.1 Thermal - A well designed, installed, and maintained rail should not experience plastic strain due to thermal cycles alone. It is difficult to say what the combined effects of thermal and operational loads are on residual stress formation. In the subject study, it has been assumed that the thermal contribution is minimal.

4.1.1.2 Flaws - Flaw free rails were used for the residual stress measurements so that the magnitude and distribution of the residual stresses could not be affected by the presence of flaws.

4.1.1.3 Wear - Wear rates are not necessarily a direct function of tonnage. However, the differences may not affect the residual stress pattern significantly. It has been assumed that if wear affects the shakedown question, it will be manifested in the tonnage parameter.

4.1.1.4 Construction/Maintenance - Analyses (under DOT/TSC-1038) of normal operating stresses (other than contact stresses) in a normally supported rail have shown that these stresses should not contribute directly to the residual stress formation. This is not true in the joint region, but the program emphasis has been placed on analysis of the midrail (continuous) region. [See reference 2.]

4.1.1.5 Traffic Speed - Recently collected data under DOT/TSC-1051 have shown that the loads that a rail sees are definitely a function of the train speed. It must be assumed that speed also affects the residual stress formation. A study of this variable was omitted on the grounds that obtaining specimens with all other parameters equal but at two distinct levels of traffic speed would be difficult. The more likely situation is that the speed is constant (the FAST specimens are all at 45 mph) or extremely varied. In any event, some documentation or estimation of the constant speed or speed range has been annotated to the measurements that were made. [See reference 5.]

4.1.1.6 Traffic Density - It is known (DOT/TSC-1044) that traffic density can affect the life of a rail. Though it is not clear what the mechanism would be, it is likely that residual stress formation would also be affected. The test matrix (Figure 1) includes density after a fashion. The heavy traffic specimens (FAST) also reflect heavy density. The general traffic specimens are of lower density but do not represent low density. [See reference 6.]

4.1.1.7 Manufacture/Mill - It has been assumed that there will be little difference in the residual stress formation in rail from one mill versus another, particularly for standard strength rail. However, the baseline "new" rail data are needed and may be a subject for future work. Two of the specimens US Steel is examining are new rail. (4)

The parameters shown in Table 3 were discussed with technical investigators of the Transportation Systems Center (TSC). The reasoning behind the further deletions that resulted in the text matrix (Figure 1) is outlined below.

4.1.1.8 Size - It is likely that the mechanisms of residual stress formation do not change greatly with rail sizes, provided that these rail sizes are within a reasonable range. Therefore, no effort was made to control the size variable; however, 132-pound rail was preferred since this size predominates now and probably will be used in the future.

4.1.1.9 Grade - For the vast majority of track, it is likely that there is little grade effect. The effect that the grade parameter may have on residual stress formation (if any) is entirely dependent on train handling. For the specimens in the test matrix the grade was minimal.

4.1.1.10 Metallurgy - High strength rail may well have a significant effect on the residual stresses that are formed in a rail. There is, however, little high strength rail in use.

4.1.2 Test Matrix

The parameters that were selected for inclusion in the test matrix of Figure 1 are tonnage, traffic, and curvature.

4.1.2.1 Tonnage - The question of shakedown can only be answered by examining the residual stress pattern at different levels of track usage. The range of 60 to 150 MGT tonnage for the first level was chosen on the basis of indications in the literature that shakedown may have occurred by 40 MGT. The second level of tonnage to be investigated was set at from 200 to 300 MGT, which was considered to be sufficiently advanced beyond the first level to show differences in residual stress patterns, if they exist. The first two specimens of tangent track that saw the heavy traffic of FAST were pulled from service after 83 and 270 MGT, respectively. The general traffic specimens were collected at either 100 or 300 MGT.

4.1.2.2 Traffic - The extremes of traffic type, heavy and light, were chosen to provide the maximum potential for detecting the effects of this parameter. The heavy traffic specimens all came from FAST where the traffic density is heavy. Light traffic specimens could not be readily located in the industry, so general traffic specimens were collected and used.

4.1.2.3 Curvature - Three levels of curvature are recognized as being significant in terms of rail loading. These are:

a. tangent track,
b. low curvature, where considerable lateral shear forces are in play but the flange does not come in contact on the gage side, and
c. high curvature, where the flange is in contact.

The transition between low and high curvature is not well defined, since it depends on several track parameters, but it is generally thought to be between 1 and 2 degrees of curvature. While it would have been desirable to examine a low-curvature specimen, it is not possible to obtain specimens of this type from FAST. The only place that this curvature exists at FAST is on spiral track where the loads tend to vary in an unpredictable manner. Only the two extremes of curvature, tangent and 5 degrees, were to be examined. The additional question of whether lubricated rail is to be used or avoided was not resolved. This may be a moot question since this practice has not been consistent on the FAST track.

4.1.2.4 Statistics - As cautioned above in Section 3, Major Conclusions and Results, four specimens constitute rather slim evidence from which to draw generalizations. Accordingly, the conclusions are limited to the observations that the general residual stress patterns in all four specimens are similar, and that it should not be assumed that the shakedown phenomenon exists.

4.2 BATTELLE SLICING TECHNIQUE FOR THREE-DIMENSIONAL RESIDUAL STRESS DETERMINATION IN RAIL

The Battelle slicing technique for determining the three-dimensional residual stress field in a rail consists of modifying and combining what is commonly known as the Yasojima and Machii technique with the Kalakoutsky or Meier technique. However, as is shown below, the Yasojima and Machii technique is very much modified by taking both a much thinner slice than is normally done and by subslicing (dicing) the slice. The Meier technique, as applied, is essentially unaltered. The following development shows that the first x-y slice (see Section 4.2.1, Mechanical Procedure), by relieving the z stress, causes the strains at each point in the slice (ε_x and ε_y in the x-y plane) to be incremented by a function of the original z stresses on the face. The subsequent dicing of the x-y slice permits determination of the incremented strains (ε_x' and ε_y'). Further, the Meier technique provides the original z-axis strain, ε_z. Combining ε_x' and ε_y' and ε_z (by the techniques described in Section 4.2.2, Analytical Procedure) permits the original strains ε_x and ε_y (those in the presliced condition) to be determined. Finally, from the original strains (ε_x, ε_y, and ε_z) the residual stress field (σ_x, σ_y and σ_z) is determined point by point. These can then be transformed to the principal stresses σ_1, σ_2, and σ_3, point by point.

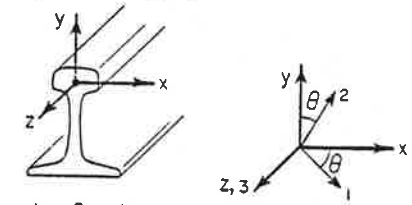

Geometric Coordinate System

Relation Between Geometric and Principal Axes

Much work went into the development of both the experimental and the analytical procedures used in the Battelle slicing technique. This evaluation/calibration work and results are detailed in Appendix A.

4.2.1 Mechanical Procedure

The mechanics of supplying this technique are now described as they were applied to specimen 1. Initially, a section of rail L inches in length is considered within which it is desired that the full three-dimensional residual stress field be determined. (See Figure 5.) For clarity, the steps of Battelle's slicing technique are listed below. The slicing of the rail (modified Yasojima and Machii technique) and the cutting of it into thin rods (Meier technique) are described separately even though some of the steps are similar and are done at the same time.

This technique involves cutting two slices, as shown in Figure 5, called the Yasojima-Machii slice and the Meier section. From the Yasojima-Machii slice, the strains ε_z and ε_t (ε_t is the tangential strain) on the periphery are determined along with the incremental strains ε_x' and ε_y' and γ_{xy} on the face of the slice. The Meier section provides the z-axis strain, ε_z', corresponding point by point to the ε_x' and ε_y' strains determined from the Yasojima-Machii slice. These are then combined in a manner, detailed later in this report, to produce the three-dimensional stress field in the rail.

4.2.1.1 Modified Yasojima and Machii Technique

Step 1. The rail is laid out for the initial x-y slicing. For the modified Yasojima-Michii technique, a thin x-y slice on the order of t = 0.160 inch is required.

Step 2. The strain gages are applied prior to slicing in order to measure the released strains/deformations on the periphery of the rail from slicing. Biaxial strain gages (Micromeasurements EA-06-S1224-120) oriented in the z and in the tangential direction are applied around the periphery of what is to be the Yasojima-Machii slice; see Figure 6. The number or frequency of gage locations depends on the fineness desired for inferring surface strains. Forty-three peripheral gages were used on specimen 1.

Step 3. The Yasojima-Machii x-y slice of the rail is cut using a new bandsaw blade with slow feed and air coolant.

Step 4. Strain gages on the periphery of the slice are read and recorded. The maximum strain change registered in the peripheral gages on specimen 1 due to the slab cut was 2630 x 10^{-6} inch/inch. This value was in the longitudinal direction near the edge of the wear lip on the gage side of the rail.

Dimensions (inches) on Specimen No. 1

L = 48
ℓ = 24-1/32
$\ell_{1,2...}$ = 23.94
t = 0.160
h = 7-1/4
w = 2-7/8

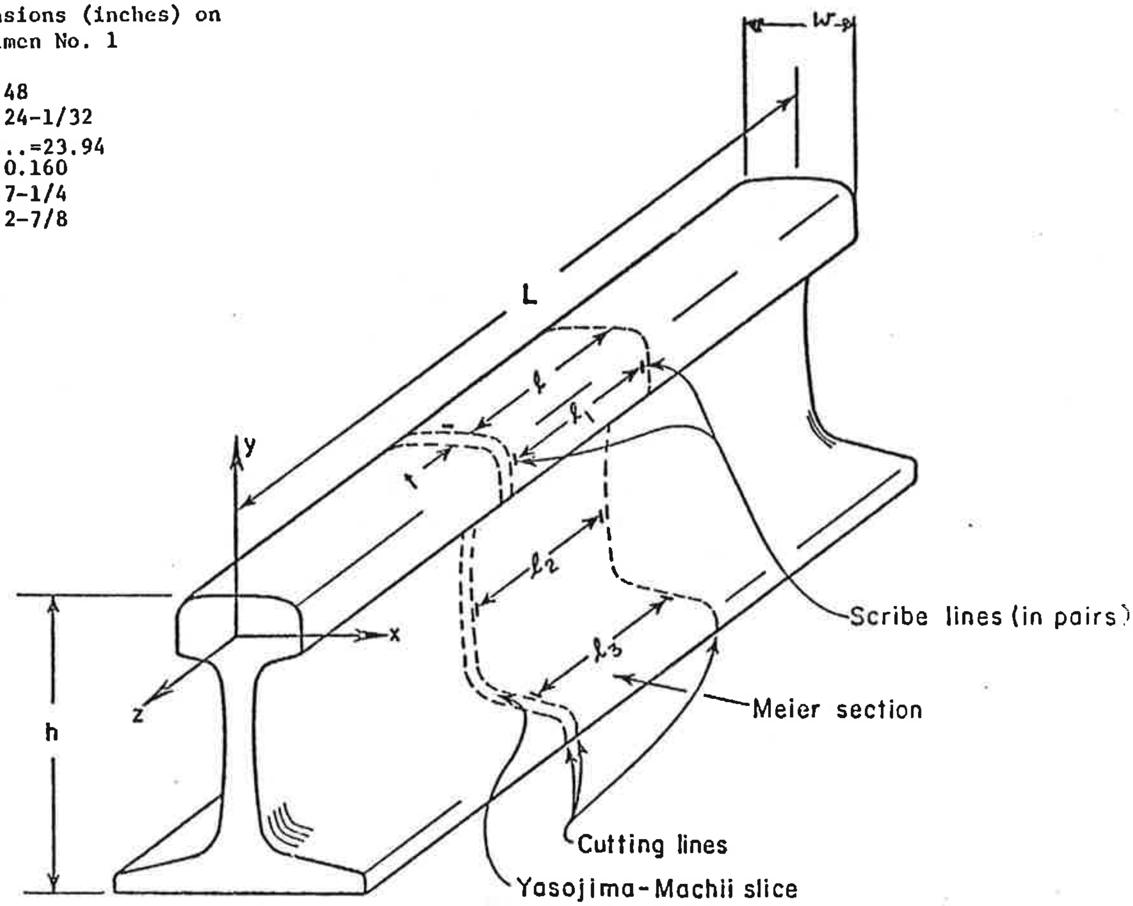

FIGURE 5. INITIAL SECTIONING OF RAIL

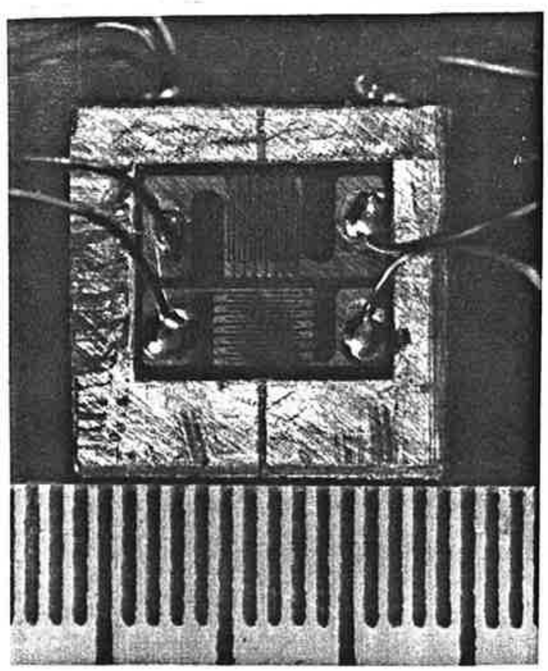

FIGURE 6. DETAIL OF BIAXIAL PERIPHERAL GAGE ON YASOJIMA-MACHII SLICE (SHOWN AFTER DICING)

Step 5. One face of the Yasojima-Machii x-y slice is hand sanded with emery cloth to smooth the surface for strain gaging. Then this surface is laid out and instrumented for dicing. This slice is laid out in the same size pattern as for the Meier section. (See step D below.) Then at the center of each x-y area, a three-gage strain rosette (Micromeasurements EA-06-015-RJ-120) is placed with a given orientation to the x-y coordinate system; see Figures 7 and 8. (The biaxial gages on the periphery of this slice were placed there in step 2 above.)

Step 6. The rosette gages are all zeroed and then the slice is diced into cubes 0.160 inch on a side, each containing a peripheral gage and/or a rosette gage; see Figure 9. A bandsaw with slow feed and air coolant is used in this dicing. The change in strain as measured by the strain rosettes for each x-y area is determined. Also, on the periphery σ_z and σ_t (σ_t is the tangential stress perpendicular to the z axis) are determined directly.

4.2.1.2 Meier Technique

Step A. The rail is laid out for the initial x-y slicing. For the Meier technique, a section approximately three to four times as long as the height of the rail is required (longer lengths are better). However, it is necessary to stay away from the ends of the specimen -- perhaps 1 to 1.5h from each end. Consequently, the above length, ℓ, is a tradeoff (depending on L) between eliminating end effects and improving measurement accuracy over the length ℓ. The longer ℓ is, the greater the accuracy of measuring $\Delta\ell$ and thus calculating $\varepsilon_z = \Delta\ell/\ell$. Therefore, a minimum specimen length is defined as

$$3h + 2h < L_{min} < 4h + 2(1.5h)$$

or

$$5h < L_{min} < 7h \quad .$$

In the case of specimen 1:

$$36.25 < L = 48 \text{ inches} < 50.75 \; .$$

$$3h = 21.75$$

$$21\text{-}3/4 < \ell = 24 \text{ inches for specimen number 1.}$$

To facilitate the slow bandsaw cutting operation, specimens having a Meier length ℓ of 18 inches are used. This is justified because of the fact that the end effects to be avoided tend to be localized in the various major portions of the rail cross section (base, web, and head). The use of h as the fundamental dimension is, therefore, conservative. The portion of the rail of greatest concern is the head. Its fundamental dimension is its width, w = 2-7/8 inches.

$$3w = 8\text{-}5/8 < \ell = 18 \text{ inches} \; .$$

The extent of the end effect was checked on one specimen, and the results readily supported the use of an 18-inch specimen length. This check is described in Appendix A.

Step B. Scribe marks are applied prior to slicing to measure the released strains/deformations from slicing. Parallel scribe marks are placed inside the slice lines for the Meier slice. Measurements of the change in length between these lines on slicing and grinding (see step D below), divided by the original length, give an indication of the z-axis strain change caused by slicing, e.g., $\varepsilon_z \sim\Delta\ell_1/\ell$, etc. For specimen 1, these strains range from -41 to 76 x 10^{-6} inch/inch.

Step C. The Meier section of the rail is cut using a new bandsaw blade with slow feed and air coolant.

Step D. The ends of the Meier slice are ground flat and parallel. A grid work is laid out for subslicing the rail into longitudinal rods denoted by (x_1, y_1), (x_3, y_3), etc.; see Figure 10. These should correspond to the (x_1, y_1), (x_2, y_2),

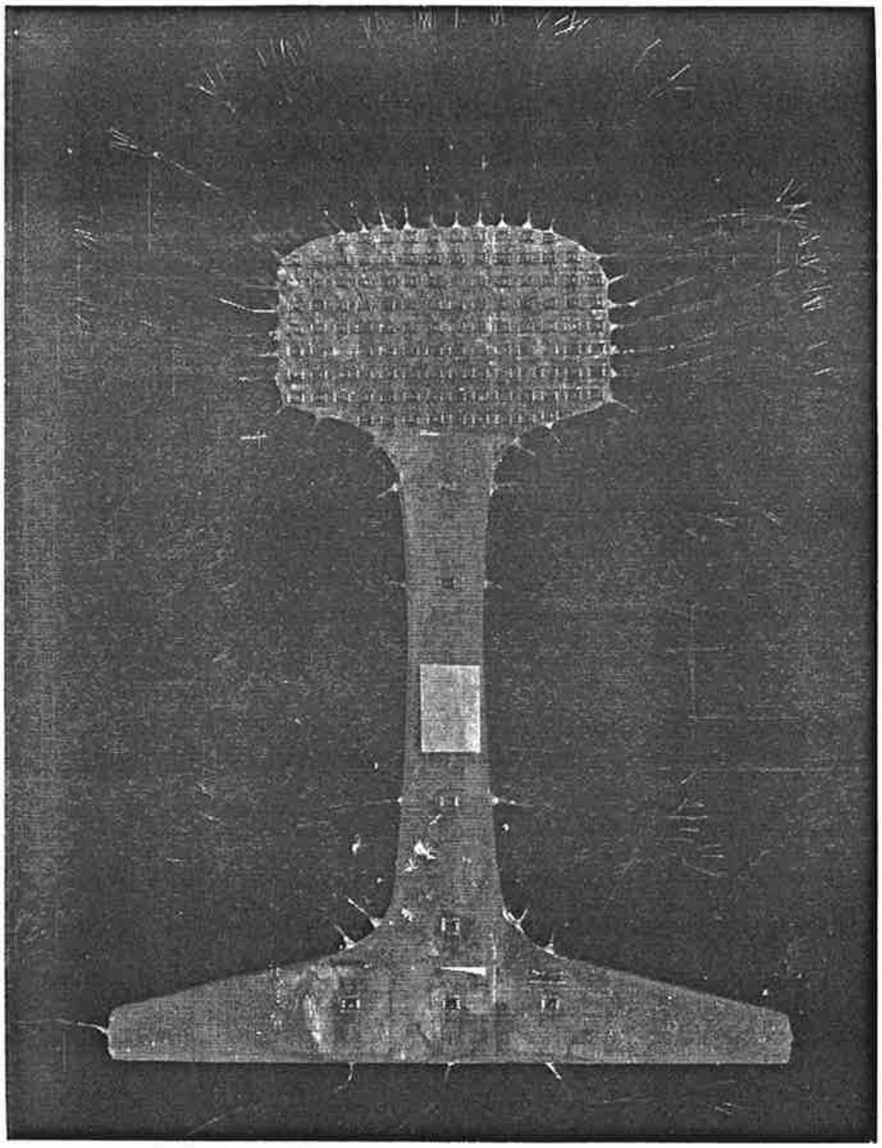

FIGURE 7. FULL ARRAY OF GAGES ON YASOJIMA-MACHII SLICE FROM SPECIMEN 1

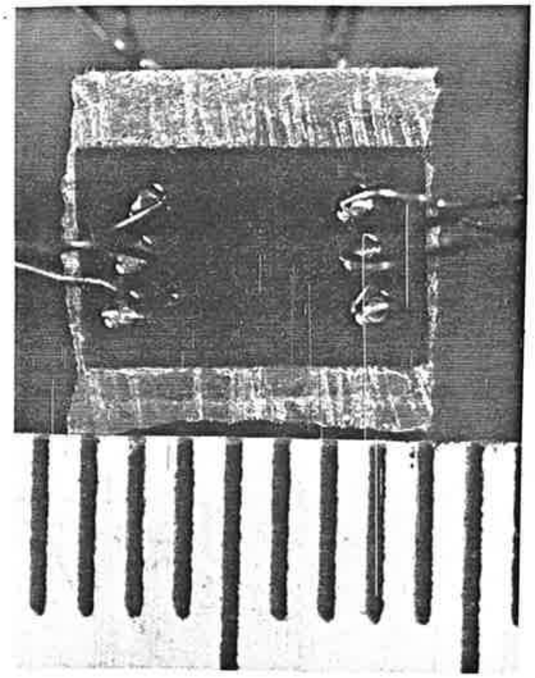

FIGURE 8. DETAIL OF ROSETTE GAGE ON FACE OF YASOJIMA-MACHII SLICE (SHOWN AFTER DICING)

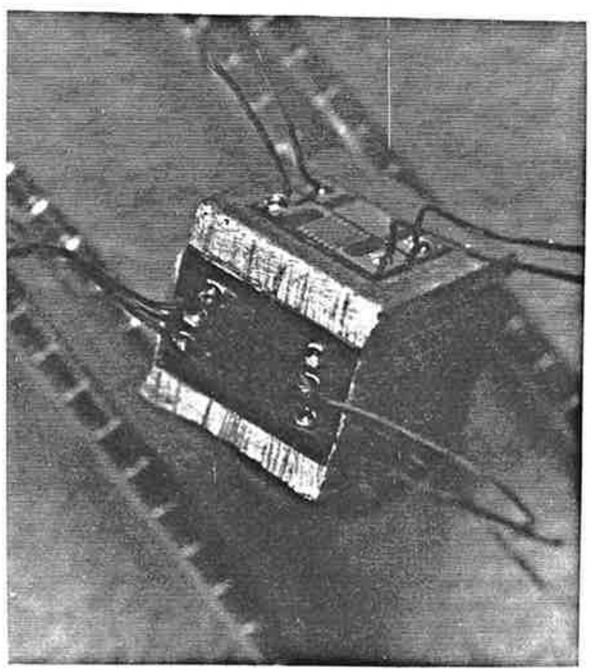

FIGURE 9. GAGED CUBE DICED FROM YASOJIMA-MACHII SLICE

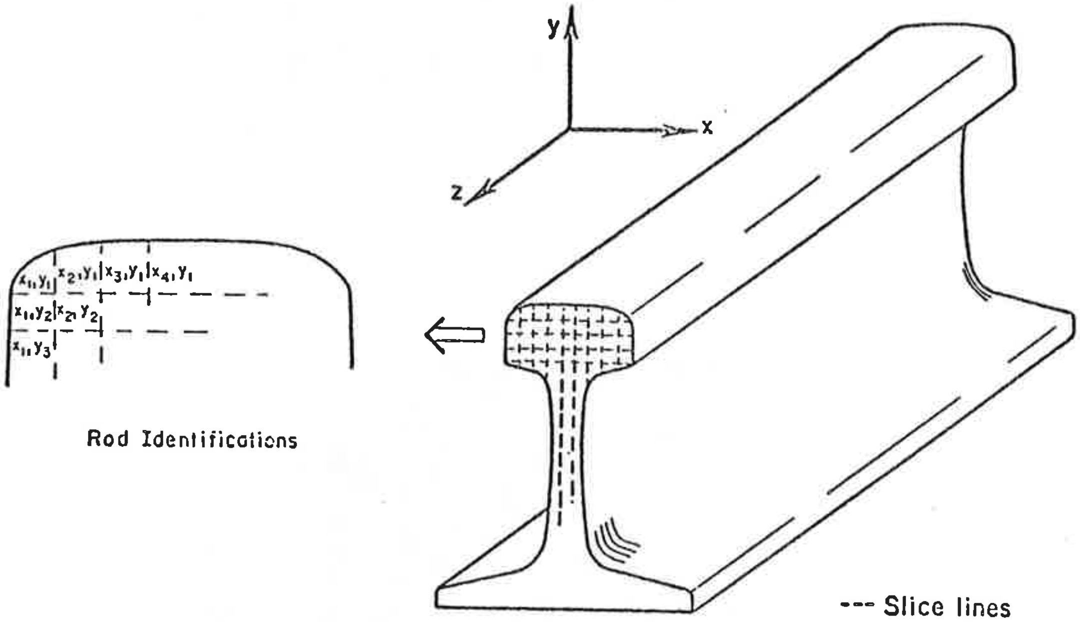

FIGURE 10. LAYOUT OF MEIER SLICE FOR SUBSLICING

(y_3, y_3) grid on the Yasojima-Machii slice. (See step 5 above.) For each rod position, the lengths, e.g., ℓ_{11}, ℓ_{12}, ℓ_{13}, etc., are measured if different from ℓ (these are not different if the ends are flat and parallel). See Figure 11.

Step E. The overall change in length at each pair of scribe marks is measured and recorded; see step B (above) and Figure 12.

Step F. The indicated cuts are made using new saw blades with slow feed and air coolant. (See Figures 13, 14, and 15.) The rod ends are deburred if necessary. The change in length for each x-y rod is determined (see Figure 16), and the z-axis strain calcualted by

$$[\varepsilon_z]_{ij} = \frac{\ell_{ij}-\ell}{\ell} \qquad i,j = 1,2,...$$

Finally, after these two sets of steps have been completed, the strains ε_x', ε_y', and γ_{xy} are known from the dicing of the Yasojima-Machii slice, and ε_z is known from the Meier section point by point (at the selected points) in the rail. Also, σ_z and σ_t are known on the periphery of the rail at selected points. Then, using the method described in the following section on analytical procedure, the residual stress field, i.e., σ_x, σ_y, σ_z, and τ_{xy}, in and on the rail can be determined. From the strains ε_x, ε_y, and γ_{xy}, the principal stress direction θ can be determined,

where

$$\theta = 0.5\tan^{-1}\frac{\gamma_{xy}}{\varepsilon_x-\varepsilon_y} .$$

Should they be desired, the principal stresses σ_1, σ_2, and σ_3 at these points can also be determined.

4.2.2 Analytical Procedure

The analytical procedure must take the various sectioning strains as measured in the mechanical procedure and combine them in a proper sequence of calculations so that the unrelaxed residual strain state (and thereby the residual stress state) that existed in the rail specimen before sectioning is determined. The calculations to do this rely on the following three assumptions:

a. The residual stresses σ_x, σ_y, σ_z, and τ_{xy} and principal residual stresses σ_1, σ_2, and σ_3 are not a function of z; therefore, the direction of the principal stress, σ_3, is parallel to the z axis. Thus $\sigma_z = \sigma_3$, and $\tau_{xz} = 0$.

b. The stresses or strains that originally exist in the rail are not increased during slicing so as to move them into the plastic range. In addition, the unloading stress/strain, σ and ε, curve is the tangent modulus line, i.e., $\varepsilon = \sigma/E$ for a uniaxial stress state.

c. The material everywhere is homogeneous, linear elastic, and orthotropic. In the calculations for specimen 1 the material properties are assumed to be isotropic (with a Young's modulus of $E = 28.9 \times 10^6$ psi, and a Poisson's ratio of $\nu = 0.3$).

Based on the third assumption, the principal residual stresses in the rail are given by: (For simplicity, the isotropic constitutive equations are presented; however, the method is equally well suited for orthotropic materials.)

$$\sigma_x = \frac{E}{(1+\nu)(1-2\nu)}\left[(1-\nu)\varepsilon_x + \nu(\varepsilon_y+\varepsilon_z)\right]$$

$$\sigma_y = \frac{E}{(1+\nu)(1-2\nu)}\left[(1-\nu)\varepsilon_y + \nu(\varepsilon_x+\varepsilon_z)\right]$$

$$\sigma_z = \frac{E}{(1+\nu)(1-2\nu)}\left[(1-\nu)\varepsilon_z + \nu(\varepsilon_x+\varepsilon_y)\right]$$

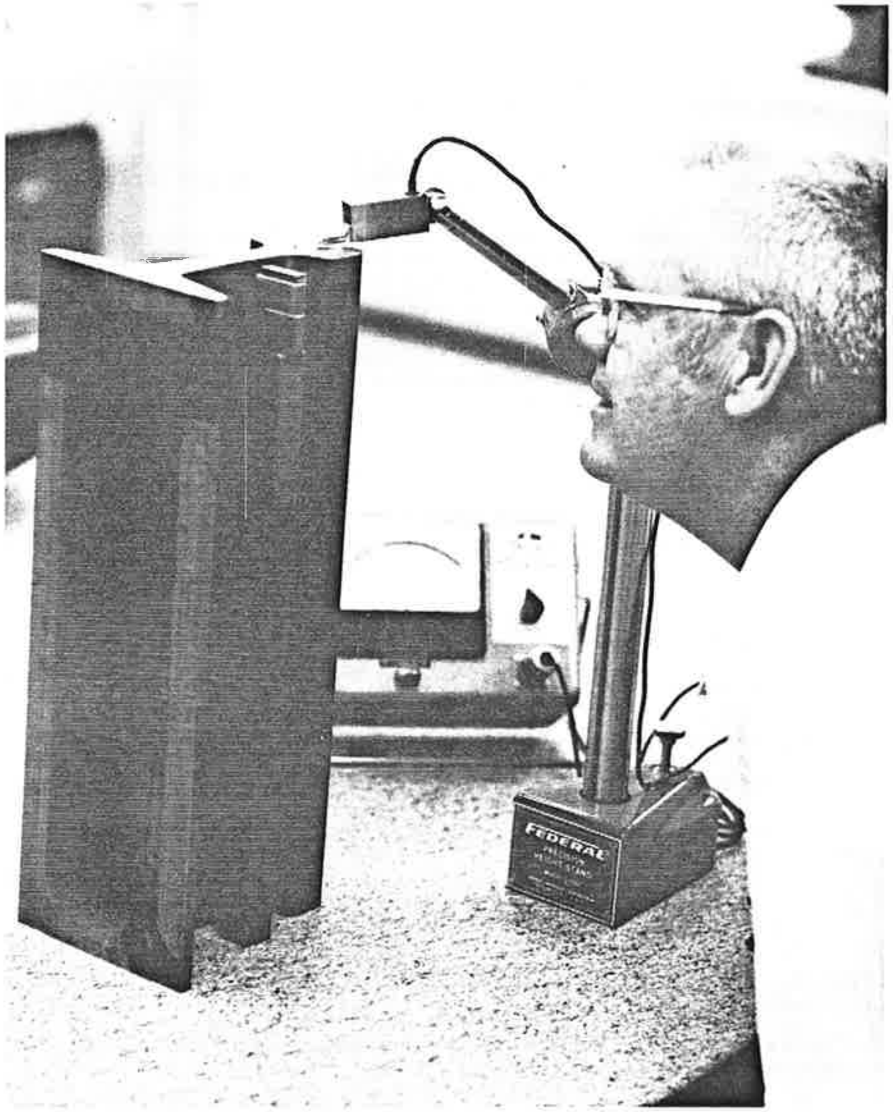

FIGURE 11. MEASURING LENGTH OF MEIER SECTION BEFORE SAWING OF RODS

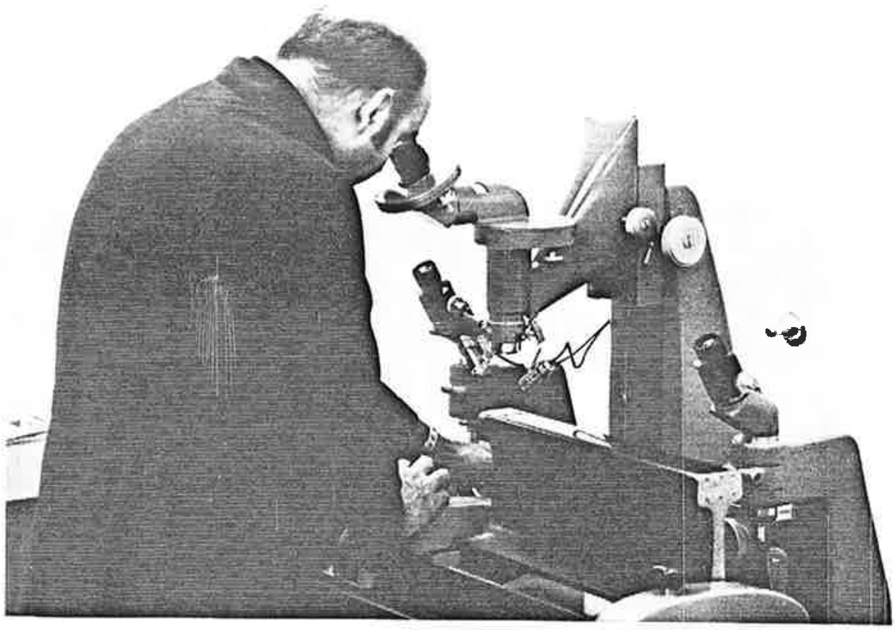

FIGURE 12. MEASURING CHANGES IN LENGTH DUE TO SLICING AND GRINDING MEIER SECTION

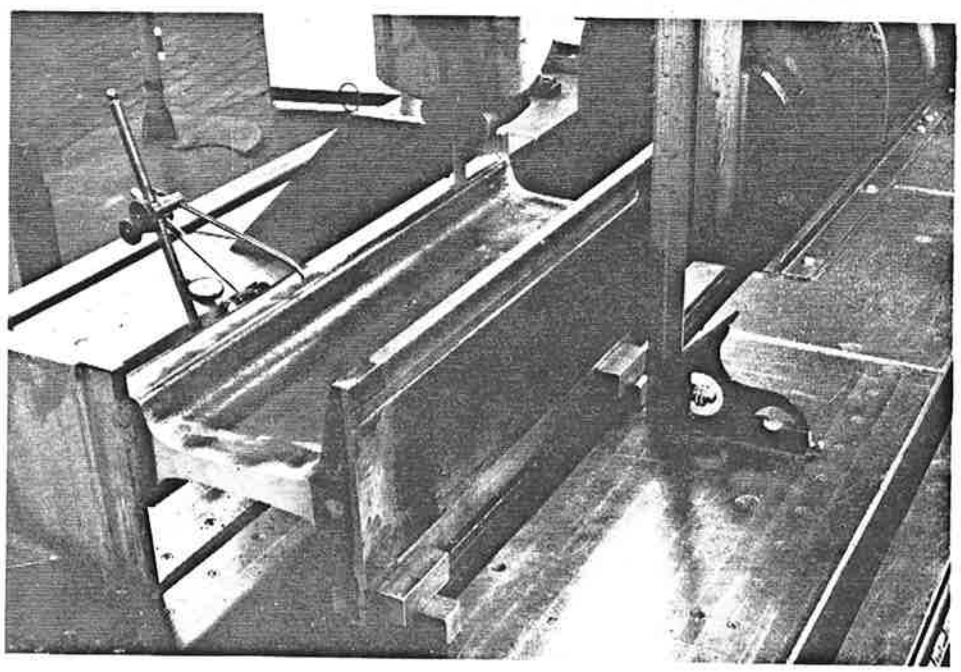

FIGURE 13. INITIAL RAIL HEAD REMOVAL AS PART OF MEIER ROD SLICING

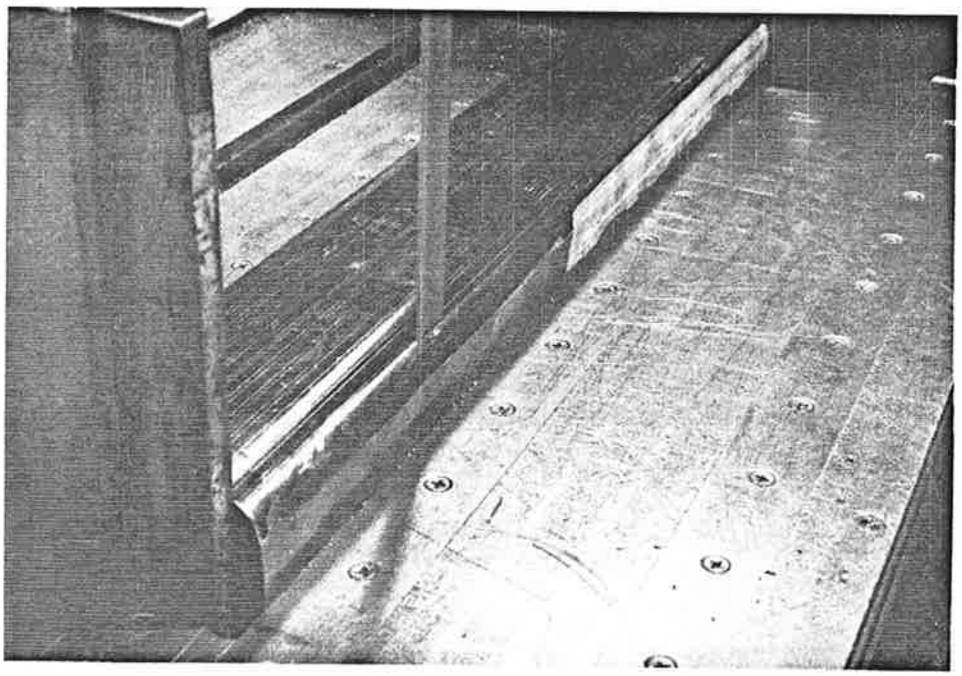

FIGURE 14. FURTHER CUTTING OF RAIL HEAD TO OBTAIN MEIER RODS

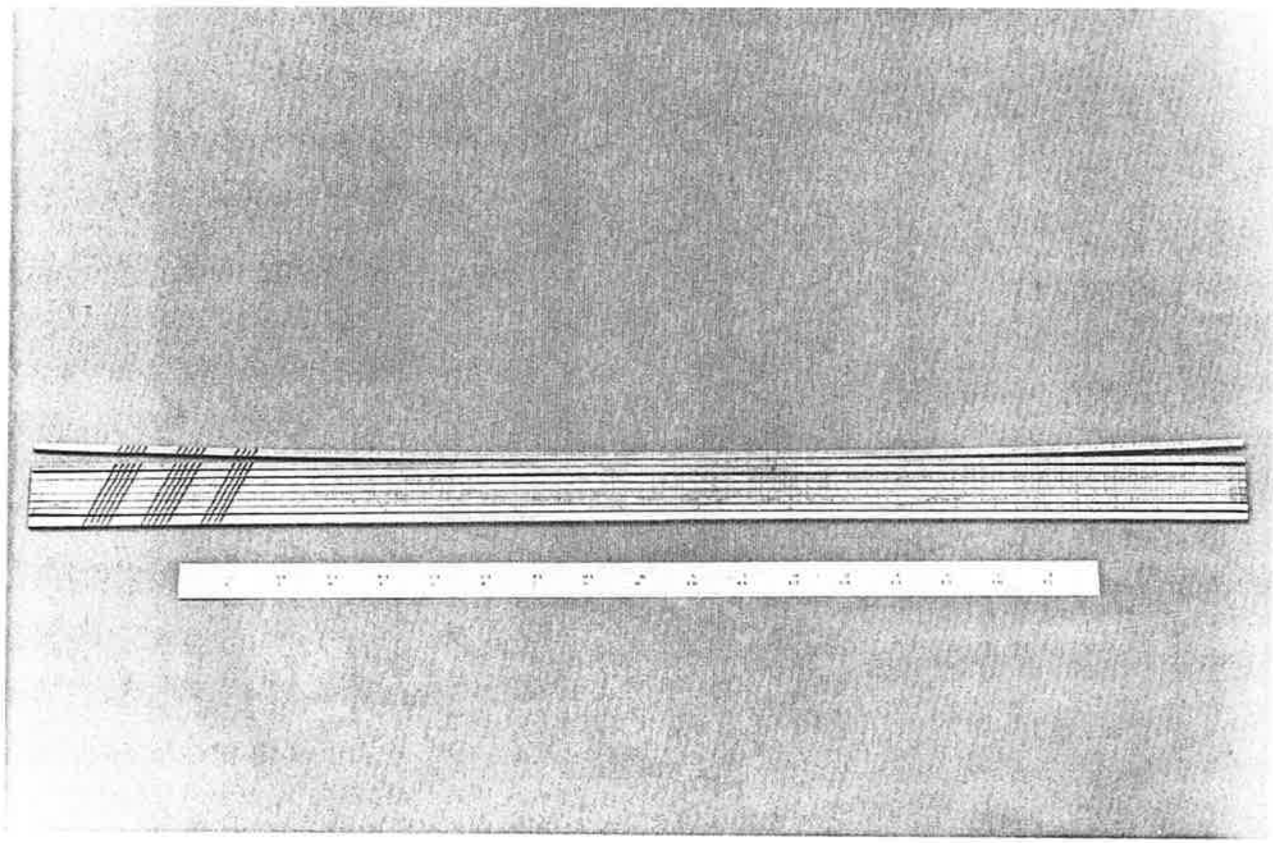

FIGURE 15. RODS FROM ONE VERTICAL SLICE OF RAIL HEAD

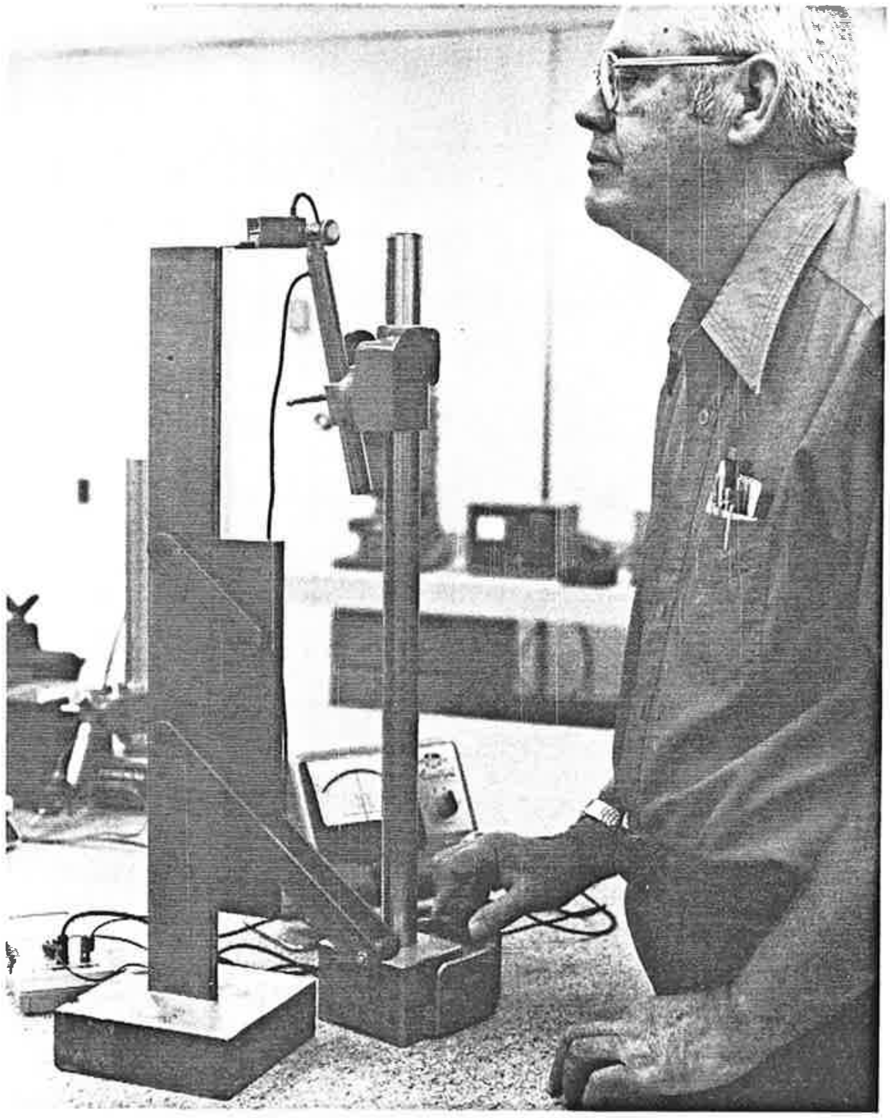

FIGURE 16. MEASUREMENT OF FINAL MEIER ROD LENGTH IN HOLDING FIXTURE

where σ_x, σ_y, and σ_z are the residual stresses and ε_x, ε_y, and ε_z are the residual strains. Likewise, the actual strains in the rail expressed in terms of the stresses are given by:

$$\varepsilon_x = \frac{1}{E}\left[\sigma_x - \nu(\sigma_y+\sigma_z)\right]$$

$$\varepsilon_y = \frac{1}{E}\left[\sigma_y - \nu(\sigma_x+\sigma_z)\right] \qquad (2)$$

$$\varepsilon_z = \frac{1}{E}\left[\sigma_z - \nu(\sigma_x+\sigma_y)\right]$$

Two methods of analyzing the strain data have been developed, a complex but accurate analysis and a simplified approximate analysis. The approximate analysis technique was selected for the reduction of the data from all specimens. The reasoning behind this choice is discussed below. Calculations that were run to develop the accurate analysis technique and calculations that were run to compare the two techniques (using data from specimen 1) are described in Appendix A. Since an understanding of the accurate analysis helps in understanding the assumptions employed in the approximate analysis, both techniques are described below.

4.2.2.1 Accurate Analysis - The original strains at all points on a cross section of the rail that are eventually to become the face of the Yasojima-Machii slice are the sets:

$$\varepsilon_x,\ \varepsilon_y,\ \text{and}\ \varepsilon_z.$$

When the Yasojima-Machii slice is removed, the sets of strains become:

$$\varepsilon_x',\ \varepsilon_y',\ \text{and}\ \varepsilon_z'.$$

When the Yasojima-Machii slice, with the rosette strain gages attached, is modified by dicing around each gage, the strain sets ε_x' and ε_y' are measured, since these are the strains that are relieved by the dicing. The sets of stress components in the x-y plane that are relieved by this dicing are:

$$\sigma_x' = \frac{E}{1-\nu^2}(\varepsilon_x' + \nu\varepsilon_y')$$

$$\sigma_y' = \frac{E}{1-\nu^2}(\varepsilon_y' + \nu\varepsilon_x'). \qquad (3)$$

The stress components in the z direction throughout the dicing are $\sigma_z' = 0$ by virtue of the fact that cutting the Yasojima-Machii slice relieves all longitudinal stresses on the face of the slice. However, the set of strains in the longitudinal direction that are relieved by the dicing can be calculated by:

$$\varepsilon_z' = \frac{-\nu}{E}(\sigma_x' + \sigma_y') \qquad (4)$$

We now introduce the Meier sectioning which, through the cutting out of the longitudinal rods, provides a direct measure of the original longitudinal strain set ε_z. By combining these measured strains with the results of calculation (4), the set of longitudinal strain changes, $\Delta\varepsilon_z$, that occur when the Yasojima-Machii slice is made can be determined by:

$$\Delta\varepsilon_z = \varepsilon_z' - \varepsilon_z \qquad (5)$$

By taking this set of strains and applying them to a finite element model of the Yasojima-Machii cross section, the sets of x-y strain changes, $\Delta\varepsilon_x$ and $\Delta\varepsilon_y$, that occur during the slicing operation can be computed.

The original x-y strain sets are then directly calculated by

$$\varepsilon_x = \varepsilon_x' - \Delta\varepsilon_x$$

and

$$\varepsilon_y = \varepsilon_y' - \Delta\varepsilon_y \quad . \tag{6}$$

The stresses are then calculated by applying the strain sets to Equation (1).

4.2.2.2 Approximate Analysis - The above analysis requires the use of a finite element model to determine the x-y strain changes during the slicing out of the Yasojima-Machii slab section. The analysis described below, by adopting an additional assumption, allows the direct point-by-point calculation of stress from the measured strains of the mechanical procedure.

On the rail in question, let us apply a stress on the rail cross section, x-y plane, everywhere equal but opposite to the set of stresses σ_z. In doing this, the ε_x and ε_y sets of strains of Equation (2) become incremented in the manner

$$\varepsilon_x' = \frac{1}{E}\left[\sigma_x - \nu(\sigma_y+\sigma_x)\right] + \frac{\nu}{E}\sigma_z$$

$$\varepsilon_y' = \frac{1}{E}\left[\sigma_y - \nu(\sigma_x+\sigma_z)\right] + \frac{\nu}{E}\sigma_z . \tag{7}$$

Thus the sets of strains ε_x and ε_y everywhere in the x-y plane are incremented by the set $\frac{\nu}{E}\sigma_z$.

Due to the absence of the τ_{xz} and τ_{yz}, the set of stresses σ_z must be self-equilibrating and does not upset the equilibrium of stresses in the x-y plane. The particular distribution of σ_z stresses on the x-y plane affects the relative distributions of σ_x and σ_y, but overall equilibrium is not affected. If it is assumed that the relative distributions of σ_x and σ_y sets of stresses are not substantially changed by addition or removal of the σ_z set of stresses, it can be concluded that applying a σ_z opposite to the σ_z in the rail is the same as slicing the rail into a thin x-y section. Further, if the x-y section is subsliced, then the incremented strains ε_x' and ε_y' can be determined point by point in the x-y plane utilizing strain rosettes on the x-y surface. These incremented strains are by definition given as the original strains, ε_x and ε_y, plus the increment $\frac{\nu}{E}\sigma_z$ Equation (7), or

$$\varepsilon_x' = \varepsilon_x + \frac{\nu}{E}\sigma_z \text{ and } \varepsilon_y' = \varepsilon_y + \frac{\nu}{E}\sigma_z, \tag{8}$$

but from Equation (1)

$$\frac{\nu}{E}\sigma_z = \frac{\nu}{(1+\nu)(1-2\nu)}\left[(1-\nu)\varepsilon_z + \nu(\varepsilon_x+\varepsilon_y)\right] . \tag{9}$$

Therefore,

$$\varepsilon_x' = \varepsilon_x + \frac{\nu}{(1+\nu)(1-2\nu)}\left[(1-\nu)\varepsilon_z + \nu(\varepsilon_x+\varepsilon_y)\right] \tag{10}$$

and

$$\varepsilon_y' = \varepsilon_y + \frac{\nu}{(1+\nu)(1-2\nu)}\left[(1-\nu)\varepsilon_z + (\varepsilon_x+\varepsilon_y)\right] . \tag{11}$$

From the Meier technique the original z-axis strain, ε_z, is determined. (Also, $\varepsilon_3 = \varepsilon_z$.) Substituting this value in Equation (10) permits ε_x and ε_y, the original strains, to be determined since ε_x' and ε_y' were previously determined from the diced x-y slice. Knowing the original strains, ε_x, ε_y, and ε_z, point by point in the rail now permits, from Equation (1), the residual stresses σ_x, σ_y, and σ_z to be determined point by point. By placing 45-degree rosettes at each location, the residual shear strain γ_{xy} is also determined, yielding the residual shear stress.

It follows that the principal stresses σ_1, σ_2, and σ_3 can be derived from σ_x, σ_z, and τ_{xy} in the x-y-z system, realizing that $\sigma_3 = \sigma_z$, and that

$$\sigma_1 = \frac{\sigma_x + \sigma_y}{2} + \frac{\sigma_x - \sigma_y}{2} \cos 2\theta + \tau_{xy} \sin 2\theta \tag{12}$$

and

$$\sigma_2 = \frac{\sigma_x + \sigma_y}{2} - \frac{\sigma_x - \sigma_y}{2} \cos 2\theta - \tau_{xy} \sin 2\theta , \tag{13}$$

where

$$\theta = 0.5\tan^{-1} \left(\frac{2\tau_{xy}}{\sigma_x - \sigma_y} \right) .$$

4.2.2.3 Comparing the Two Procedures - The approximate analysis procedure described above has the distinct advantage of requiring only a closed form calculation of the stresses at any point, using the measured data for that point on the cross section. The accurate analysis procedure requires the generation and application of a finite element computer model of each rail section for which data are collected. Furthermore, the accuracy of the computer modeling is greatly dependent upon the number of points measured; the more points, the more accurate the model.

The possibility that the approximate technique provides reasonably accurate stress values was examined using the data from specimen 1. The stresses were calculated using both procedures and the results were compared. At points where the accurate analysis showed a maximum principal stress in excess of $\pm$ 10,000 psi, the approximate analysis matched the stress within $\pm$ 10 percent. This was true for the entire rail cross section except at the edge of the tread wear surface, particularly on the gage side. Here the steep compressive stress gradient caused a disagreement of 44 percent between the two methods. This is not viewed as a serious problem since even the "accurate" technique is suspect in this region due to the probable presence of plasticity in the measurement process and due to the coarseness of the finite element gridwork compared to the steep stress gradient.

4.2.3 Accuracy Checks

Other than comparison with independent data, there is only one check that can be applied to see if the analytical assumptions and experimental errors have combined to produce unreasonable results. This check is to see if the stress results provide force equilibrium conditions at various cross sections through the rail head. These checks were made using the extensive data from specimen 1. A typical horizontal section taken for this type of check is shown in Figure 17. Equilibrium of the "freed" portion of the head requires that a summation of each force component (normal, shear, and moment) over the cut cross section total up to zero.

Equilibrium was checked on 10 horizontal sections down through the head and on 9 vertical sections taken at either side of the web intersection with the head. Axial equilibrium can be determined only on the one transverse cross section. This was also done but only for the head, i.e., the low stresses in the web and base were not included in the equilibrium balance.

The check results showed reasonably close balances for equilibrium. When equilibrium was checked with cross section not immediately at the surface*, the force or moment imbalances would generally run from 1 to 18 percent of the absolute total of the absolute total of force (moment) components on the section. The horizontal forces and moments in the transverse plane were in particularly good balance. The vertical forces in the plane and the axial forces tended to be overly compressive.

*As discussed previously, the resolution of the technique is inadequate to define the sharply varying compressive stress gradients near the rail surface.

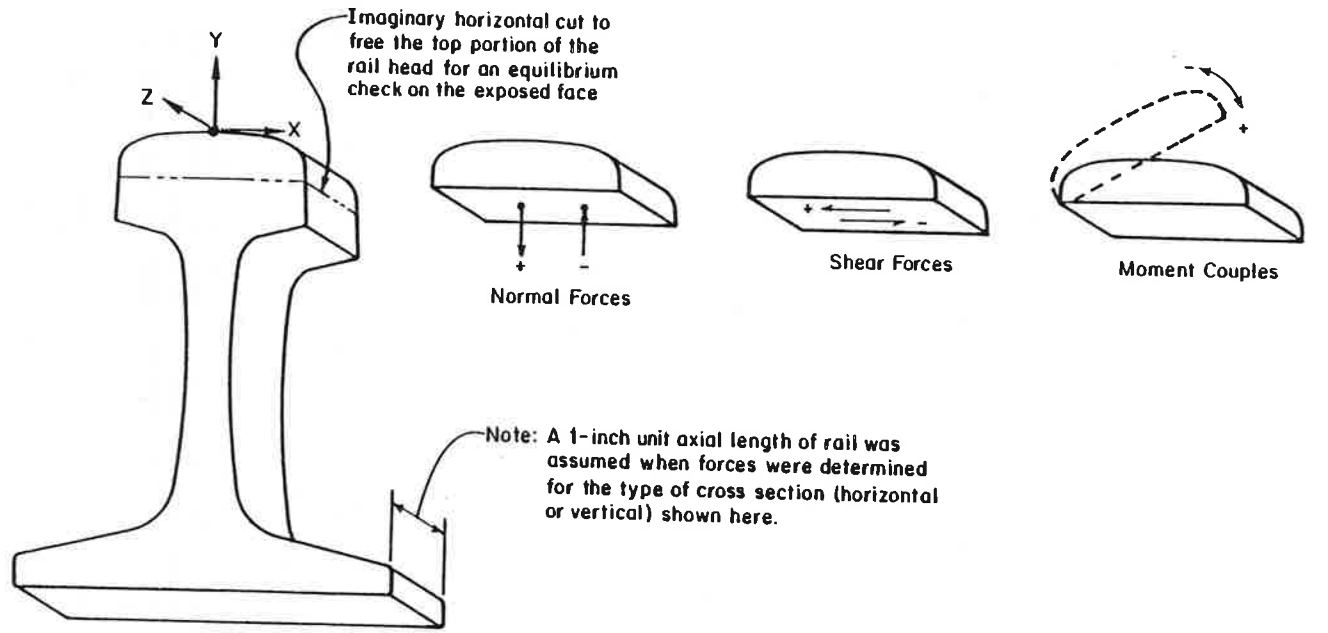

FIGURE 17. HORIZONTAL SECTION FOR EQUILIBRIUM CHECK

For example, the total normal (vertical) forces on a horizontal cross section generally ran about -24,000 pounds (compressive) versus only 17,000 pounds (tensile). Obviously the normal forces on the cross section are overly compressive; however, if the tensile forces were 17 percent higher and the compressive forces 17 percent lower, the forces would have balanced at -19,900 pounds (compressive) and +19,900 pounds (tensile). The error might be said to be 17 percent. The worst case occurred on the horizontal cut passing through the knot of compressive stress in the lower field-side portion of the head. Very little vertical tensile force, +3,000 pounds, was present here while a very high vertical compressive force, -47,500 pounds, was totalled for the section. This condition suggests that this knot of compressive stress is a local phenomenon and does not extend along the length of the rail; therefore, this knot may have been balanced by some longitudinal stress gradient at this point in the cross section.

The axial forces in the head were +20,500 pounds (tensile) and -29,500 pounds (compressive). This figures to an 18 percent error in each type of force, if they are reconciled in the above manner. Inclusion of the web and base axial stresses in this equilibrium balance may have justified the axial stresses in the head, but the low stresses were not measured with enough definition over the web and base regions to allow this to be done with accuracy.

4.3 RESIDUAL STRESSES IN TANGENT RAIL

The general characteristics of the residual stress patterns in the four tangent rail specimens examined in this program were described in Section 3, Major Conclusions and Results. The results from each specimen are presented here.

a. A vector plot of the principal stresses in the transverse plane of the rail cross section. This is the only way that the direction of these stresses can be realized. The number and distribution of the measurement points on each cross section are also clearly demonstrated by the vector set plots.

b. A contour plot of the maximum (tensile) principal stress distributions in the transverse plane. Though this plot does not show the orientations of the tensile stresses, it provides a ready visual display of regions and magnitudes of the tensile stresses in the transverse plane.

c. A contour plot of the minimum (compressive) principal stress distributions in the transverse plane. This plot displays the regions and magnitudes of the compressive stresses in the transverse plane.

d. A contour plot of the axial stresses over the head cross section of the rail specimen. Here the stress orientation is always directly out of (or into) the page on which the cross section and the contours are displayed.

The actual numerical values of the stresses determined at each point of measurement on each specimen are documented in Appendix B. The exact location of each measurement point on each cross section (including the web and base measurement points) is also documented in Appendix B.

4.3.1 Specimen 1, Stresses in Heavy Traffic Rail at 83 MGT

The results from specimen 1 were used in Section 3, Major Conclusions and Results, to demonstrate the general patterns of all four specimens. Significant details in the stress patterns of specimen 1 are described below.

In the principal stress vector plots of Figure 18, the largest residual stresses in the transverse plane are the compressive stresses at both edges of the wear pattern and at the knot of stress in the lower field side of the head. The tensile stresses in this plane run horizontally in a deep band across the middle of the head cross section and point diagonally up toward the edges of the wear pattern.

In Figure 19, the principal tensile stress contour plot shows the in-plane tensile stress to peak out at +41,000 psi where the tensile stresses point towards the field-side edge of the wear pattern.

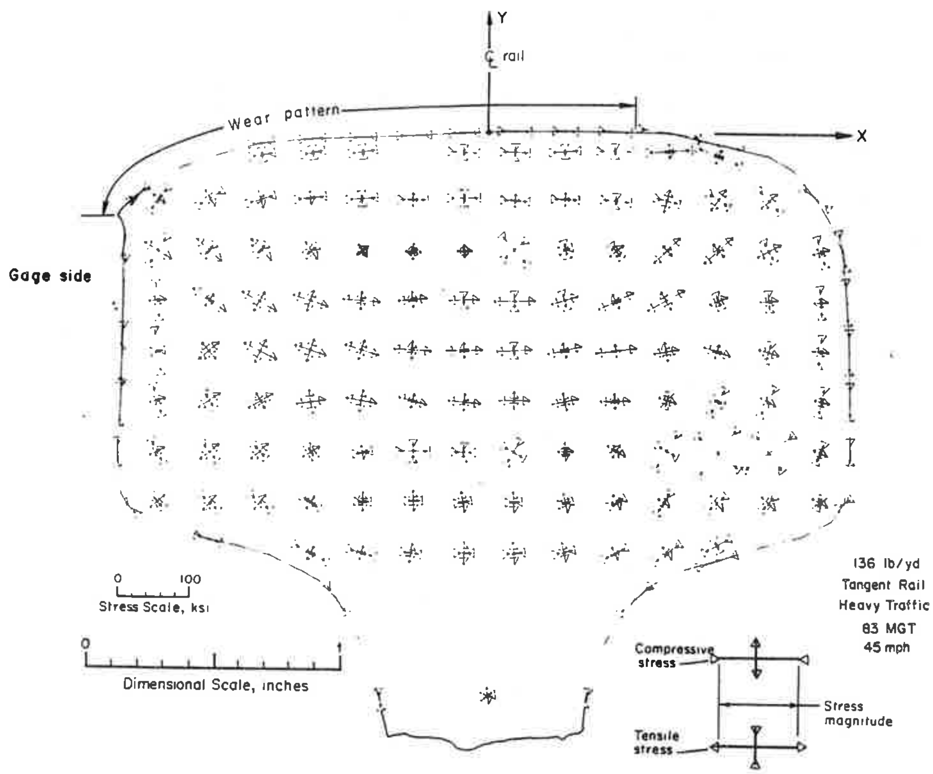

FIGURE 18. SPECIMEN 1, IN-PLANE PRINCIPAL STRESS VECTORS

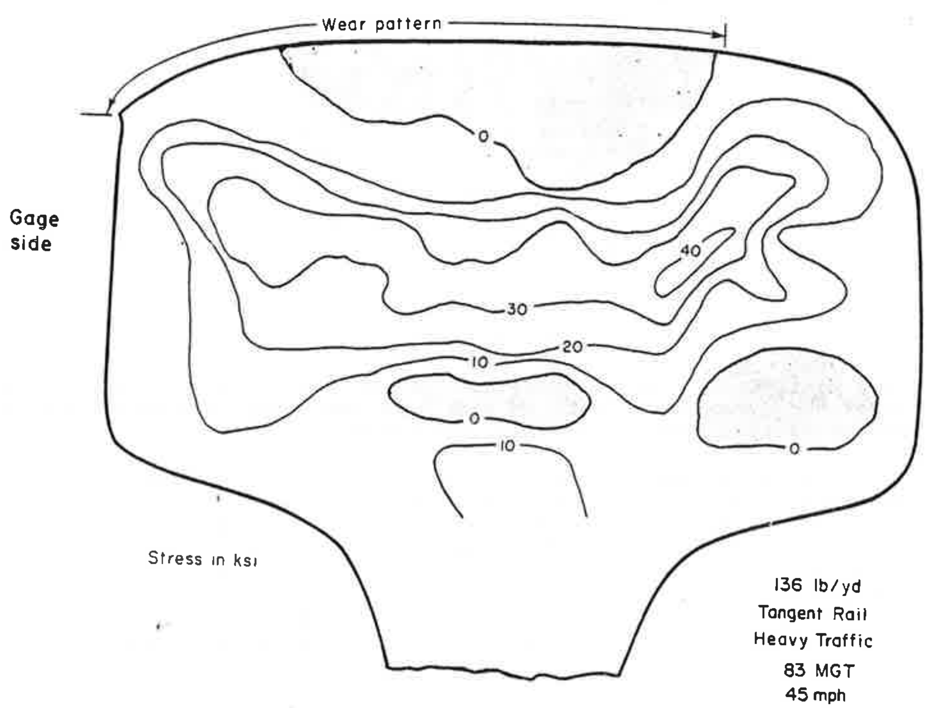

FIGURE 19. SPECIMEN 1, IN-PLANE TENSILE STRESS MAGNITUDE CONTOURS

In Figure 20, the principal compressive stress contour plot shows the in-plane compressive stress to peak at -142,700 psi at the flow lip on the gage-side edge of the wear pattern. A stress of -69,000 psi occurs at the field-side edge of the wear pattern and a stress of -69,000 psi is found in the knot of compressive stress deep inside the head on the field side. Only the central region of the rail cross section displays completely tensile residual stresses.

In Figure 21, the axial (out-of-plane) residual stress contours are shown. Here there is no question of stress direction; it is always normal to the plane of the transverse cross section. The compressive stresses peak at the same locations that the in-plane stresses peak, but the magnitudes are substantially reduced. The axial tensile stress magnitudes are also significantly reduced from the in-plane values. A peak axial tensile stress of +17,300 psi occurs beneath the surface near the gage-side edge of the wear pattern.

4.3.2 Specimen 2, Stresses in Heavy Traffic Rail at 270 MGT

As described earlier, two thin (Yasojima-Machii) slices were taken on this specimen in order to verify the longitudinal consistency of the stress pattern. The actual gaged slices are shown, prior to dicing, in Figure 22. These slices were approximately 18 inches apart at either end of the Meier section. The contour plots presented below were prepared using the averaged values from the two slices. The stress magnitudes discussed here and listed in Table 1 are the maximum values from the two slices.

In the principal stress vector plots of Figures 23 and 24, the consistency of the stress pattern over the 18-inch length is evident. As for the pattern itself, it bears more than a superficial resemblance to the pattern from specimen 1, Figure 18. Again, there are the large compressive stresses in the surfaces associated with the edges of the now broader wear pattern. The tensile stresses run horizontally across the central portions of the head and then point diagonally up toward the edges of the wear (flow) pattern.

In the principal tensile stress contour plots of Figure 25, we see a peak stress of +64,300 psi in the transverse plane. This "finger" of maximum tensile stress points towards the edge of the wear pattern on the field side.

In the principal compressive stress contour plots of Figure 26, the high compressive stresses are again at the edges of the expanded wear pattern, but the magnitudes of from -70 to -100,000 psi are lower than the extremes (-142,700 psi) seen in specimen 1. The region of tensile stresses is broader, and the knot of compressive stresses seen in the low field side of the rail head in specimen 1 is nonexistent in this specimen.

In the axial stress plots of Figure 27, the maximum compressive stresses are again at the surfaces near the edges of the expanded wear pattern. The peak stress of -63,700 psi is lower in magnitude than on specimen 1, and occurs on the field side of the wear pattern rather than on the gage side. The peak axial tensile stress of +22,000 psi also occurs on the field side up near the edge of the wear pattern, whereas the peak stress on specimen 1 was lower (+17,300 psi) and was associated with the gage-side edge of the wear pattern.

4.3.3 Specimen 5, Stresses in General Traffic Rail at 100 MGT

This specimen had a slightly wider wear pattern on the field side than heavy traffic specimen 1 (83 MGT), and it did not have a pronounced flow lip on the gage side as did specimen 1. The principal stress vector plots, shown in Figure 28, display a pattern similar to those of the heavy traffic specimens. The general pattern is one of high surface compressive stresses toward the edges of the wear pattern and horizontally oriented tensile stresses through the central portion of the head with a shift to pointing diagonally up toward the top corners of the rail. There are a few isolated points of compressive stress deep within the rail head.

The principal in-plane tensile stress contours of Figure 29 show a peak tensile stress of +35,700 psi where the stresses point diagonally up toward the gage-side corner of the head. The tensile stress level of +30,000 psi runs broadly across the center of the head around a small region of compressive stress.

Principal in-plane compressive stresses are shown in Figure 30. A surface compressive stress maximum of -59,200 psi occurs at the edge of the wear pattern on the field side. An even higher surface compressive stress may have been present on the gage side

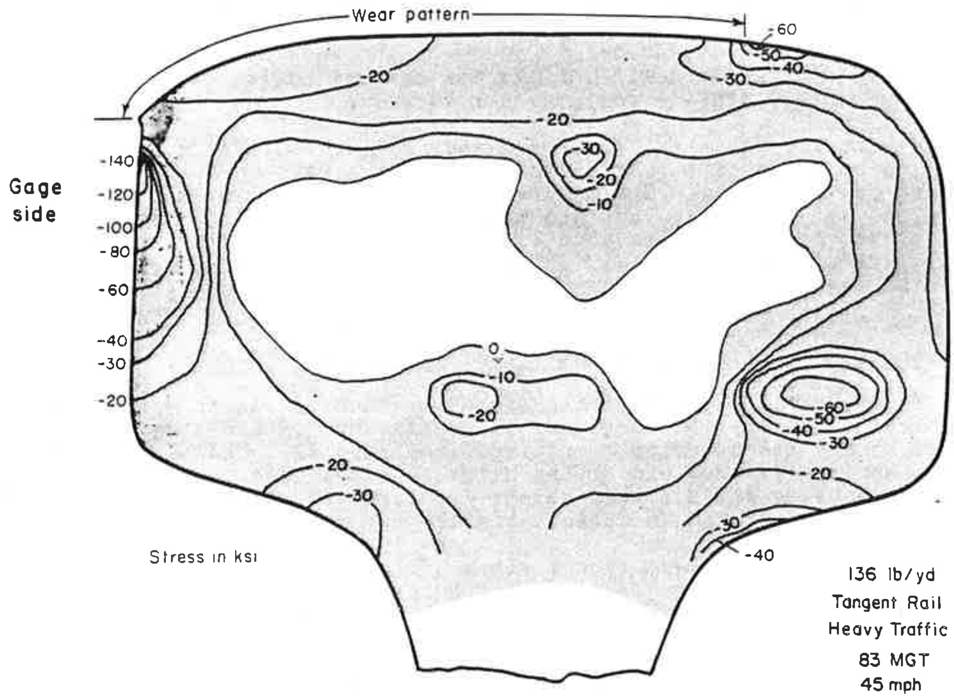

FIGURE 20. SPECIMEN 1, IN-PLANE COMPRESSIVE STRESS MAGNITUDE CONTOURS

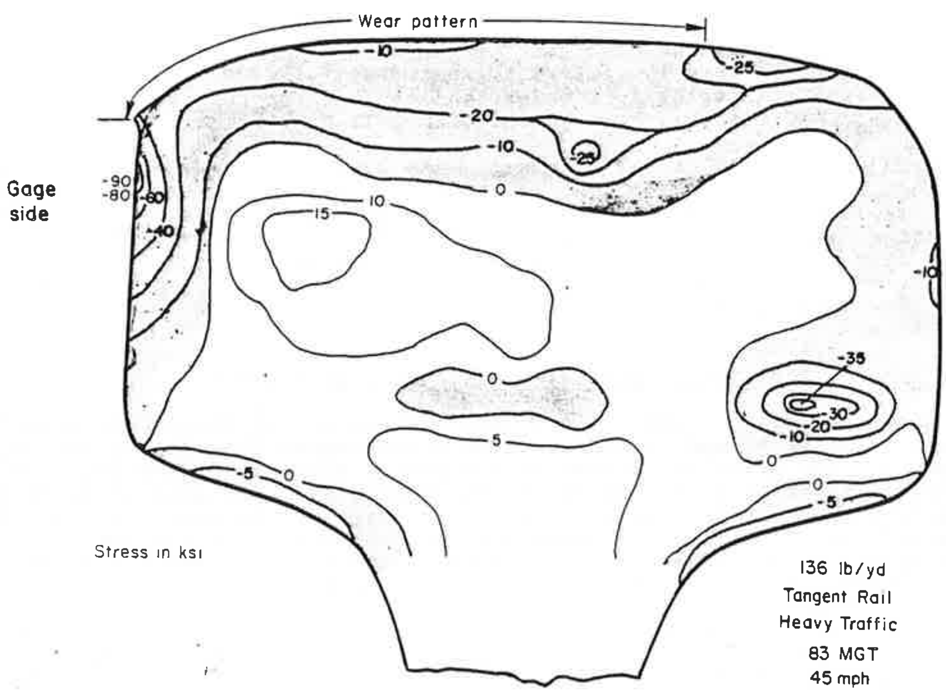

FIGURE 21. SPECIMEN 1, AXIAL STRESS CONTOURS

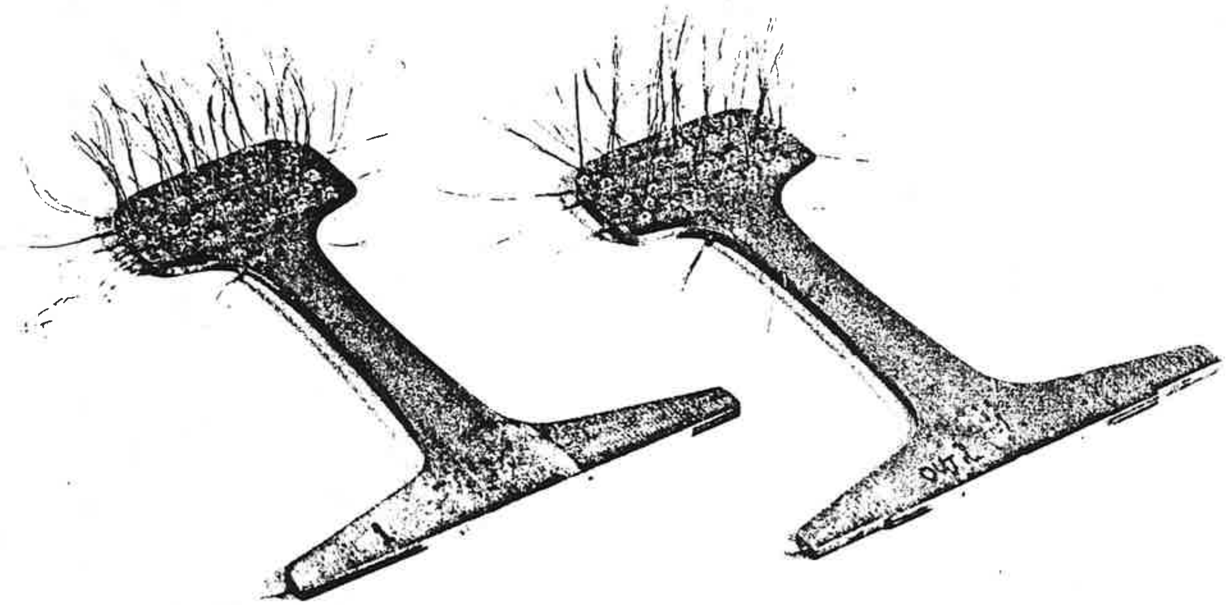

FIGURE 22. TWO YASOJIMA-MACHII SLICES FROM SPECIMEN 2

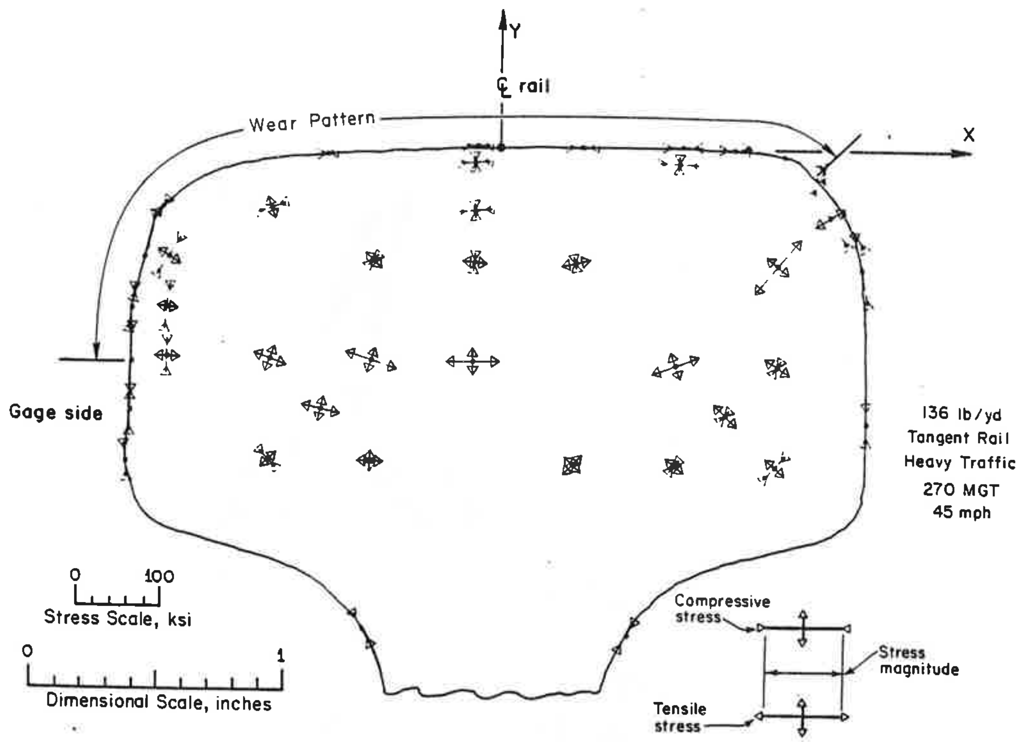

FIGURE 23. SPECIMEN 2, IN-PLANE PRINCIPAL STRESS VECTORS (SLICE 1)

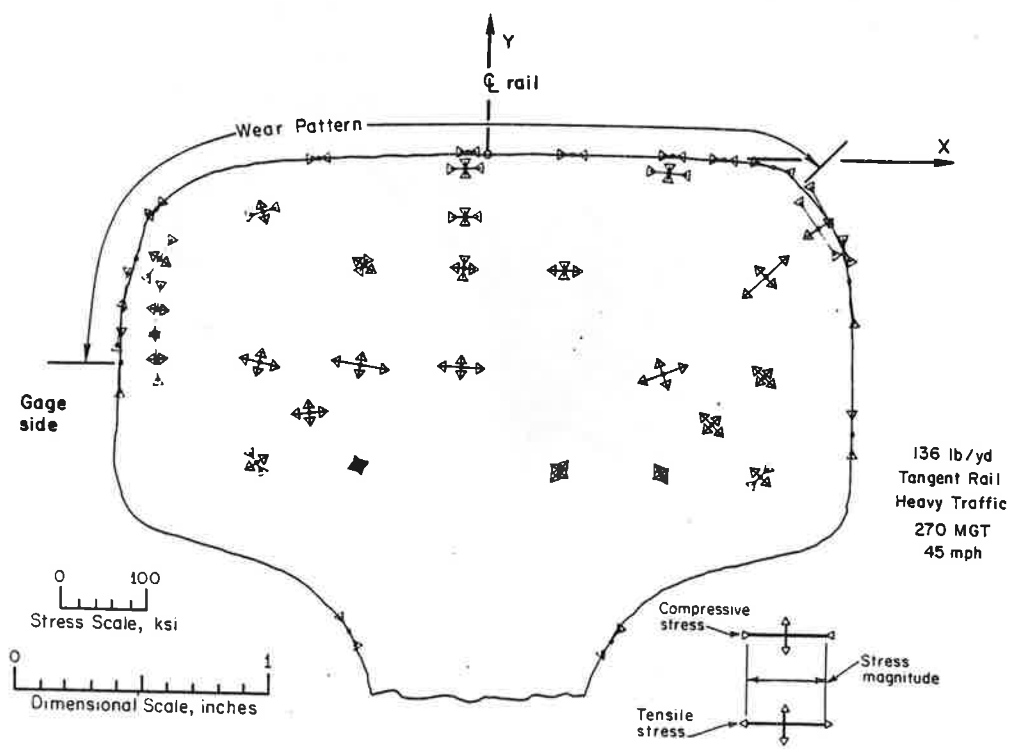

FIGURE 24. SPECIMEN 2, IN-PLANE PRINCIPAL STRESS VECTORS (SLICE 2)

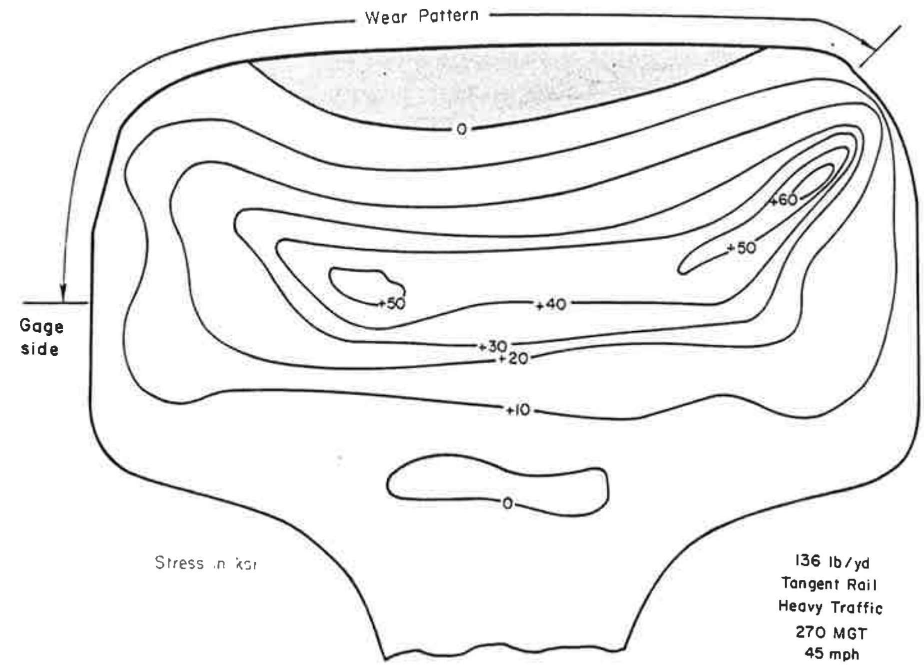

FIGURE 25. SPECIMEN 2, IN-PLANE TENSILE STRESS MAGNITUDE CONTOURS

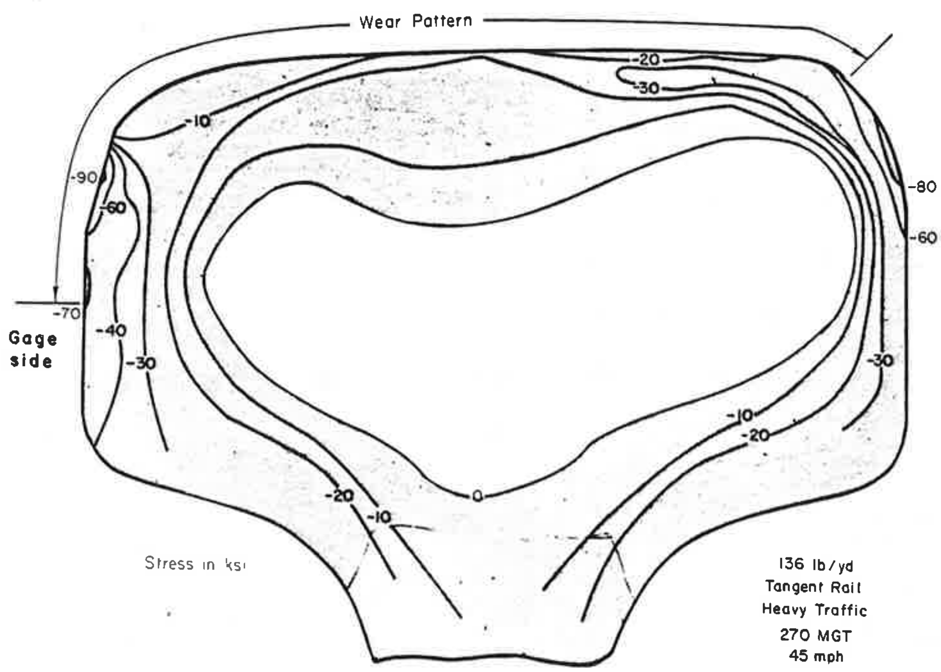

FIGURE 26. SPECIMEN 2, IN-PLANE COMPRESSIVE STRESS MAGNITUDE CONTOURS

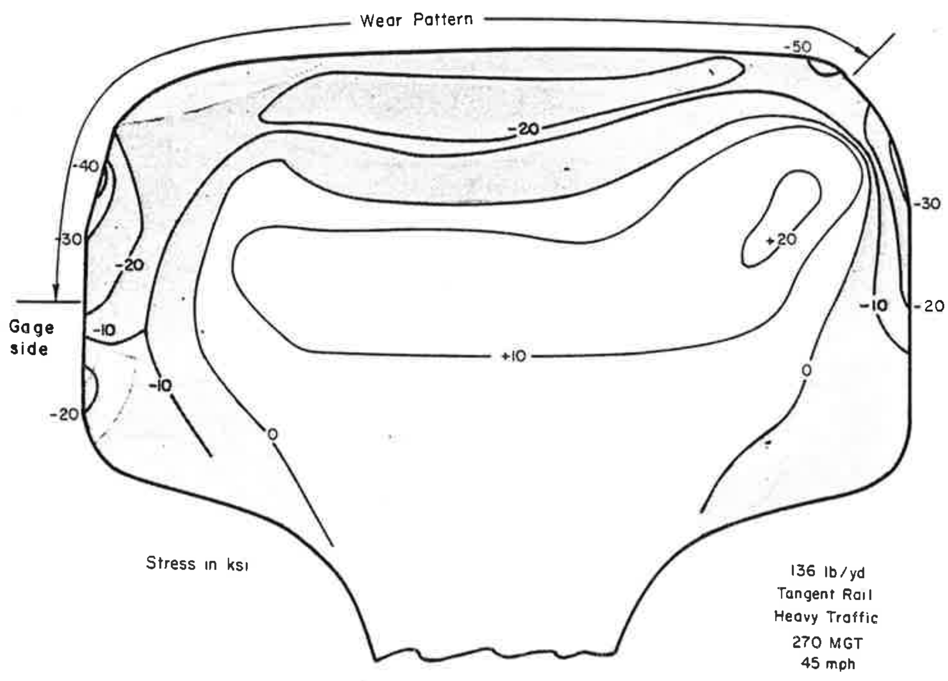

FIGURE 27. SPECIMEN 2, AXIAL STRESS CONTOURS

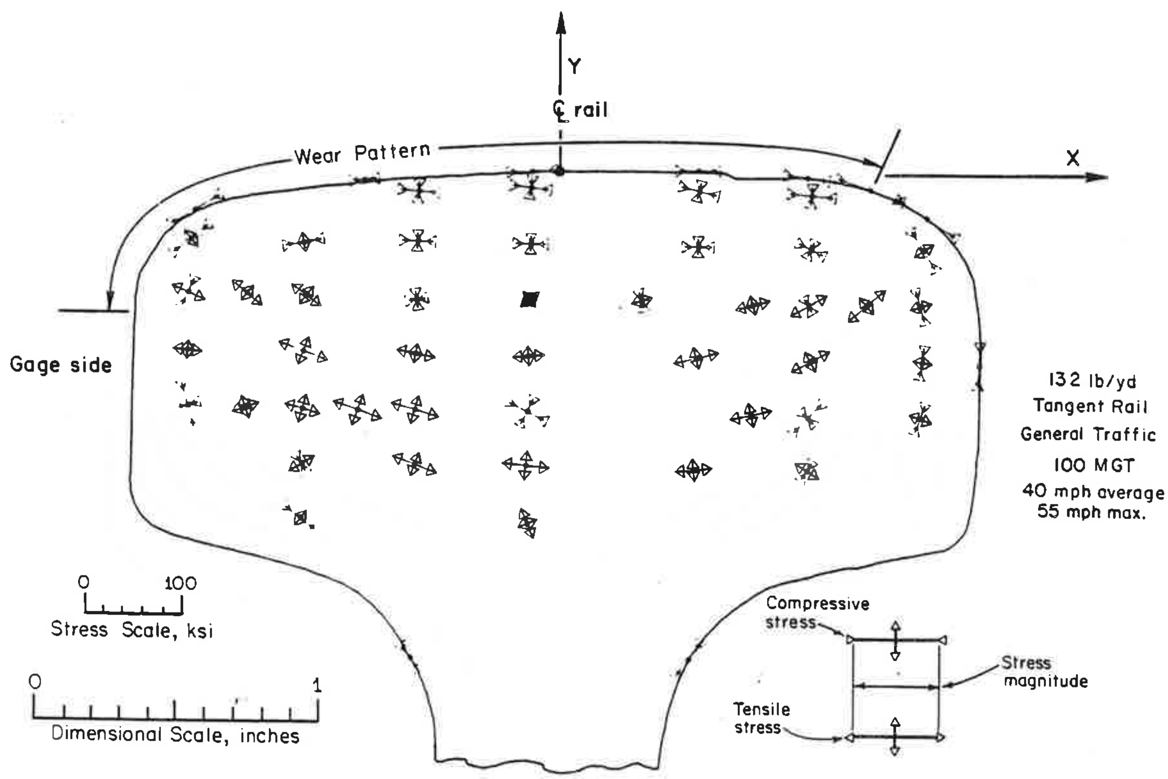

FIGURE 28. SPECIMEN 5, IN-PLANE PRINCIPAL STRESS VECTORS

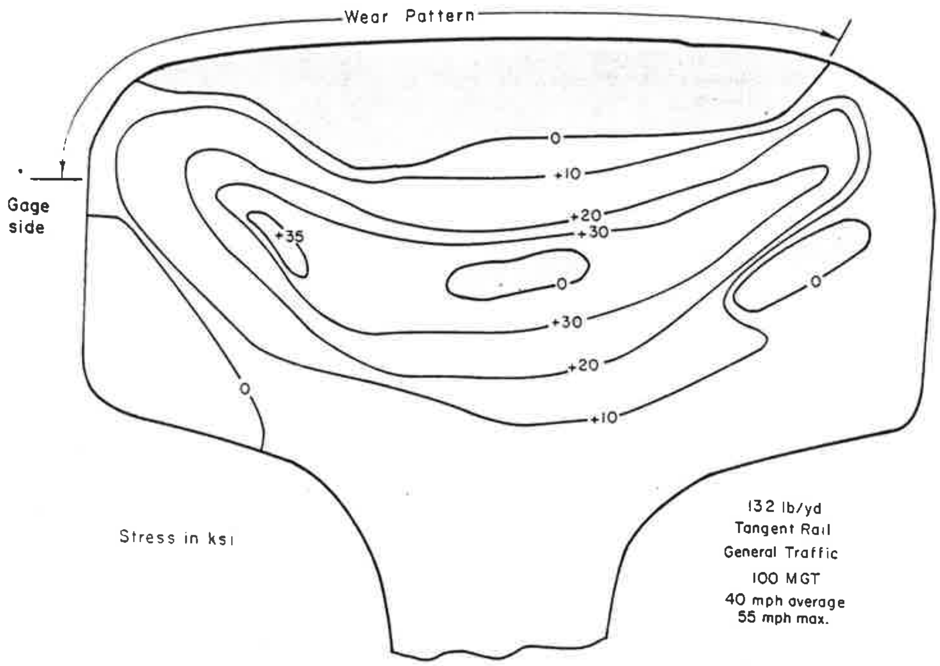

FIGURE 29. SPECIMEN 5, IN-PLANE TENSILE STRESS MAGNITUDE CONTOURS

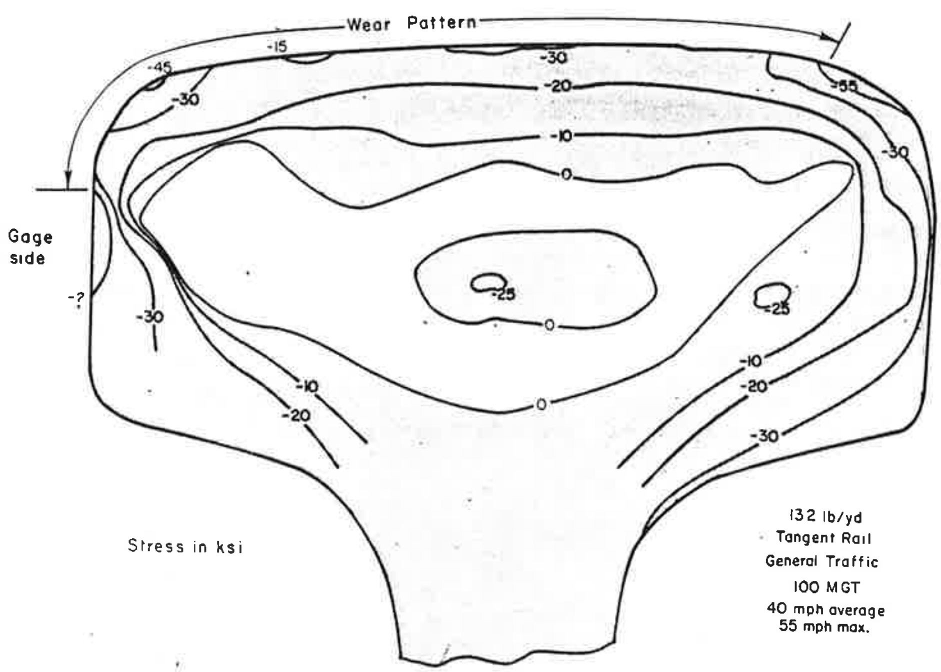

FIGURE 30. SPECIMEN 5, IN-PLANE COMPRESSIVE STRESS MAGNITUDE CONTOURS

of the wear pattern, but the gage location system did not allow sufficient material on this side of the specimen for gaging.

The axial stress contours of Figure 31 show both compressive and tensile stress levels well below the in-plane levels. A maximum axial compressive stress of -39,700 psi occurs on the gage-side corner of the wear surface. A maximum axial tensile stress +18,900 psi occurs in the diagonal run of stress pointing toward the top gage-side corner of the rail cross section.

4.3.4 Specimen 6, Stresses in General Traffic Rail at 300 MGT

The most notable difference between general traffic specimens 5 (100 MGT) and 6 (300 MGT) is that the metal flow at the edges of the wear surface on specimen 6 forms distinct lateral protrusions or "lips." On specimens 1 and 2, the small gage side flow present (or evident) at 83 MGT was completely worn away at 270 MGT, and the gage side of the rail was indented by wheel flange action. The presence of the gage-side lip on the 300 MGT specimen 6 suggests that very little flange contact occurred in this section of tangent track.

The in-plane principal stress vector plots of Figure 32 show the same general stress patterns of the previous three specimens with the exception that gages could not be applied near the edges of the flow lips to adequately verify or disprove the existence of high compressive surface stresses at these points. The usual broad region of tensile stresses runs horizontally through the interior of the head and tips diagonally upward at the edges.

Figure 33 shows the principal in-plane tensile stresses. The peak tensile stress of +41,300 occurs in the same gage-side diagonal location as the tensile peak stress in specimen 5 (+35,700). As well as being higher, the in-plane tensile stresses of specimen 6 cover a broader area of the rail head than those in specimen 5. An interesting point about the general traffic specimen is that, while the in-plane tensile stresses increase in both general and heavy traffic specimens with increased MGT, the peak stress location does not shift from the gage-side diagonal to the field-side diagonal as it does with the two heavy traffic specimens.

The in-plane compressive stress contours of Figure 34 are remarkable only in the one point of compressive stress low in the gage-side portion of the head which measured -59,800 psi. There were inadequate measurements to define the surface stresses near the edges of the wear pattern.

Axial stresses for specimen 6 are shown in Figure 35. The tensile stresses are more solidly established within the rail head than those in specimen 5. The peak tensile stress of +18,400 is relatively unchanged from that of specimen 5 (+18,900 psi) and the location has not shifted to the field side as occurred in the heavy traffic specimens. The compressive stresses where measured on the tread surface are substantially lower than those on specimen 5; see Figure 31.

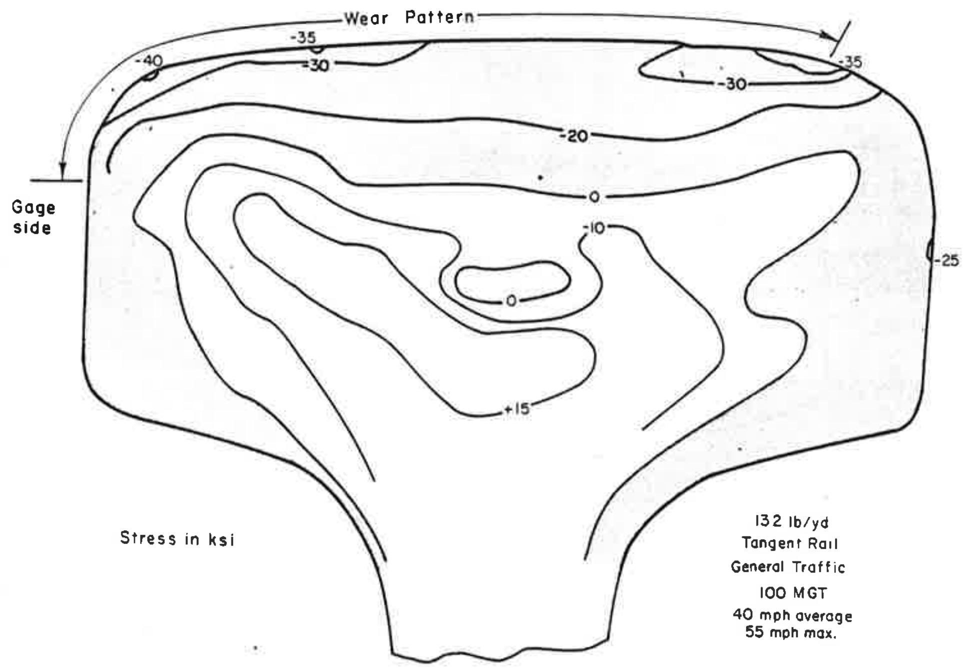

FIGURE 31. SPECIMEN 5, AXIAL STRESS CONTOURS

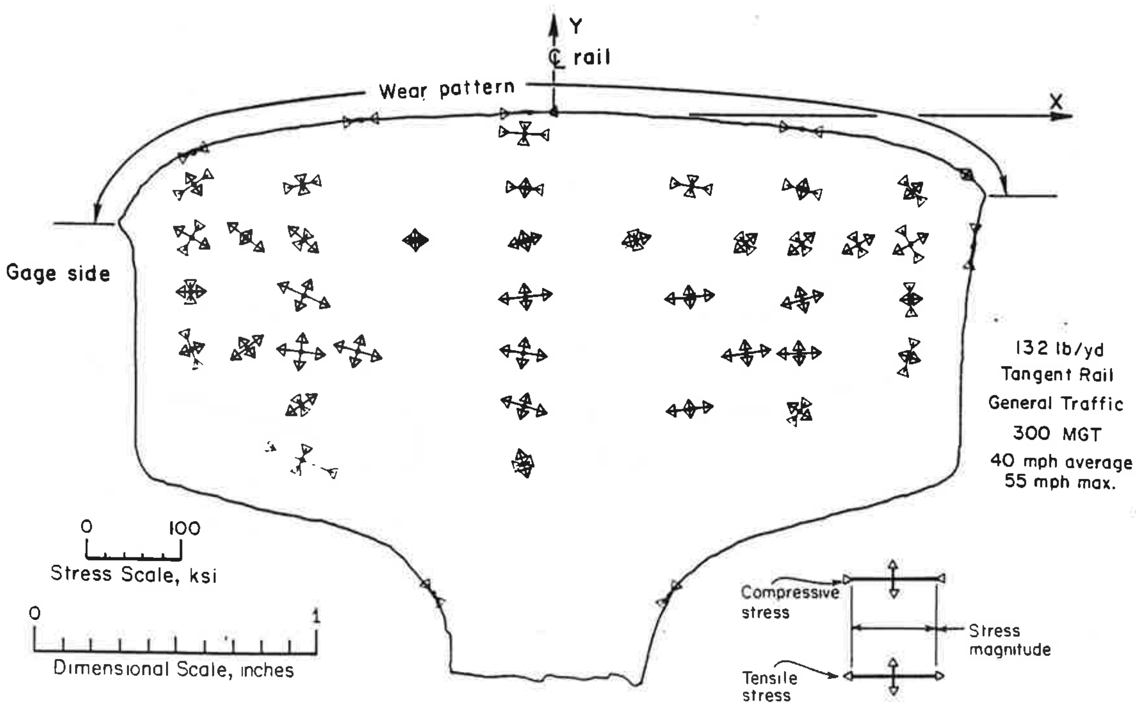

FIGURE 32. SPECIMEN 6, IN-PLANE PRINCIPAL STRESS VECTORS

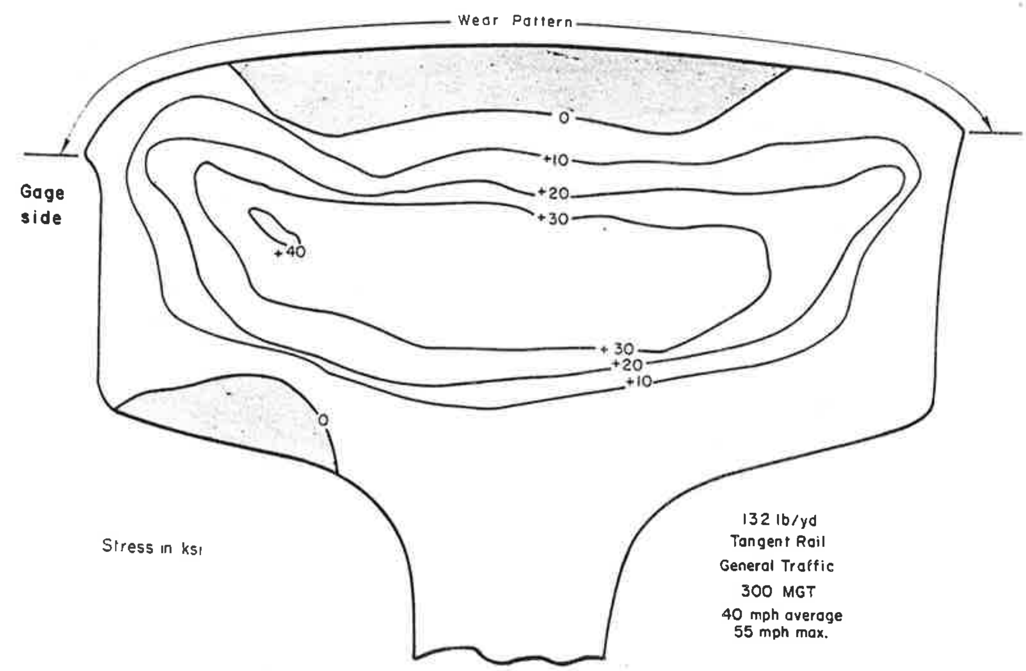

FIGURE 33. SPECIMEN 6, IN-PLANE TENSILE STRESS MAGNITUDE CONTOURS

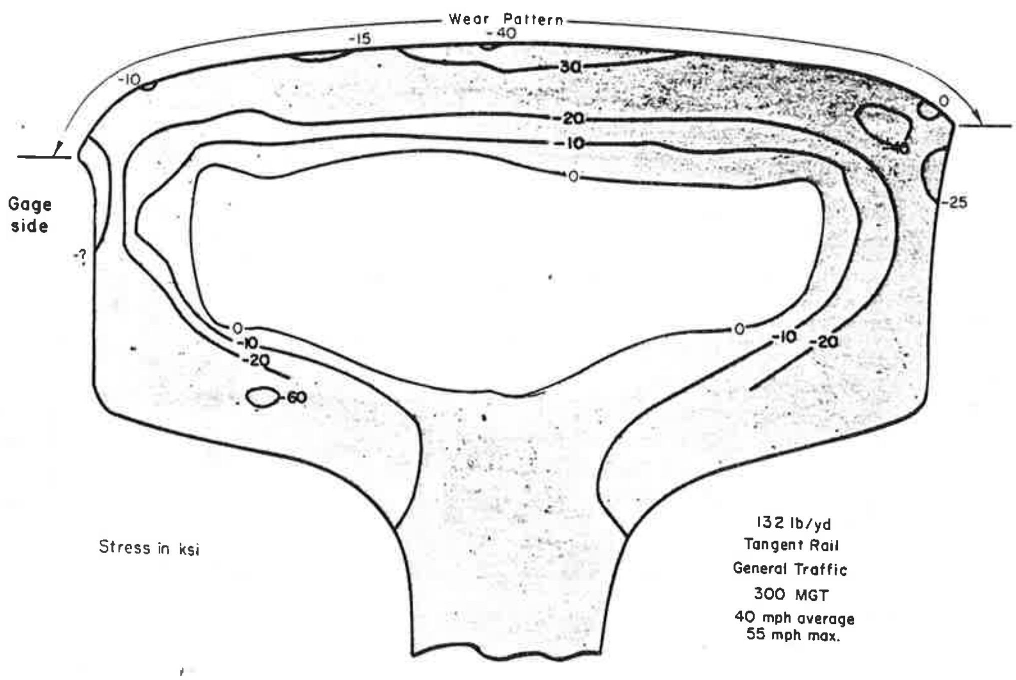

FIGURE 34. SPECIMEN 6, IN-PLANE COMPRESSIVE STRESS MAGNITUDE CONTOURS

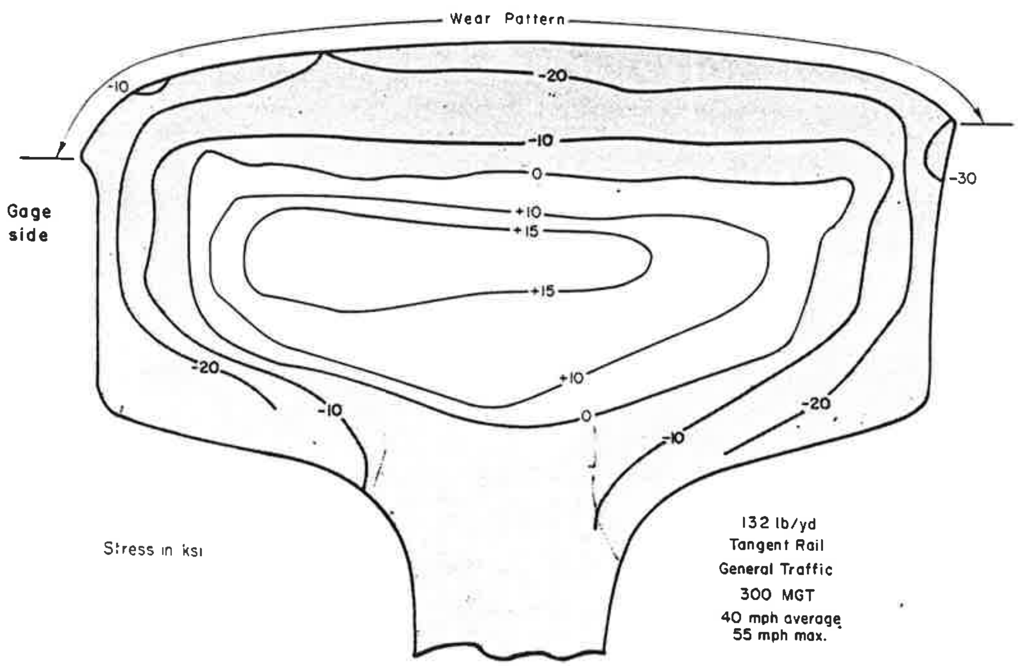

FIGURE 35. SPECIMEN 6, AXIAL STRESS CONTOURS

REFERENCES

1. Martin, G.C., and W.W. Hay, "The Influence of Wheel-Rail Contact Forces on the Formation of Rail Shells," Trans. ASME, 72-WA/RT-8, 1972.

2. Johns, T.G., Sampath, S.G., Bell, J.C., and Davies, K.B., "Engineering Analysis of Stresses in Railroad Rails," Federal Railroad Administration, FRA/ORD-81/51, 1981. National Technical Information Service No. PB 82-129610.

3. Office for Research and Experiments of the International Union of Railways, "Study of Fatigue Phenomena of the Rail in the Contact Zone with the Wheel," Rail International, 3, (13), 741-794, September 1973.

4. Schilling, C.G., and Blake, G.T. "Measurement of Triaxial Residual Stresses in Railroad Rails," Association of American Railroads, Technical Report R-447, Rail Analysis, Volume 10, March 1981.

5. Ahlbeck, D.R. et al, "Measurements of Wheel/Rail Loads on Class 5 Track, Federal Railroad Administration, FRA/ORD-82/24, 1980. National Technical Information Service PB 80-196868.

6. Prause, R.H., Kennedy, J.C. and Arnlund, R.C., "An Evaluation of Performance Requirements for Cross Ties and Fasteners," Federal Railroad Administration, FRA/ORD-78/37, 1978. National Technical Information Service PB 294 431.

APPENDIX A

EXPERIMENTAL AND ANALYTICAL DEVELOPMENT OF RESIDUAL STRESS MEASUREMENTS TECHNIQUE

A number of the assumptions involved in the experimental and analytical procedures of the Battelle slicing technique were subjected to checks, tests, and calibrations. These various evaluation efforts and their results are described below.

Experimental Evaluations

In developing the Battelle slicing technique procedures, special tests were conducted to define the amount of error stemming from the mechanical aspects of the technique itself. Some of these tests were concerned with the sectioning/cutting procedures used in applying the technique, and others were concerned with the consistency of the stress patterns within what were assumed to be axially uniform specimens. These experimental evaluations are discussed in this section.

Cutting Stresses

All of the sectioning of the specimens that took place as part of the Battelle slicing technique was done by bandsaw cutting. Table A-1 lists the various parameters of the bandsaw cutting. Bandsaw cutting does produce some erroneous stress indications in the specimen (through work hardening, heating, etc.), and there are other more delicate techniques, such as Electric Discharge Machining (EDM). But EDM and the other possible techniques are extremely time-consuming and expensive. Previous Battelle experience indicated that bandsaw cutting could be used economically and that the cutting errors could, with care, be controllable to the extent that they could be accounted for by applying a correction factor to the as-measured strains.

A series of tests were run to quantify the errors resulting from the cutting procedures. These tests consisted of applying the procedures to thoroughly stress-relieved rail material and assuming that the resulting residual stress indications were due entirely to technique.

TABLE A-1. BANDSAW CUTTING PARAMETERS

TYPE OF CUT	TYPE OF BLADE*	BLADE SPEED, fpm	BLADE PRESSURE ON WORKPIECE, lb
Heavy Slab	3/4 - 10 Bimetal	68	40
Thin Rod	3/4 - 10 Bimetal	68	25
Dicing	3/8 - 10 Standard	65	4

*The bandsaw blades were changed at the operator's discretion, but this was done long before a blade would be judged worn under normal cutting conditions.

The stress-relieved rail specimens that were left over from the DOT/TSC-1038 program were used to determine cutting stresses. Under the 1038 program, the rail had been held at a temperature of from 1250°F to 1263°F for 14 hours. It was then cooled down to near room temperature at a rate of less than 10°F/hour. A tensile test on this stress-relieved material gave a yield stress of only 47.3 ksi, an indication that the cold/hot working effects had been relieved.

This material was then used in simulations of the Battelle slicing technique wherein all the procedures that were being used to measure the specimens in the subject program were duplicated on the stress-relieved rail. The results, for gage locations beneath the rail surfaces, are shown in Table A-2 as if the measured stresses were actual residual stresses. In applying the technique to actual rail specimens, the average stress values shown in Table A-2 were subtracted from the values indicated by the measurements on the specimens*, i.e., the apparent readings were corrected for error due to technique. No corrections were made for the angle Ø since it depends on the sequence of bandsaw cuts, and it is nearly symmetrical.

TABLE A-2. PRINCIPAL INTERNAL STRESS INDICATIONS DUE TO TECHNIQUE*

COMPONENT**	AVERAGE, psi	RANGE ABOUT AVERAGE, psi	
		OVER	UNDER
σ_1	-4,800	2,400	-4,000
σ_2	-7,600	3,100	-4,500
σ_3	-6,800	2,300	-3,600
Ø (degrees)	8.42	23.02	-27.5

*Stresses σ_1 and σ_2 were determined using seven rosette gages applied to a 0.160-inch thick slab sawed from a stress-relieved portion of rail. The longitudinal stress, $\sigma_3 = \sigma_z$, was determined from 10 2-foot long rods cut from another stress-relieved section of rail. The strains from the two types of measurements were combined, using the approximate analysis procedure described above. In this one case, where the measurements were being made on stress-relieved material, the approximate analysis procedure is theoretically valid and accurate.

**σ_1 and σ_2 are located in the vertical-transverse plane (x-y plane). The angle between the upward-vertical y-axis and the orientation of σ_1 is given by Ø where +Ø is counterclockwise from +y and -Ø is clockwise from +y.

Table A-2 shows a range of stress, about the average for σ_2, of from +3,100 to -4,500 psi. This error range is reasonable for the bandsaw procedures that were used and should not cause problems where rail residual stress levels on the order of 30 ksi and higher are of concern. The results that went into the compilation of Table A-2 are shown graphically in Figure A-1. Also shown are the correction factors for cuts producing data on the surface of the rail. The surface dicing data show considerable variation (+600 to -12,300 psi) on the transverse/peripheral stress. These latter data are also compiled in Table A-3. The surface cutting variation combined with the natural variability of the rail surface stresses means that all surface stress measurements made with bandsaw cuts should be viewed as approximate.

TABLE A-3. APPARENT SURFACE STRESSES DUE TO BANDSAW AND DRILL TREPANNING CUTS

STRESS COMPONENT	AVERAGE STRESS, psi	RANGE ABOUT AVERAGE, psi	
		OVER	UNDER
Bandsaw Cutting			
Longitudinal	-4,900	3,000	-2,600
Transverse/Peripheral	-3,100	3,700	-9,200
Drill Trepanning			
Longitudinal	-4,000	1,000	-2,600
Transverse/Peripheral	-2,900	800	-1,200

*In the actual calculation procedure, the machining corrections were made on the measured strain components before these components were used in the stress calculation.

Additional test cuts were made on the stress-relieved material using the dental drill trepanning technique for surface residual stress measurements. The apparent stresses produced by this techinque are shown in Figure A-1 and are listed in Table A-3. Various survey measurements, using the dental drill trepanning technique, were made on rail specimens. In these cases, the apparent measured stresses were corrected by subtracting the average values shown in Table A-3.

Axial Consistency of Surface Stresses

The first two specimens received (from FAST, specimens 1 and 2) were tested for the axial consistency of their tread surface stresses. Surface trepanning measurements were made at six points along the head centerline of each specimen. The results of these measurements are shown in Figure A-2. Though the trends in the data are clear and moderately consistent, there is considerable variation in the stress values along the length at this one point on the rail cross section. Subsequent data, discussed in the body of this report, show that the surface stresses are much more axially variable than stresses within the cross section. The data do show a surprising amount of agreement in going from specimen 1 at 83 MGT to specimen 2 at 270 MGT. However, the presence of shakedown cannot be judged on the basis of surface stresses alone.

End Effects in the Meier Section

The question of the appropriate length for the Meier section in a specimen was discussed in the text of this report under Section 4.2.1, Mechanical Procedure. The main concern was to choose an economical section length (for rod cutting) in which the longitudinal extent of the effect of freeing the ends represented a small length compared to the unaffected length.

To check the axial extent of the strain effect of cutting out the Meier section, axial strain gages were attached at various points along the length of what was to become the 18-inch long Meier section in specimen 2. All the gages were at the same point on the cross-sectional profile, just below the wear pattern on the gage side of the rail. Based on the results from specimen 1, it was thought that this represented the point of highest longitudinal strain. The Meier section was then bandsawed from the rail specimen, and the ends of the Meier section were ground flat and parallel.

The longitudinal strain change resulting from the Meier sectioning procedure is shown as the heavy line in Figure A-3. Most of the strain change due to sectioning occurred in the first inch into the section from the section face, dropping from 1000 microstrain at the face to 67 microstrain at approximately 1 inch. This means that if there had been no correction on the final Meier rod length reading for this initial sectioning shift, the rod strain would have been low by about 98 microinch/inch. If this had been converted to a uniaxial stress, the z residual stress at this point would have had to be corrected by adding -2,800 psi.

However, all the Meier section rod readings were given an approximate correction to account for the end effects of initial sectioning, as described in the text under Section 4.2.1, Mechanical Procedure. This correction was determined by the length change between surface scribe lines (tick marks) located very close to the ends of the Meier section (see Figures 5 and A-3). For example, the rod corresponding to the above surface gages was corrected for a 115 microinch/inch shift, i.e., approximately -3,300 psi was added to the z stress via the corrected rod reading.

The other plots in Figure A-3 show the total strain changes at the gage locations as the Meier rod was cut out and then specially cut at each gage location to produce a cube similar to those from the modified Yasojima-Machii slices on each end of this specimen. The final (corrected) strains are low, and show much variation along the length among themselves and in comparison with the modified Yasojima-Machii gage readings for this cross section location. What happened is that the peripheral strains at this location (shown on the two modified Yasojima-Machii slices) were much higher than the longitudinal strains (1,900 to 2,300 microstrain, peripheral, versus 60 to 220 microstrain, longitudinal). Longitudinal consistency cannot be judged on the basis of secondary components of biaxial strains such as these (see the discussion of longitudinal consistency of the residual stress pattern in Section 3, Major Conclusions and Recommendations).

Analytical Evaluations

Two separate analytical methods of converting the experimental measurements into residual stresses were described in Section 4, Discussion. Both techniques were developed to the point where they were applied to the common set of data from specimen 1.

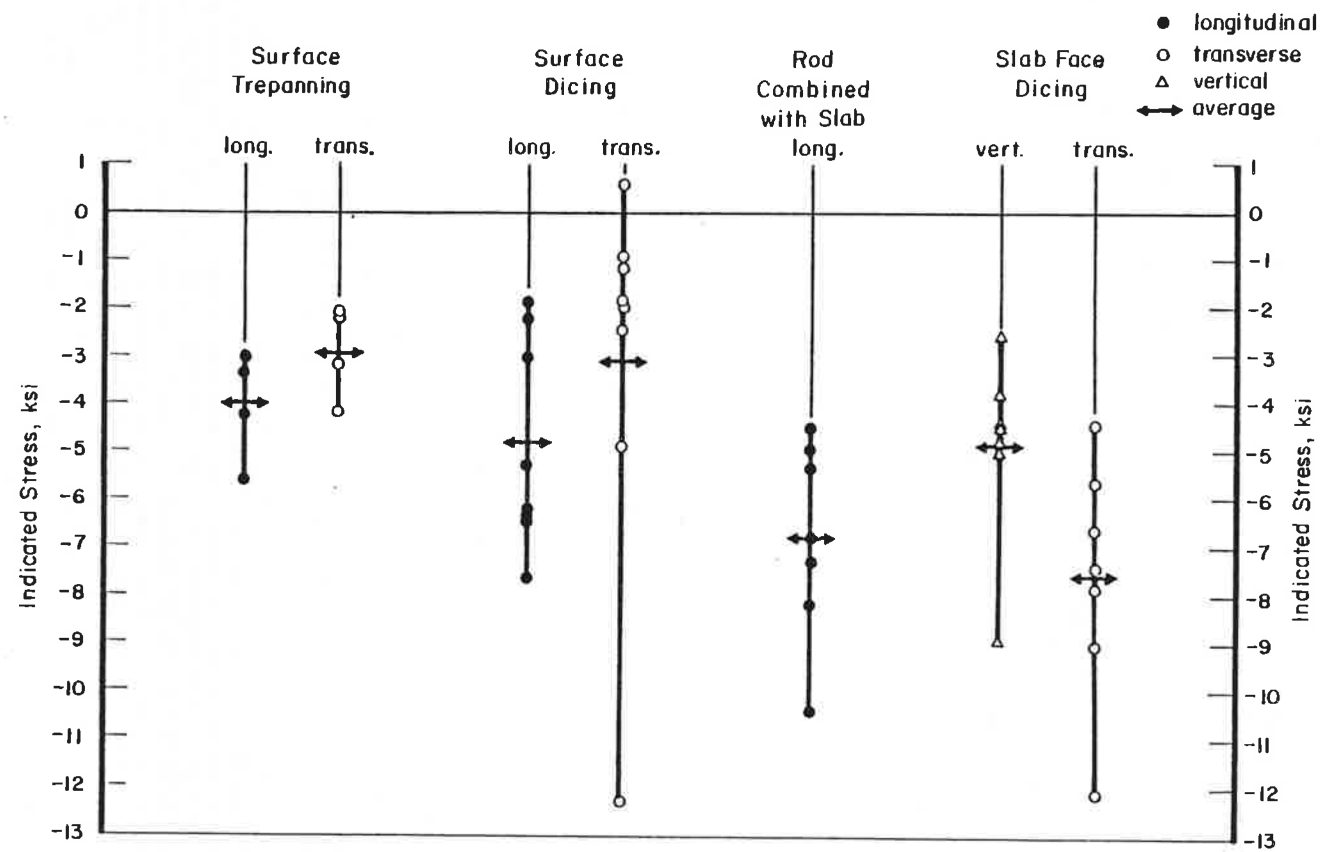

FIGURE A-1. CUTTING PROCEDURE EFFECTS IN STRESS-RELIEVED RAIL MATERIAL

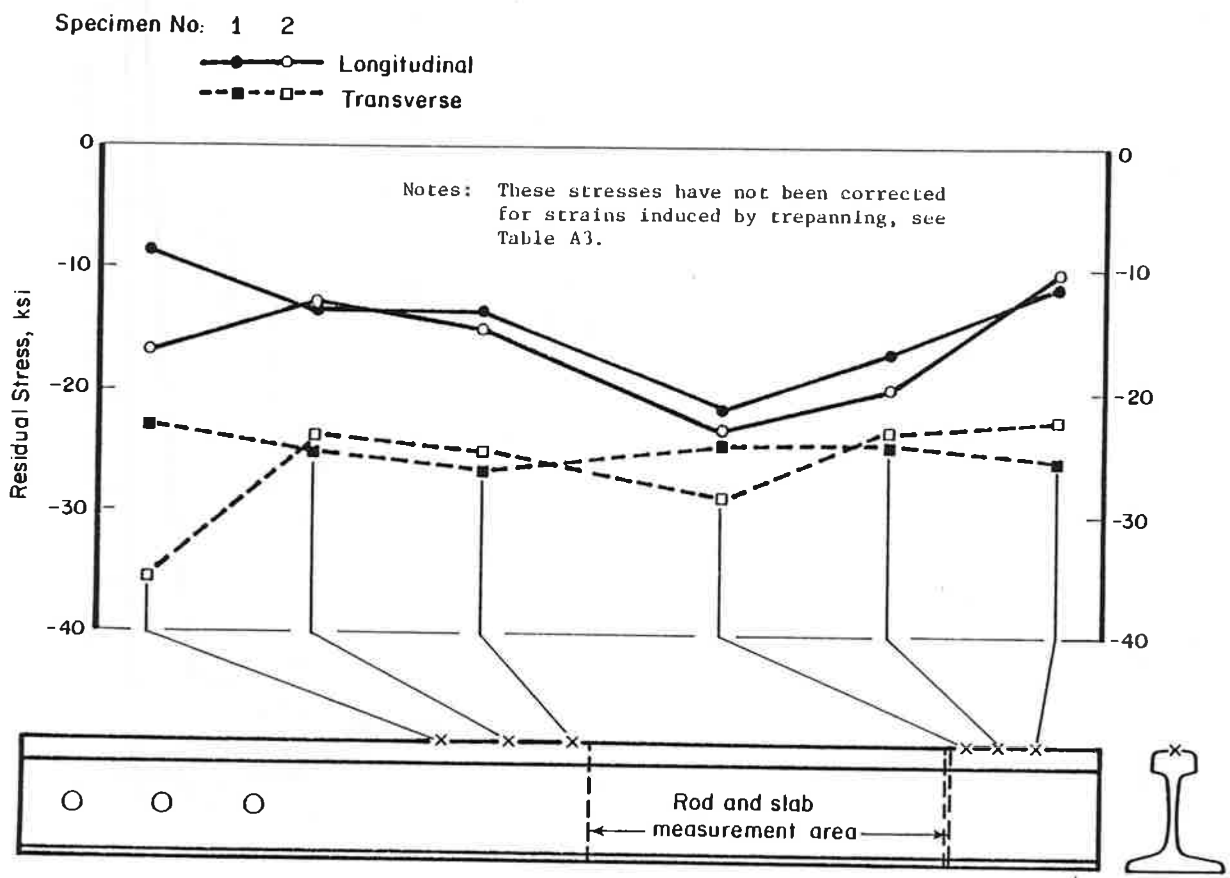

FIGURE A-2. SURFACE STRESS ALONG TREAD CENTERLINE

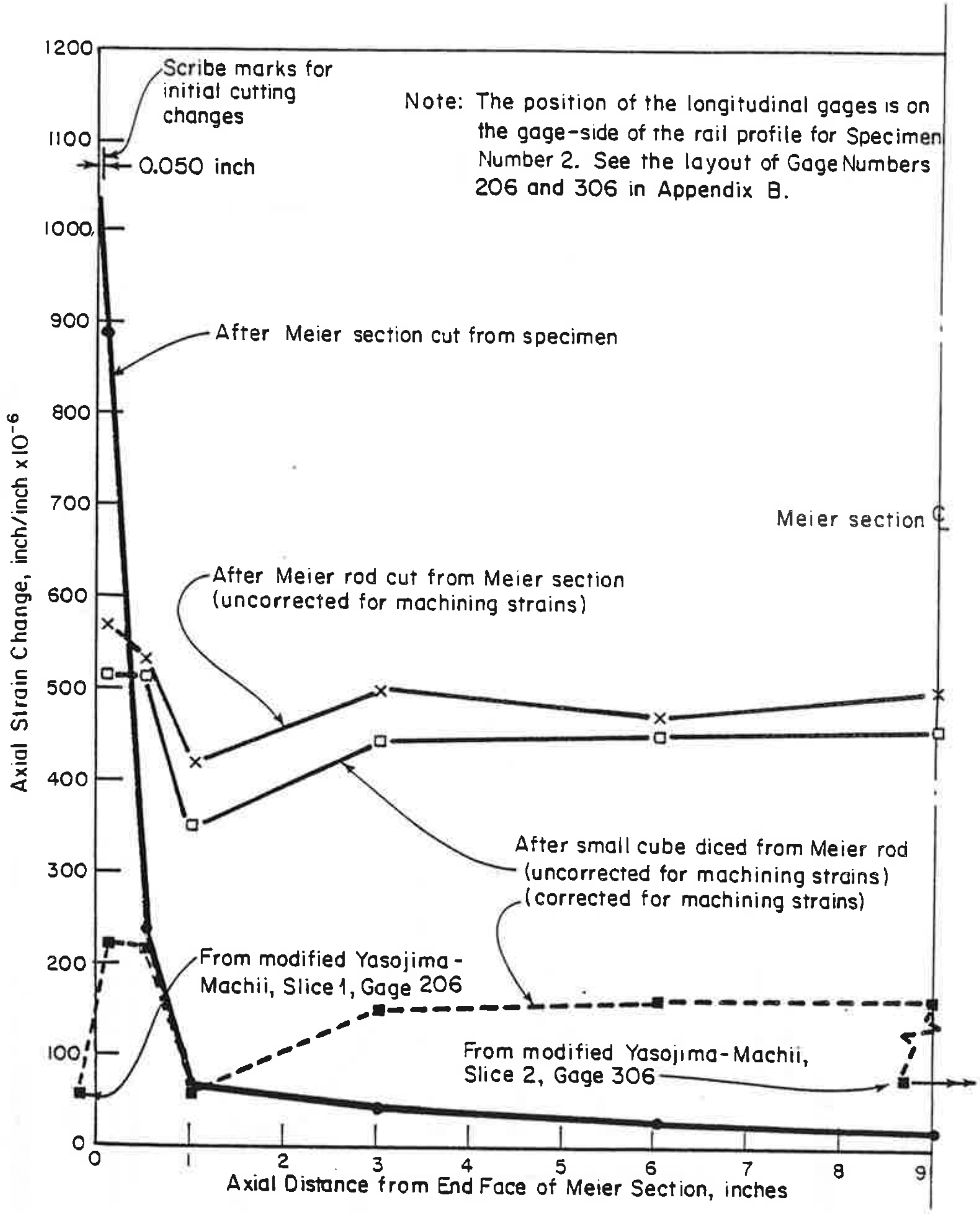

FIGURE A-3. SPECIAL LONGITUDINAL STRAIN CHANGE MEASUREMENTS ON MEIER SECTION OF SPECIMEN 2

The results of this comparison of the two techniques are also discussed in the body of this report under Section 4. As a result of this comparison, the approximate analysis technique was adopted as the method for reducing the data from all specimens.

Part of the development of the methodology in these two techniques involved running both analyses through a test case. This case allowed the procedures to be checked for correct execution, and gave an additional basis for comparing the two techniques. This test case effort is described below.

Analytical Test Case

The test case was derived by conceiving of a stressed body that had the following three attributes:

1. The initial stress state would be known throughout the body.
2. The stress pattern would not vary along one axis of the body.
3. It would be possible to determine all the strain changes that would occur when various portions of the body were removed. (Erroneous strains due to machining would not exist in this hypothetical case.)

The case that was derived is as follows:

a. The body is an infinitely long thick-walled axisymmetric cylinder having a 10-inch inside diameter and 40-inch outside diameter.
b. The cylinder is in an initially stressed state arising from the condition of an axisymmetric temperature field that does not vary along the length of the infinite cylinder.
c. The temperature varies linearly along the radius, going from 0 degrees on the ID to 200 degrees on the OD of the cylinder.
d. The material properties of this cylinder are

$$E = 30 \times 10^6 \text{ psi},$$

$$\nu = 0.26,$$

$$\alpha = 10.8 \times 10^{-6} \text{ inch/inch/degree}.$$

The complete initial stress state in the body under the above condition can be determined with a closed form solution.* Once the stress state of the body was determined, the thermal nature of the problem was ignored. In other words, the thermally derived stress state was viewed as a residual stress condition existing within the infinitely long cylinder, the manner in which the body got to be in this condition of equilibrium being unimportant to the test case requirements.

The internally stressed cylinder was then "dissected" using various conventional two- and three-dimensional finite element computer codes. The dissection simulated the steps of the mechanical procedure used in the Battelle slicing technique.

One three-dimensional finite element model used in the dissection analysis is shown in Figure A-4. The pie-shaped segment of the cylinder (shown with each element as shrunken 20 percent) represents the Yasojima-Machii slice in the procedure. The appropriate strain components resulting from the dissection simulation were then applied in the accurate analyses and apprxoimate analyses and the original stress state of the cylinder was predicted by each procedure.

Since the accurate technique involves a reversal of some of the finite element techniques used in the dissection analyses, it is not surprising that the accurate technique did faithfully reproduce the original stress state. (This calculation merely provided a debugging check for the linking software used in the accurate solution.)

The results of applying the approximate technique in the test case are shown in Figure A-5. As shown, the stresses are in close agreement for the longitudinal (axial) direction; the approximate stresses are 16 percent lower than the true stress for the circumferential (hoop) direction. The radial stresses are generally lower when the approximate solution is used. The irregularity at the 11-1/2-inch radial dimension in the radial stress curve for the approximate solution is due to finite element modeling problems, and not due to the solution technique.

---

*Timoshenko, S.P., and Goodier, J.N., Theory of Elasticity, McGraw-Hill, NY, 3rd Edition p. 448.

A. GLOBAL
B. ERASE--REDRAW
C. ERASE--NO REDRAW

SELECT MODE BY WHICH
PICTURE WILL BE CHANGED

D. ZOOM
E. SPLIT SCREEN
F. SHRINK ELEMENTS BY 2
G. CHANGE PLOT LIMITS

I. PERSPECTIVE VIEW
J. AXES
K. ROTATE
L. RESTORE ORIGINAL PIC
M. RETURN
N. QUICK RETURN

SELECT ELEMENTS ON
SCREEN OR ALL

D. ALL
E. CHOOSE ELEMENTS
F. RETURN

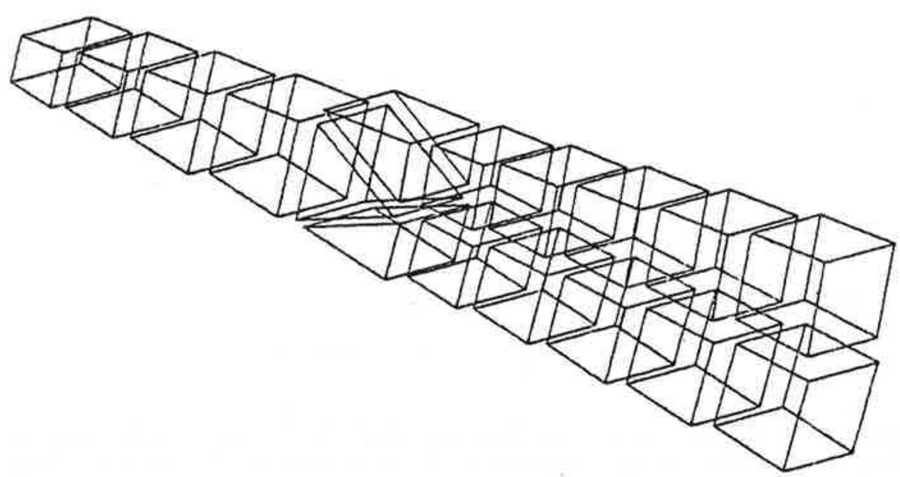

FIGURE A-4. THREE-DIMENSIONAL SECTION OF TEST CASE CYLINDER

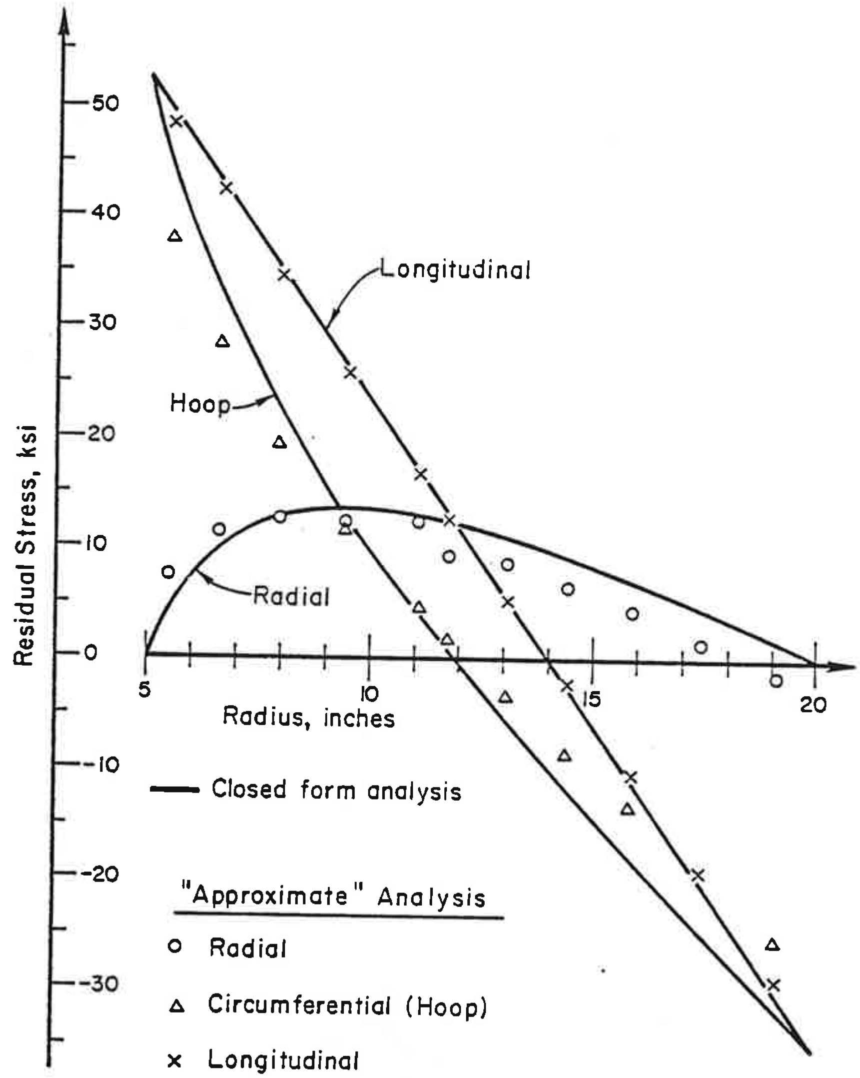

FIGURE A-5. TEST CASE, THICK-WALLED CYLINDER, RESULTS

With respect to maximum stresses, there is a reasonable amount of agreement between the two techniques when smoothly varying residual stresses are encountered. It It was thought that the actual rail residual stress conditions might introduce problems with both techniques. This reservation was not realized when the techniques were applied to the data from specimen 1. In this case both techniques yielded reasonable results (see Sections 4.2.2 and 4.2.3 in the text of the report). Figure A-6 shows the finite element modeling of the Yasojima-Machii slice from specimen 1 that was part of the accurate analysis.

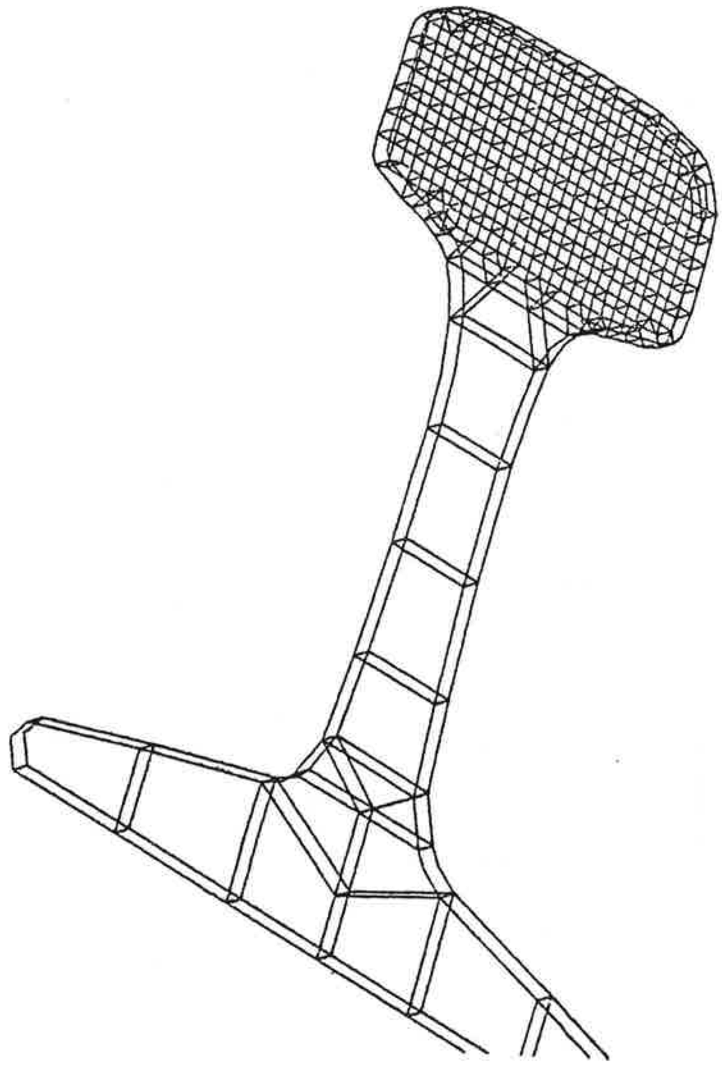

FIGURE A-6. FINITE ELEMENT MODEL OF SLICE FROM SPECIMEN 1

APPENDIX B

MEASURED RESIDUAL STRESSES IN SPECIMENS 1, 2, 5, AND 6

The residual stresses, determined by measurements and calculations, for the tangent track specimens 1, 2, 5, and 6 are presented in this appendix. The location of each measurement point in the rail's x-y cross section is shown on a cross section profile and as a set of x-y coordinates in the tables. The principal stresses σ_1 and σ_2 which lie in the x-y plane, their orientation (θ_1) with the horizontal x axis, and the axial stress (σ_z), are listed in the accompanying tables. The stresses listed for specimen 1 are the result of the accurate analysis technique, although the approximate analysis technique produced similar results (see Section 4, Discussion). Six figures and five tables follow in this appendix.

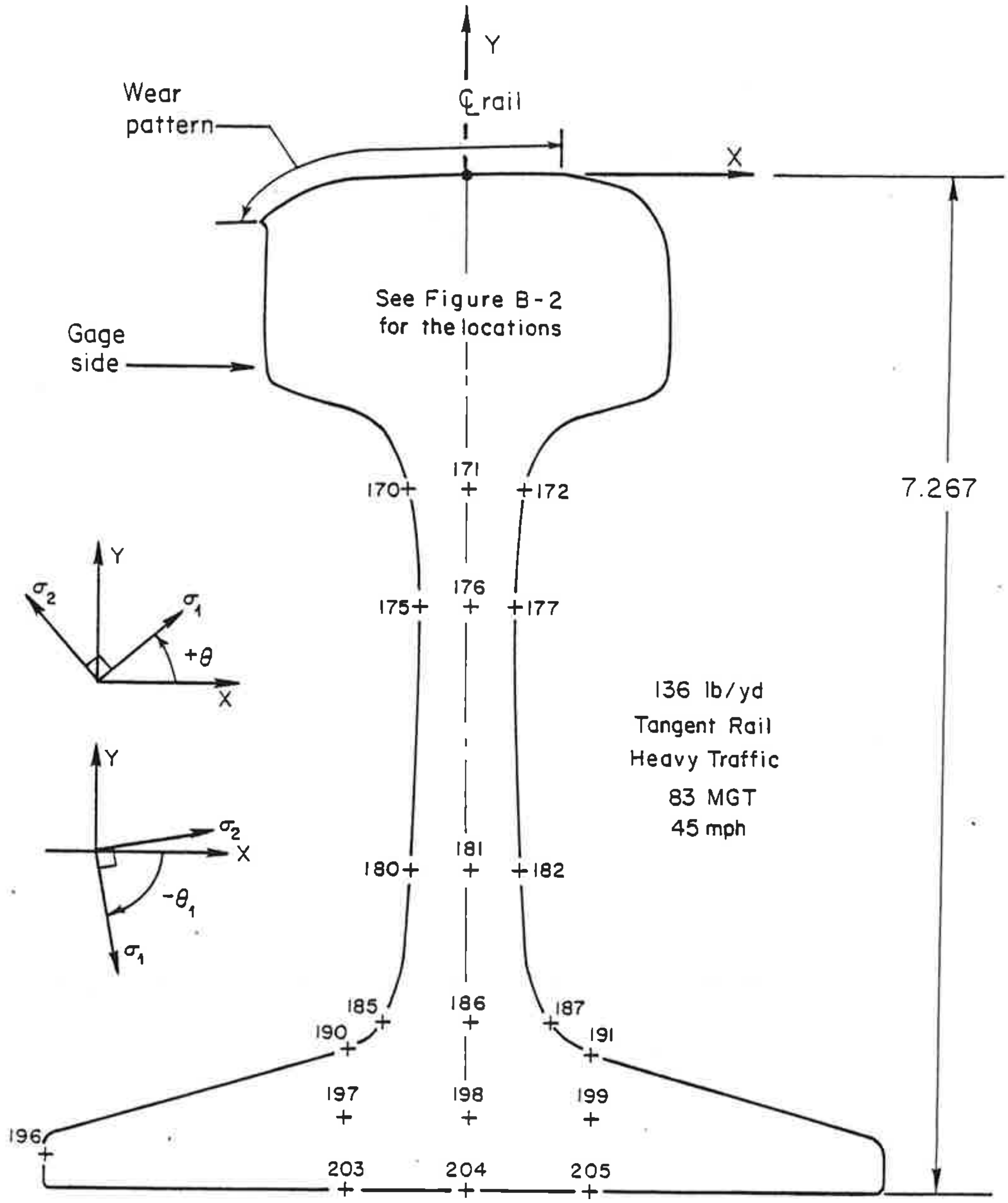

FIGURE B-1. SPECIMEN 1, DATA POINT LOCATIONS (RAIL WEB AND BASE)

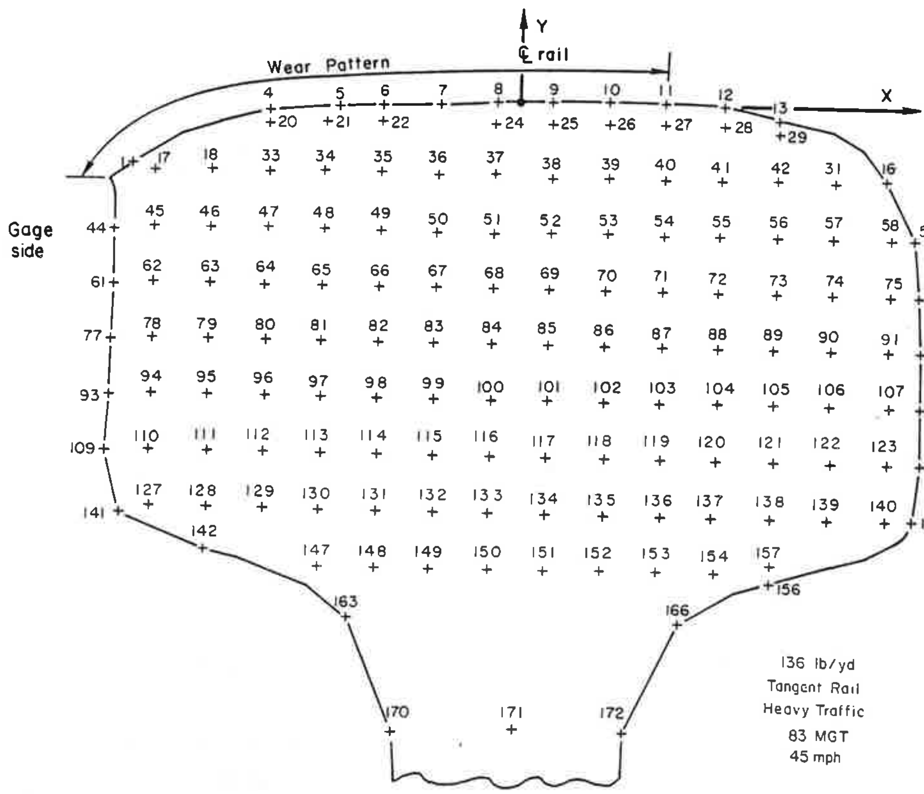

FIGURE B-2. SPECIMEN 1, DATA POINT LOCATIONS (RAIL HEAD)

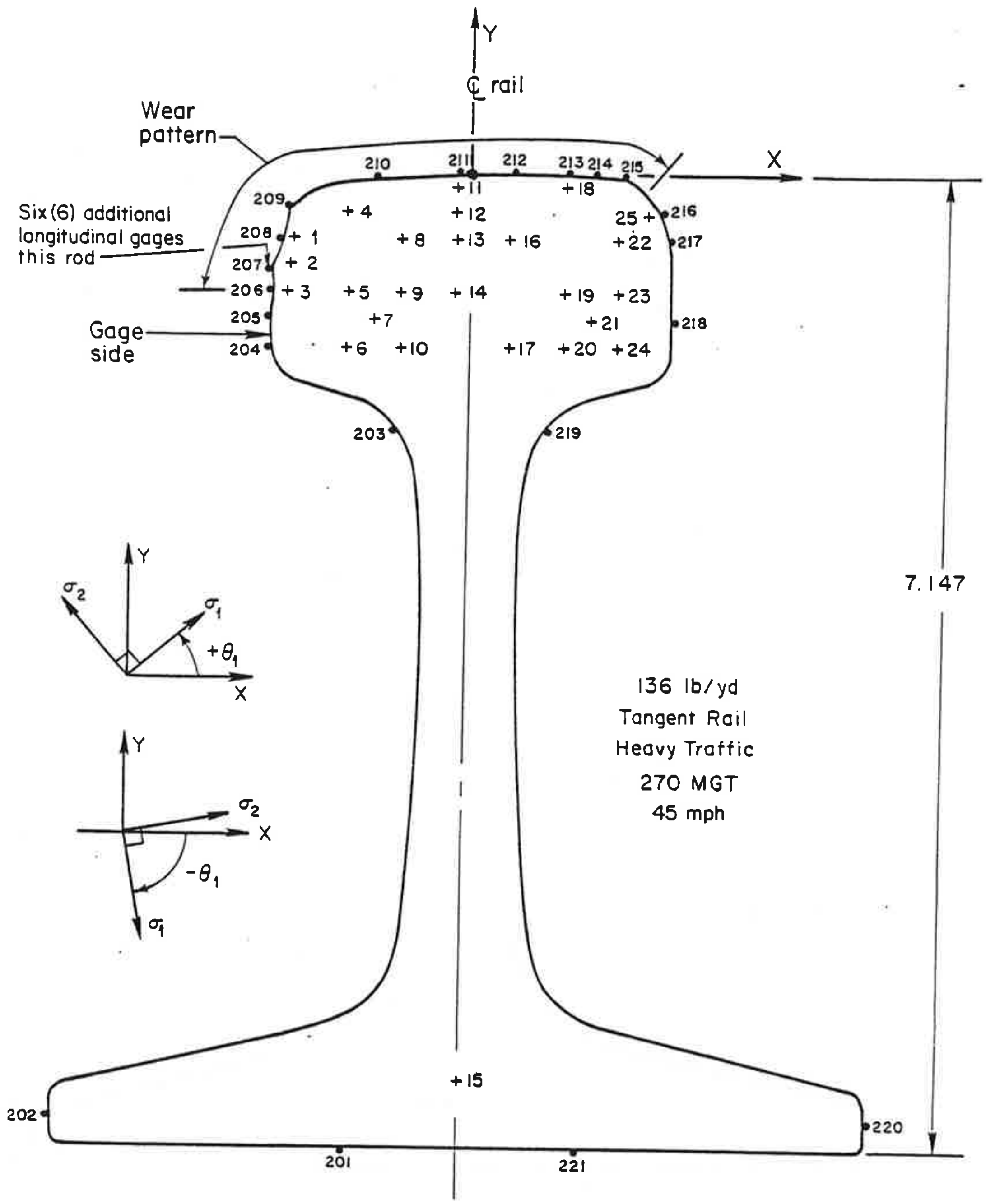

FIGURE B-3. SPECIMEN 2, SLICE 1, DATA POINT LOCATIONS

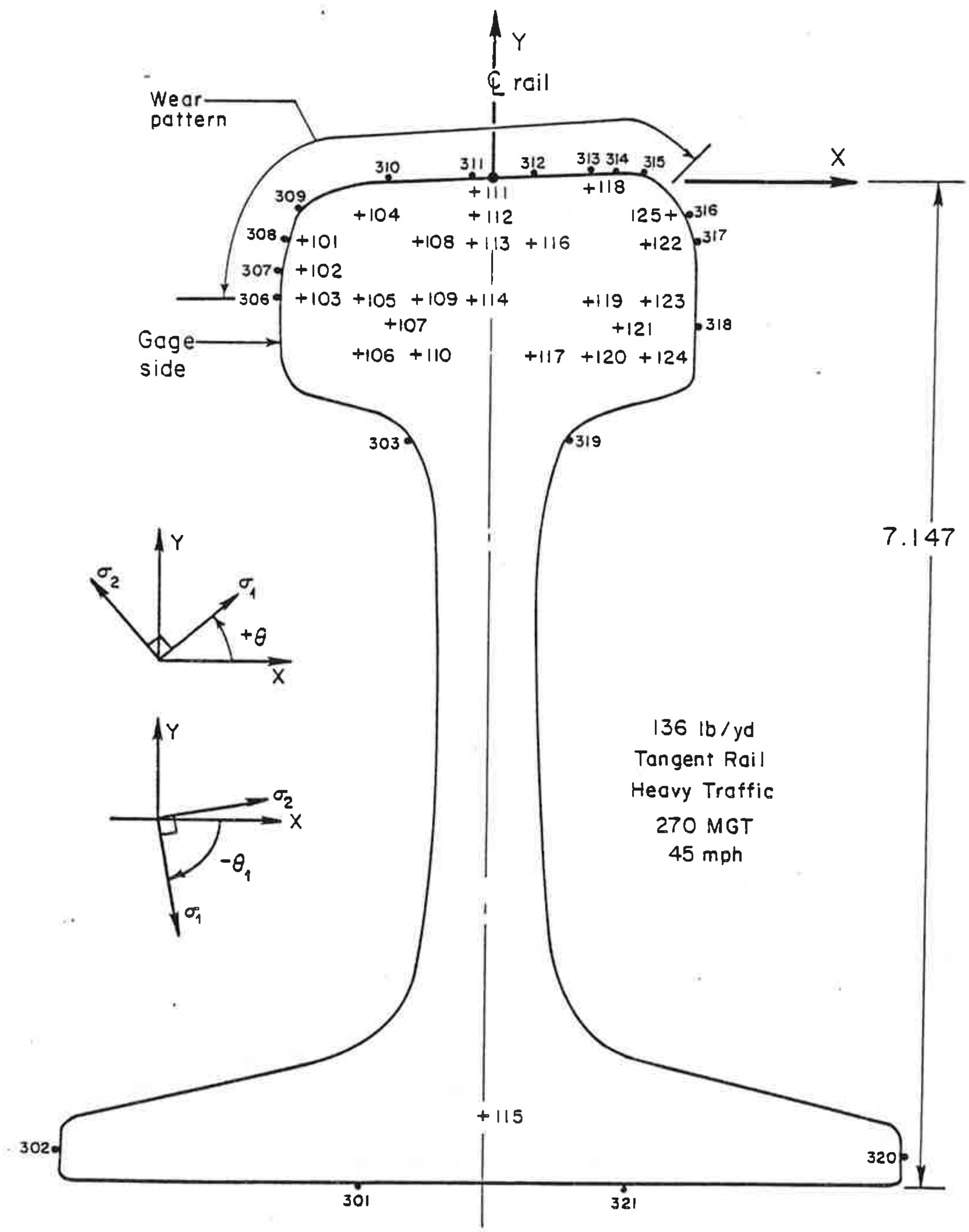

FIGURE B-4. SPECIMEN 2, SLICE 2, DATA POINT LOCATIONS

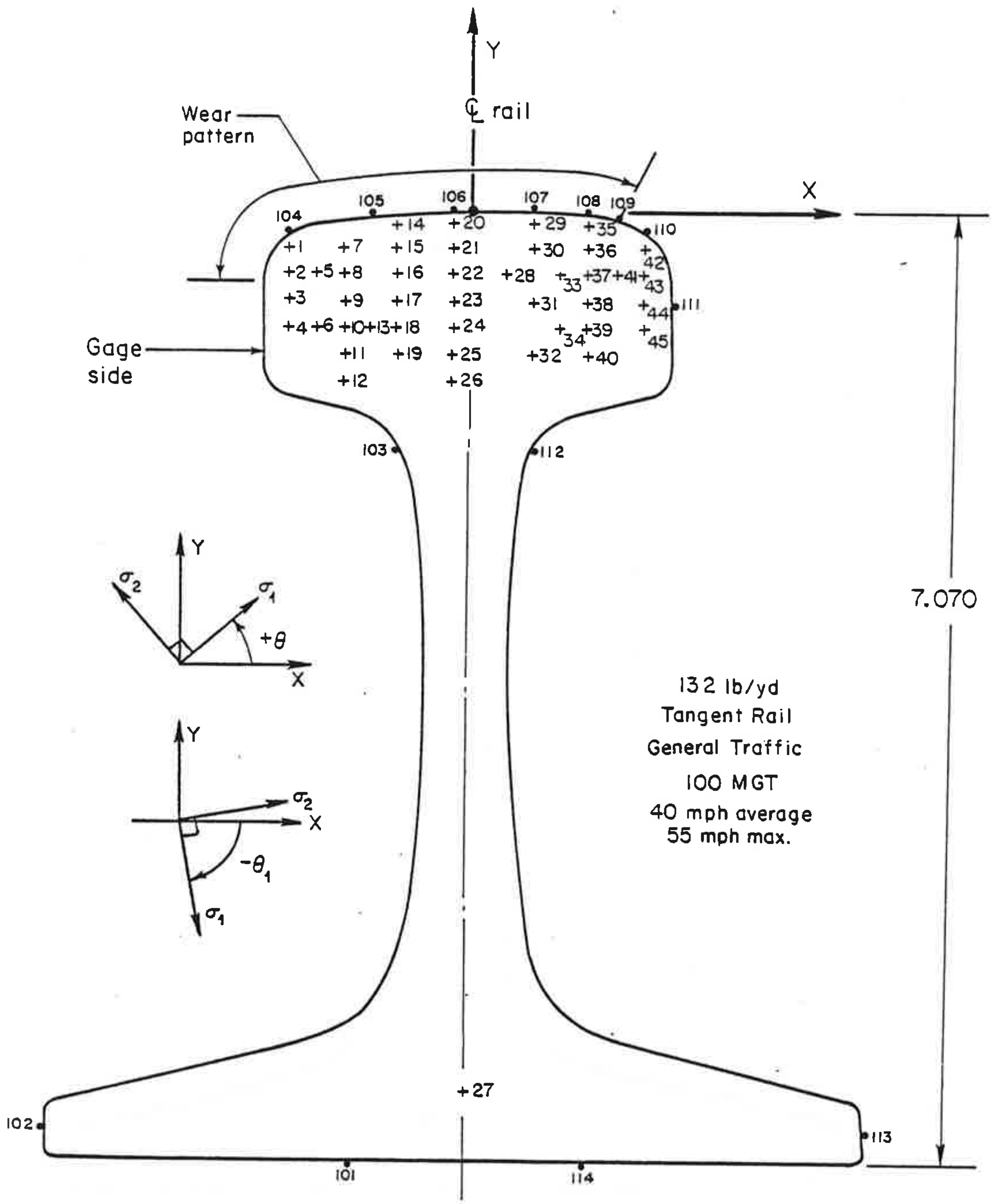

FIGURE B-5. SPECIMEN 5, DATA POINT LOCATIONS

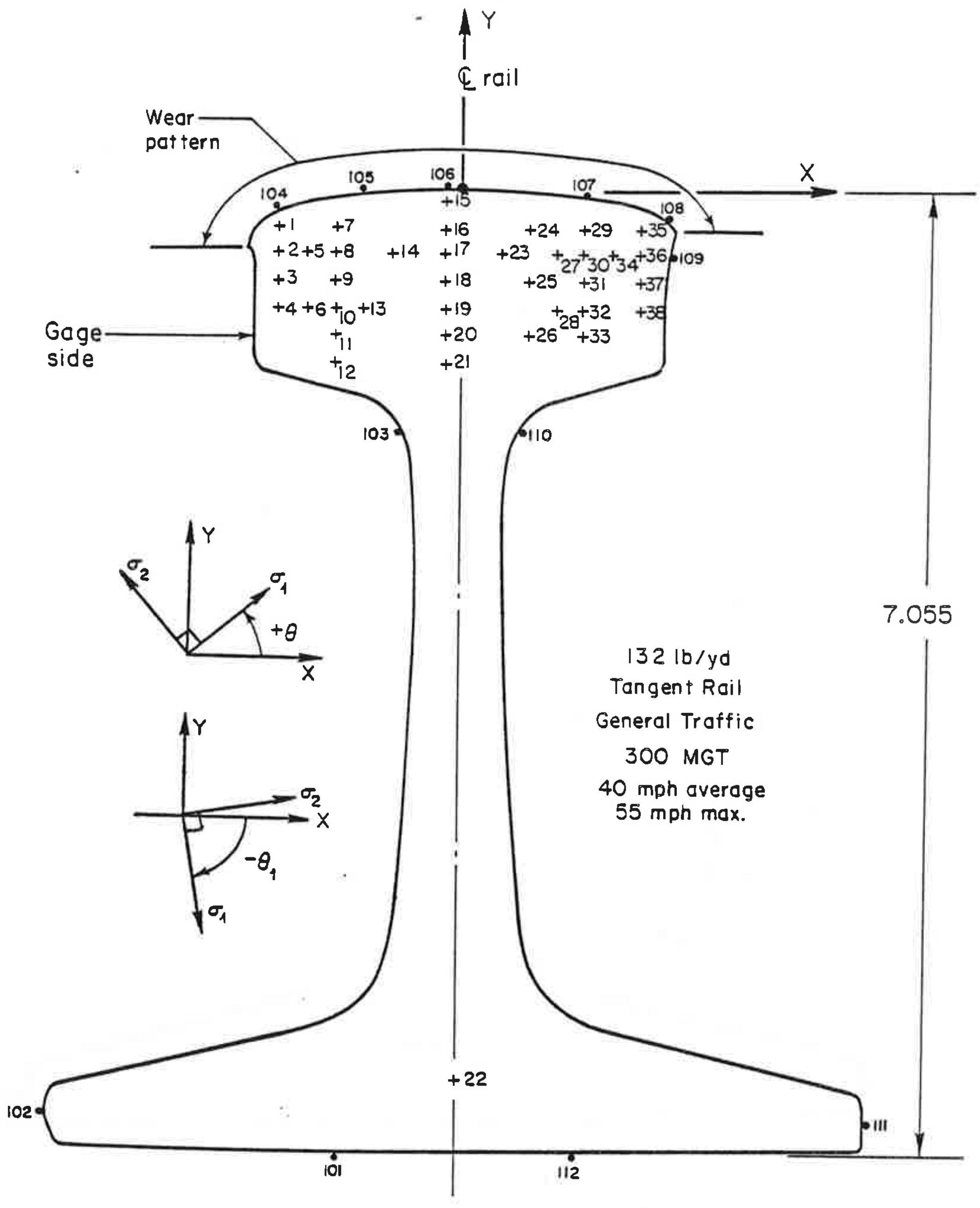

FIGURE B-6. SPECIMEN 6, DATA POINT LOCATIONS

TABLE B-1. SPECIMEN 1 STRESSES (See Figures B-1 and B-2 for gage locations)

GAGE NO.	GAGE COORDINATE, INCHES		PRINCIPAL STRESS, psi (IN x-y PLANE)			ANGLE, DEGREES	GAGE NO.
	X	Y	σ_1	σ_2	σ_z	θ_1	
1	-1.375	-0.258	0	-15900	-17100	-48.7	1
4	-0.897	-0.051	0	-16800	- 9300	-83.3	4
5	-0.695	-0.031	0	-17200	-11000	-85.5	5
6	-0.497	-0.024	0	-18300	- 8200	-88.2	6
7	-0.297	-0.015	0	-29200	-10100	-88.3	7
8	-0.097	-0.003	0	-23200	-12500	-88.3	8
9	0.104	0.005	0	-28400	-14000	89.4	9
10	0.303	0.008	0	-16700	- 9900	88.8	10
11	0.499	0.008	0	-26900	-18000	86.8	11
12	0.711	0.004	0	-69000	-35800	81.8	12
13	0.903	-0.040	0	-51500	-26400	78.5	13
16	1.289	-0.248	0	-31300	- 8000	53.3	16
17	-1.297	-0.277	2400	-25300	-20000	-36.2	17
18	-1.096	-0.272	8600	-24300	-14900	-57.7	18
20	-0.896	-0.098	-600	-17500	-13200	-80.3	20
21	-0.695	-0.088	0	-14700	-12100	-78.8	21
22	-0.499	-0.083	-1100	-20800	-13700	-81.3	22
24	-0.099	-0.081	-2200	-25000	-16000	87.3	24
25	0.105	-0.079	-4500	-22600	-16000	88.0	25
26	0.302	-0.074	- 600	-24600	-17500	-85.4	26
27	0.499	-0.071	-2000	-32300	-23000	89.3	27
28	0.710	-0.068	2100	-45600	-26500	-85.8	28
29	0.905	-0.088	2700	-48600	-22200	67.8	29
31	1.106	-0.261	12600	-28000	- 5100	43.1	31
33	-0.893	-0.275	6500	-22800	-15900	-72.7	33
34	-0.697	-0.267	500	-25100	-20200	-83.1	34
35	-0.496	-0.269	-1800	-24600	-21800	-85.7	35
36	-0.296	-0.271	500	-22300	-20200	89.6	36
37	-0.096	-0.262	-3900	-27600	-23300	-88.6	37
38	0.108	-0.270	100	-21600	-20600	86.4	38
39	0.305	-0.264	400	-19900	-21200	88.0	39
40	0.504	-0.269	-2400	-23700	-22000	83.9	40
41	0.703	-0.265	14100	-17600	- 9200	75.9	41
42	0.905	-0.260	18000	-17400	- 900	55.2	42
44	-1.432	-0.493	0	-142700	-91000	- 9.5	44
45	-1.293	-0.481	25800	-29900	-17800	-31.3	45
46	-1.095	-0.478	28500	- 4300	5800	-41.4	46
47	-0.892	-0.474	23600	- 3000	3100	-45.6	47
48	-0.693	-0.477	11000	- 4000	- 3300	-53.7	48
49	-0.493	-0.476	3100	1600	- 5000	-54.0	49
50	-0.293	-0.477	4400	3900	- 3900	-87.1	50
51	-0.092	-0.473	3200	600	- 4100	2.5	51
52	0.106	-0.466	-24600	-37200	-24900	41.1	52
53	0.308	-0.463	- 400	- 6800	- 7700	15.3	53
54	0.508	-0.467	6800	- 6900	- 2700	39.4	54
55	0.706	-0.463	33100	500	9000	44.3	55
56	0.908	-0.461	36300	5400	11800	42.2	56
57	1.107	-0.460	18800	-15300	- 300	28.0	57
58	1.312	-0.462	6400	-26800	- 5900	16.1	58
59	1.397	-0.455	0	-39000	- 8800	12.3	59
61	-1.429	-0.688	0	-114200	-60800	- 2.3	61
62	-1.293	-0.679	6200	-38500	-26100	5.8	62
63	-1.092	-0.676	39000	2300	13100	-35.3	63
64	-0.896	-0.680	37300	12400	17300	-29.3	64
65	-0.694	-0.675	34100	12200	16000	-18.2	65
66	-0.495	-0.674	34200	7400	13400	- 4.2	66
67	-0.293	-0.668	22500	4100	8900	5.9	67
68	-0.092	-0.667	25400	- 3200	6800	2.2	68
69	0.109	-0.669	40400	- 9100	9900	1.3	69

TABLE B-1. SPECIMEN 1 STRESSES (CONT.)
(See Figures B-1 and B-2 for gage locations)

GAGE NO.	GAGE COORDINATE, INCHES		PRINCIPAL STRESS, psi (IN x-y PLANE)			ANGLE, DEGREES	GAGE NO.
	X	Y	σ_1	σ_2	σ_z	θ_1	
70	0.306	-0.665	21000	- 8900	3700	17.6	70
71	0.508	-0.667	37000	4400	13000	26.3	71
72	0.704	-0.662	41000	11500	14900	29.7	72
73	0.911	-0.662	9600	- 5900	- 1000	22.1	73
74	1.110	-0.659	8000	-11300	- 2400	5.7	74
75	1.314	-0.663	1900	-28000	- 7800	4.5	75
76	1.417	-0.659	0	-46800	-10900	3.8	76
77	-1.432	-0.889	0	-67600	-36500	- 2.3	77
78	-1.290	-0.881	- 800	-49000	-21900	8.3	78
79	-1.092	-0.877	18900	12300	11200	40.9	79
80	-0.890	-0.877	33700	17600	16900	-26.2	80
81	-0.692	-0.871	28800	14600	15000	-17.9	81
82	-0.492	-0.870	31600	10000	14300	-17.0	82
83	-0.293	-0.868	35100	6900	14800	- 3.3	83
84	-0.089	-0.868	33700	3500	11000	1.4	84
85	0.109	-0.865	32200	- 3600	9300	3.9	85
86	0.309	-0.863	31200	3900	10100	13.1	86
87	0.510	-0.863	40500	100	11900	7.7	87
88	0.707	-0.865	18200	9000	7600	10.1	88
89	0.907	-0.862	21400	1700	6100	-18.2	89
90	1.111	-0.862	11600	-12000	- 700	-16.5	90
91	1.314	-0.858	5800	-28400	- 5800	- 5.9	91
92	1.429	-0.857	0	-44900	-11000	1.5	92
93	-1.436	-1.087	0	-46100	-12400	- 2.9	93
94	-1.290	-1.076	4800	-28600	- 3900	16.3	94
95	-1.089	-1.075	18500	- 8500	4300	33.8	95
96	-0.887	-1.075	22200	7300	11000	30.4	96
97	-0.689	-1.077	24000	16400	14300	8.5	97
98	-0.491	-1.072	25600	12700	12200	-10.1	98
99	-0.290	-1.071	22700	1900	8100	-14.6	99
100	-0.086	-1.074	28700	6000	11000	- 5.2	100
101	0.113	-1.064	25900	6600	10000	0.1	101
102	0.313	-1.068	20500	7800	8300	12.0	102
103	0.509	-1.064	24200	3700	8100	1.5	103
104	0.714	-1.059	8400	- 5000	800	-17.9	104
105	0.912	-1.061	- 300	-24900	- 7200	-30.8	105
106	1.110	-1.058	6200	-29100	- 4600	-27.7	106
107	1.322	-1.058	3500	-24500	- 2600	-12.7	107
108	1.434	-1.054	0	-33600	- 6500	0.6	108
109	-1.446	-1.283	0	-20700	- 2200	0.4	109
110	-1.290	-1.279	5500	-19400	400	28.2	110
111	-1.086	-1.279	16100	-15100	3300	39.1	111
112	-0.889	-1.276	14900	- 8400	5400	42.3	112
113	-0.686	-1.276	9600	- 3700	4800	32.2	113
114	-0.485	-1.278	600	- 8200	- 1400	-79.6	114
115	-0.286	-1.270	-12800	-28100	- 7400	90.0	115
116	-0.087	-1.273	- 7300	-14300	- 2600	88.0	116
117	0.112	-1.270	-17900	-21800	- 8300	-29.5	117
118	0.316	-1.266	7300	3800	7700	-87.3	118
119	0.516	-1.263	12200	2500	8300	-29.7	119
120	0.714	-1.260	-15600	-43400	-12900	-31.5	120
121	0.915	-1.264	-59600	-69800	-35300	-38.6	121
122	1.117	-1.261	-47500	-69800	-31900	-53.3	122
123	1.319	-1.261	2800	-14700	100	-23.0	123
124	1.437	-1.254	0	-18000	- 5500	0.6	124
126	1.417	-1.457	0	- 6100	1000	-56.6	126
127	-1.287	-1.478	8400	- 6900	9400	41.7	127
128	-1.084	-1.482	9500	-15600	6600	48.9	128
129	-0.886	-1.478	8000	-18900	4200	52.0	129

TABLE B-1. SPECIMEN 1 STRESSES (CONT.)
(See Figures B-1 and B-2
for gage locations)

GAGE NO.	GAGE COORDINATE, INCHES		PRINCIPAL STRESS, psi (IN x-y PLANE)			ANGLE, DEGREES	GAGE NO.
	X	Y	σ_1	σ_2	σ_z	θ_1	
130	-0.687	-1.477	2500	-12100	4500	56.6	130
131	-0.483	-1.473	8400	- 4600	8200	89.5	131
132	-0.283	-1.468	10700	- 5500	7100	-87.6	132
133	-0.087	-1.471	11000	- 5300	6200	-80.2	133
134	0.115	-1.468	11600	- 4200	6500	-86.8	134
135	0.319	-1.470	8500	- 2200	6400	-76.0	135
136	0.520	-1.465	5000	- 8300	3900	-61.7	136
137	0.705	-1.466	2000	-18600	900	-32.3	137
138	0.913	-1.465	10100	-16500	3100	-49.6	138
139	1.117	-1.462	9300	-10800	4200	-43.3	139
140	1.319	-1.457	6700	- 2200	4900	-27.0	140
141	-1.391	-1.507	0	- 9700	- 400	43.7	141
142	-1.091	-1.627	0	-18700	- 9800	73.2	142
147	-0.683	-1.678	2400	-36100	- 2700	62.0	147
148	-0.484	-1.675	1100	-21900	2100	73.5	148
149	-0.289	-1.674	8200	-10000	7300	81.9	149
150	-0.079	-1.672	13200	- 9000	6500	-89.9	150
151	0.118	-1.671	12300	-12200	6700	-85.0	151
152	0.315	-1.664	9400	-12300	5900	-76.7	152
153	0.516	-1.667	1000	-19500	1400	-62.6	153
154	0.720	-1.664	4100	-28200	- 300	-53.1	154
156	0.917	-1.693	0	-40300	-11300	-71.7	156
157	0.915	-1.632	- 1900	-24900	- 3000	-61.4	157
163	-0.577	-1.860	0	-31900	- 5300	35.6	163
166	0.597	-1.850	0	-41300	- 7400	-46.7	166
170	-0.406	-2.260	0	-10600	- 4500	9.5	170
171	0.021	-2.240	4300	- 1300	3400	-82.0	171
172	0.410	-2.244	0	- 6400	600	-12.2	172
175	-0.321	-3.108	0	- 4400	- 100	0.6	175
176	0.029	-3.098	4400	100	2300	-19.4	176
177	0.351	-3.096	0	- 5100	- 2800	- 3.8	177
180	-0.368	-5.012	0	-11600	- 8200	- 4.3	180
181	0.046	-5.005	3600	800	1900	- 7.8	181
182	0.409	-4.997	0	- 3300	- 2800	3.8	182
185	-0.565	-6.102	0	-11700	- 3600	-44.0	185
186	0.053	-6.091	5400	2300	8000	- 8.1	186
187	0.630	-6.088	0	2000	5900	37.6	187
190	-0.808	-6.300	0	- 5800	0	-72.7	190
191	0.925	-6.324	0	- 5200	- 400	78.0	191
196	-2.942	-7.087	0	-10400	-19000	- 2.0	196
197	-0.814	-6.779	5000	3800	7200	-30.0	197
198	0.062	-6.774	5300	1600	9300	-14.7	198
199	0.932	-6.764	- 2600	- 3200	2100	- 9.3	199
203	-0.800	-7.303	0	- 700	- 2700	90.0	203
204	0.067	-7.300	0	-11000	-14100	90.0	204
205	0.941	-7.299	0	-24700	-35300	90.0	205

TABLE B-2. SPECIMEN 2, SLICE 1 STRESSES (See Figure B-3 for gage locations)

GAGE NO.	GAGE COORDINATE, INCHES		PRINCIPAL STRESS, psi (IN x-y PLANE)			ANGLE, DEGREES	GAGE NO.
	X	Y	σ_1	σ_2	σ_z	θ_1	
1	-1.318	-0.461	12600	-38700	-23200	-32.4	1
2	-1.320	-0.663	5600	-40500	-24500	- 6.0	2
3	-1.319	-0.860	10400	-27700	-12400	- 0.9	3
4	-0.916	-0.261	7800	-20300	-17400	-70.3	4
5	-0.913	-0.862	21200	12800	8400	-20.1	5
6	-0.913	-1.264	5900	-14100	- 1400	43.3	6
7	-0.711	-1.059	27100	10600	10400	-12.2	7
8	-0.511	-0.463	7500	- 2900	- 7300	-44.6	8
9	-0.515	-0.862	44100	11300	16000	-18.0	9
10	-0.513	-1.264	11600	5700	5700	- 1.9	10
11	-0.118	-0.065	- 3000	-21500	-19000	-86.0	11
12	-0.113	-0.258	- 3100	-25000	-25700	-84.6	12
13	-0.112	-0.464	9700	- 6500	- 7500	- 5.1	13
14	-0.113	-0.860	44000	12000	15400	1.4	14
15	-0.015	-6.717	100	- 2900	2400	45.5	15
16	0.287	-0.462	15200	- 100	- 3200	13.0	16
17	0.288	-1.265	12600	7700	4500	46.0	17
18	0.691	-0.061	- 3200	-31400	-24700	87.4	18
19	0.689	-0.864	39900	14400	13800	20.7	19
20	0.693	-1.264	8300	- 4000	900	-39.6	20
21	0.889	-1.060	19200	- 1800	3100	-44.0	21
22	1.086	-0.462	64300	14900	22000	51.1	22
23	1.091	-0.864	16000	- 3200	- 500	-32.6	23
24	1.089	-1.265	11400	-24100	- 4800	-42.7	24
25	1.289	-0.264	21500	-66500	-25700	32.6	25
201	-0.883	-7.248	2200	0	7900	0.0	201
202	-3.019	-7.002	0	- 5600	- 9400	0.0	202
203	-0.547	-1.934	0	-28500	1600	43.0	203
204	-1.457	-1.280	0	-28900	-21500	8.5	204
205	-1.455	-1.078	0	-39600	-10300	1.5	205
206	-1.459	-0.881	0	-72700	-23700	- 1.0	206
207	-1.435	-0.669	0	-39300	-23600	- 4.0	207
208	-1.394	-0.464	0	-91000	-43800	-15.0	208
209	-1.306	-0.262	0	- 5100	-10400	-37.0	209
210	-0.700	-0.041	0	- 3800	- 3100	-84.0	210
211	-0.108	0.001	0	-15700	- 6800	-87.0	211
212	0.305	0.002	0	-18400	- 7800	-88.5	212
213	0.703	0.008	0	-26400	-10600	87.0	213
214	0.908	-0.001	0	-15700	- 9200	88.0	214
215	1.103	-0.025	0	-81300	-37200	82.0	215
216	1.340	-0.245	0	-85200	-29700	30.0	216
217	1.418	-0.472	0	-70700	-25600	12.0	217
218	1.448	-1.085	0	-32000	- 4832	90.0	218
219	0.516	-1.944	0	-24900	5400	-35.0	219
220	2.968	-7.004	0	- 4200	- 100	0.0	220
221	0.870	-7.254	1600	0	7200	-90.0	221

TABLE B-3. SPECIMEN 2, SLICE 2 STRESSES (See Figure B-4 for gage locations)

GAGE NO.	GAGE COORDINATE, INCHES		PRINCIPAL STRESS, psi (IN x-y PLANE)			ANGLE, DEGREES	GAGE NO.
	X	Y	σ_1	σ_2	σ_z	θ_1	
101	-1.318	-0.461	10600	-41500	-24700	-31.0	101
102	-1.320	-0.663	6900	-46500	-25900	- 5.8	102
103	-1.319	-0.860	5200	-43300	-18700	5.5	103
104	-0.916	-0.261	10200	-19900	-16500	-70.9	104
105	-0.913	-0.862	29500	13800	11200	-12.1	105
106	-0.913	-1.264	12800	-13000	1000	34.6	106
107	-0.711	-1.059	23800	11900	9800	7.0	107
108	-0.511	-0.463	13600	- 2700	- 5400	-31.8	108
109	-0.515	-0.862	50100	12000	18000	- 8.2	109
110	-0.513	-1.264	5500	3900	3300	19.6	110
111	-0.118	-0.065	- 2300	-22500	-19100	-86.8	111
112	-0.113	-0.258	- 200	-18000	-22700	-87.2	112
113	-0.112	-0.464	13200	- 9200	- 7300	- 2.8	113
114	-0.113	-0.860	36500	9100	12300	- 1.8	114
115	-0.015	-6.717	2700	300	4100	4.7	115
116	0.287	-0.462	21300	- 400	- 1500	0.0	116
117	0.288	-1.265	13100	7100	4500	52.1	117
118	0.691	-0.061	- 2000	-30500	-24100	85.1	118
119	0.689	-0.864	43300	19600	16400	21.4	119
120	0.693	-1.264	9000	2300	3000	-55.9	120
121	0.889	-1.060	20800	10100	7100	-44.3	121
122	1.086	-0.462	55300	16900	19900	44.9	122
123	1.091	-0.864	18900	8100	3700	-42.1	123
124	1.089	-1.265	13100	-14700	- 1500	-42.6	124
125	1.289	-0.264	22800	-63100	-24300	35.7	125
301	-0.883	-7.248	3500	0	3800	0.0	301
302	-3.019	-7.002	800	0	-19700	90.0	302
303	-0.547	-1.934	0	-26400	- 4500	43.0	303
306	-1.459	-0.881	0	-62300	-20900	- 1.0	306
307	-1.435	-0.669	0	-80500	-36600	- 4.0	307
308	-1.394	-0.464	0	-100700	-49600	-15.0	308
309	-1.306	-0.262	0	- 7400	-17300	-37.0	309
310	-0.700	-0.041	0	- 6900	- 4500	-84.0	310
311	-0.108	0.001	0	- 6400	-13500	-87.0	311
312	0.305	0.002	0	-14700	-19800	-88.5	312
313	0.703	0.008	0	-10400	-20500	87.0	313
314	0.908	-0.001	0	-12200	-15100	88.0	314
315	1.103	-0.025	0	-31000	-63800	82.0	315
316	1.340	-0.245	0	-88500	-28600	30.0	316
317	1.418	-0.472	0	-89900	-34300	12.0	317
318	1.448	-1.085	0	-36900	- 8500	0.0	318
319	0.516	-1.944	0	-25200	800	-35.0	319
320	2.968	-7.004	0	-19000	-27400	0.0	320
321	0.870	-7.254	1800	0	1700	0.0	321

TABLE B-4. SPECIMEN 5 STRESSES (See Figure B-5 for gage locations)

GAGE NO.	GAGE COORDINATE, INCHES		PRINCIPAL STRESS, psi (IN x-y PLANE)			ANGLE, DEGREES	GAGE NO.
	X	Y	σ_1	σ_2	σ_z	θ_1	
1	-1.306	-0.270	3100	-32100	-31600	-50.3	1
2	-1.312	-0.463	18200	-17100	- 7800	-23.5	2
3	-1.312	-0.670	11000	200	- 200	- 5.1	3
4	-1.307	-0.869	- 7400	-34300	-15400	15.9	4
5	-1.106	-0.461	22200	900	4000	-39.2	5
6	-1.106	-0.871	10700	5700	5800	19.9	6
7	-0.909	-0.276	900	-23900	-19100	-79.1	7
8	-0.897	-0.466	19200	4600	6700	-37.2	8
9	-0.905	-0.667	35700	11600	18600	-20.4	9
10	-0.905	-0.873	18900	10900	12900	-15.3	10
11	-0.905	-1.071	11400	- 4500	5200	31.9	11
12	-0.905	-1.268	100	-25200	1000	52.3	12
13	-0.710	-0.875	35200	14800	18900	-18.7	13
14	-0.503	-0.086	- 5700	-24000	-30800	85.5	14
15	-0.504	-0.265	- 2700	-18500	-24200	88.0	15
16	-0.503	-0.475	- 2900	- 4200	- 5600	-80.6	16
17	-0.505	-0.669	21500	1500	10500	-10.4	17
18	-0.505	-0.871	33100	11000	17200	-15.7	18
19	-0.502	-1.068	30400	6500	14500	-20.1	19
20	-0.104	-0.067	- 5200	-24500	-28300	83.1	20
21	-0.101	-0.269	- 1800	-17300	-21200	88.7	21
22	-0.104	-0.467	5100	1700	- 2500	38.8	22
23	-0.104	-0.672	14500	1700	6300	4.9	23
24	-0.104	-0.871	-15800	-27600	-10200	63.7	24
25	-0.107	-1.065	30400	11700	17900	- 5.7	25
26	-0.097	-1.274	14900	2000	17200	-67.1	26
27	0.025	-6.574	10900	2700	10200	- 3.5	27
28	0.297	-0.465	3100	- 3500	- 6300	17.0	28
29	0.496	-0.070	- 3100	-23800	-32200	76.5	29
30	0.496	-0.269	- 2300	-14300	-24600	89.8	30
31	0.494	-0.669	29800	4500	6900	14.7	31
32	0.492	-1.071	19900	4600	13000	6.3	32
33	0.692	-0.475	17800	1900	- 2400	15.8	33
34	0.692	-0.870	25700	6600	7400	12.9	34
35	0.894	-0.079	- 5800	-32000	-34700	85.6	35
36	0.895	-0.271	- 1800	-13900	-17600	64.6	36
37	0.889	-0.473	25200	- 500	1500	30.7	37
38	0.899	-0.674	26600	4600	5300	29.4	38
39	0.893	-0.878	- 2600	-28000	- 7200	-43.4	39
40	0.893	-1.068	10600	- 6500	4800	-32.1	40
41	1.095	-0.469	32700	4200	9900	41.4	41
42	1.296	-0.267	4900	-32800	- 9000	33.3	42
43	1.289	-0.469	5200	-19700	- 6300	17.3	43
44	1.299	-0.670	1400	-17200	- 6600	- 8.2	44
45	1.296	-0.872	6400	-16300	- 500	-19.4	45
101	-0.832	-7.093	0	-48700	-48800	90.0	101
102	-3.025	-6.880	0	-25700	-16100	0.0	102
103	-0.506	-1.765	0	-16500	- 3200	35.8	103
104	-1.291	-0.165	0	-44700	-39700	-58.0	104
105	-0.696	-0.047	0	-11700	-36000	-84.9	105
106	-0.100	-0.007	0	-33800	-27000	-87.0	106
107	0.491	0.004	0	-27800	-23500	-89.5	107
108	0.876	-0.015	0	-29100	-34600	82.8	108
109	1.101	-0.054	0	-57500	-34900	70.9	109
110	1.305	-0.152	0	-59200	-18800	58.0	110
111	1.503	-0.678	0	-30700	-25700	- 2.0	111
112	0.489	-1.755	0	-30000	- 9100	-35.0	112
113	2.980	-6.859	0	-12100	-17900	- 5.2	113
114	0.899	-7.093	0	-23800	-20500	90.0	114

TABLE B-5. SPECIMEN 6 STRESSES (See Figure B-6 for gage locations)

GAGE NO.	GAGE COORDINATE, INCHES		PRINCIPAL STRESS, psi (IN x-y PLANE)			ANGLE, DEGREES	GAGE NO.
	X	Y	σ_1	σ_2	σ_z	θ_1	
1	-1.279	-0.269	9624	-23200	-20357	-56.05	1
2	-1.284	-0.461	24947	-17447	-10907	-30.27	2
3	-1.286	-0.656	12122	- 5269	-11357	2.20	3
4	-1.283	-0.862	8697	-22272	- 9403	21.39	4
5	-1.093	-0.458	30829	280	2520	-38.22	5
6	-1.086	-0.855	23429	8004	9064	37.81	6
7	-0.890	-0.266	- 235	-18785	-18314	-76.83	7
8	-0.887	-0.466	23823	- 854	1195	-40.98	8
9	-0.884	-0.667	41320	17441	18363	-23.47	9
10	-0.894	-0.870	33457	20722	16686	- 6.68	10
11	-0.891	-1.062	20615	- 880	6690	34.16	11
12	-0.888	-1.260	-12469	-59805	-19614	68.16	12
13	-0.691	-0.867	33652	16431	17535	-15.42	13
14	-0.488	-0.465	7390	4421	- 2483	2.25	14
15	-0.098	-0.079	- 4682	-32341	-21989	86.08	15
16	-0.095	-0.275	1105	-18723	-15830	85.20	16
17	-0.096	-0.466	17574	4264	192	17.98	17
18	-0.092	-0.667	37773	8967	14735	6.50	18
19	-0.099	-0.869	31726	13397	15710	- 7.86	19
20	-0.095	-1.061	31639	9118	13455	-16.20	20
21	-0.096	-1.268	12994	- 996	11358	-72.86	21
22	0.022	-6.527	4967	- 3935	8687	- 0.15	22
23	0.301	-0.460	12245	- 756	- 3406	16.02	23
24	0.498	-0.263	- 2463	-23672	-17601	80.84	24
25	0.493	-0.663	33268	5387	11972	6.09	25
26	0.495	-1.067	30818	561	10464	7.46	26
27	0.691	-0.468	12368	- 3089	- 2155	40.19	27
28	0.697	-0.863	33674	8539	12730	9.00	28
29	0.896	-0.271	3695	-20612	-14847	75.18	29
30	0.892	-0.468	17255	- 3287	- 2517	40.37	30
31	0.896	-0.670	27052	9124	8491	16.03	31
32	0.887	-0.862	27854	6758	8841	2.53	32
33	0.890	-1.074	11792	-10006	3592	-33.74	33
34	1.095	-0.469	20230	- 5292	- 789	29.92	34
35	1.292	-0.273	6674	-13404	-15169	42.43	35
36	1.283	-0.465	23699	-20187	- 7269	30.57	36
37	1.287	-0.665	4570	-15612	-13863	4.26	37
38	1.283	-0.873	4752	-20322	-12638	-17.51	38
101	-0.831	-7.057	0	-29758	-22764	-90.00	101
102	-2.910	-6.795	0	-40889	-19634	0.00	102
103	-0.413	-1.739	0	-10236	14	37.50	103
104	-1.276	-0.154	0	-10191	-11305	-64.60	104
105	-0.680	-0.034	0	-16507	-19706	-83.00	105
106	-0.080	-0.003	0	-40195	-22139	-87.50	106
107	0.892	-0.055	0	-24773	-24496	83.00	107
108	1.481	-0.214	696	0	-23565	-37.20	108
109	1.507	-0.471	0	-28444	-31591	- 4.00	109
110	0.430	-1.737	0	-10201	- 5181	-37.00	110
111	2.943	-6.822	0	-16990	-15185	0.00	111
112	0.871	-7.057	0	-34505	-22575	-90.00	112

APPENDIX C

REPORT OF NEW TECHNOLOGY

A technique for measuring the three-dimensional residual stresses in a length of rail removed from a track has been developed and applied. This destructive sectioning technique modifies, extends, and combines several existing techniques that were used previously to make partial measurements of residual stresses in rails. Various computer programs to reduce the experimental data for the presentation of residual stresses in rails have been developed and applied. These developments are improvements on existing techniques, and we believe that no inventions, discoveries, or improvements on inventions were made.

116 copies

U.S. Department
of Transportation

**Research and
Special Programs
Administration**

Kendall Square
Cambridge, Massachusetts 02142